The Institute of Paper Chemistry

Appleton, Wisconsin

Doctor's Dissertation

Elastic Wave Propagation in Paper

Ronald W. Mann

January, 1979

ELASTIC WAVE PROPAGATION IN PAPER

A thesis submitted by

Ronald W. Mann

B.S. 1974, University of Maine

M.S. 1976, Lawrence University

in partial fulfillment of the requirements
of The Institute of Paper Chemistry
for the degree of Doctor of Philosophy
from Lawrence University,
Appleton, Wisconsin

January, 1979

TABLE OF CONTENTS

SUMMARY

The present investigation treats paper as a three-dimensional homogeneous material. The propagation of ultrasonic waves through paper has been investigated from both experimental and theoretical points of view. The primary objective of this work was to determine the validity of applying well-established wave theories, developed for homogeneous continuous materials, to the propagation of waves in paper.

Preliminary experiments indicated that below about 1 MHz ultrasonic waves propagate in paper without severe attenuation. Furthermore, it became clear that at these relatively low frequencies, the fibrous structure of paper does not interact with the waves to produce anomalous behavior.

Techniques were developed for measuring various longitudinal and shear wave velocities for propagation through paper. Some of the techniques apply only to samples having a thickness of 15 mils or more. Most of the experimental work was conducted on two 90-lb linerboard samples and a heavy milk carton stock. For some of the velocity measurements, it was necessary to construct three-dimensional structures by gluing individual sheets into stacks.

Using these sonic techniques, the nine orthotropic constants were evaluated for the three board samples. These constants were used in conjunction with orthotropic plate wave theory to predict wave dispersion curves for X- and Y-direction propagation. Portions of these curves were determined experimentally using a plate wave resonance technique.

The comparison of experimental and predicted dispersion curves was good, particularly for the milk carton stock. It was therefore concluded that the orthotropic wave theories did apply to paper. Consequently, paper was

established as a three-dimensional orthotropic material. Orthotropic plate wave theory was subsequently used to modify the velocity measurement procedures.

These improved techniques were used to redetermine the orthotropic constants for the milk carton stock. The set of elastic constants suggested an unusual elastic material. The Z-direction moduli were found to be very low. The Z-direction Young's modulus was about 200 times less than the corresponding X-direction modulus. The out-of-plane Poisson ratios were found to be greater than 1.

INTRODUCTION

The primary objective of this thesis is to determine the validity of applying wave theories, developed for continuous homogeneous materials, to paper. Paper is a heterogeneous porous material. Even well-bonded paper sheets contain unbonded fiber regions and air spaces.

During the formation of the paper web, the fibers generally align preferentially in the plane of the sheet. In addition, the tension in the web during drying usually differs markedly in the machine and cross-machine directions. These factors help to explain the observed differences in the stiffness of machine-made paper along the machine (X), cross machine (Y), and thickness (Z) directions.

Orthotropic materials have three orthogonal symmetry axes. The orthotropic model is the simplest model which can accommodate different elastic properties along the three mutually perpendicular directions. Consequently, orthotropic wave theories, in particular, will be tested.

LITERATURE REVIEW

MECHANICAL MEASUREMENT OF PAPER ELASTICITY

IN-PLANE

Paper is relatively thin. Consequently, it is difficult to determine the elastic constants which characterize the thickness direction of paper. On the other hand, much study has been made of the in-plane elastic properties.

The mechanical properties of elastic materials are time independent. Brezinski (1) has shown that even under very low loads, the deformation of paper is time dependent. It was demonstrated, however, that at low loads the rate of time-dependent deformation is low. It is therefore possible, for example, to obtain valid estimates of the elastic modulus of paper by measuring the initial slope of the load-elongation curve.

The time-dependent mechanical properties of paper can be examined using various techniques such as creep, stress relaxation, and certain resonance techniques. These latter techniques have been used to investigate the dependency of Young's modulus, shear modulus, and viscous damping on various parameters, including strain, relative humidity, sheet density, and orientation in the sheet (2-6).

Riemen and Kurath (2), using the vibrating reed technique at about 60 Hz and at low strain amplitude, were able to determine the complex Young's modulus for handsheets of softwood bleached sulfite pulp. The real component of Young's modulus was found to be nearly independent of strain up to approximately 6×10^{-4}. The loss tangent, however, increased markedly with strain. With increasing moisture content, the real component decreased steadily, whereas the

imaginary component exhibited a minimum at about 2% moisture and a maximum at about 8%. Both in this work and in that by Horio and Onogi (3), the imaginary component of Young's modulus was found to be less than 5% of the real component.

Kubat and Lindbergson (4) used a low frequency torsional pendulum in their study of shear modulus and the damping behavior of machine-made papers. Upon increasing moisture content the shear modulus decreased, while damping increased.

In another study (6), the dynamic Young's modulus and damping were determined by applying low frequency uniaxial sinusoidal strains to paper strips. By varying strain amplitude, static strain and number of cycles, pronounced strain hardening was observed (increasing modulus). The dynamic modulus and damping were found to exhibit an inverse relationship for the several paper samples tested.

It is evident from these investigations and others that paper falls short of ideal elastic behavior. The measurement of the elastic properties of paper is complicated by factors related to the measurement technique such as strain level and strain rate, and by the ambient conditions of temperature and relative humidity. Furthermore, changes in the elastic properties may occur with mechanical conditioning.

The determination of in-plane Poisson ratios for paper is generally more difficult and less accurate than determinations of Young's and shear moduli. The more direct method of measuring Poisson ratios consists of uniaxially stressing the test specimen and measuring both the longitudinal elongation and the lateral contraction. This technique has been employed on sulfate handsheets yielding ratios of 0.4 to 0.95 (7). Glass beads were affixed to the specimens and their displacements were measured. Jones (8) used this technique

in his work with kraft sack and linerboard samples and found ν_{xy} and ν_{yx} values which fell in the ranges 0.10-0.23 and 0.21-0.57, respectively.

Gottsching and Baumgarten (9) studied the triaxial deformation of paper under tensile loads. The tensile tester used in the study was equipped with special fittings, including two pairs of blades used for measuring lateral contraction. Results for spruce sulfite handsheets indicated an increase in ν_{yx} from 0.17 to 0.32 as the extent of beating was increased. For machine-made papers, ν_{xy} and ν_{yx} values fell in the ranges 0.04-0.10 and 0.16-0.34, respectively. The authors also demonstrated that a plastic component to the lateral contraction was detected only when the longitudinal elongation exhibited a plastic component.

Biaxial testing of cruciform-shaped specimens constitutes a second technique for determining in-plane Poisson ratios. The biaxial stress field precludes potential buckling of the sheet in the direction of contraction. When used in an investigation of jack pine and southern pine kraft handsheets (10), the IPC Biaxial Load-Elongation Apparatus yielded Poisson ratios which fell between 0.27 and 0.37 with few exceptions. Contrary to the experimental results of Gottsching and Baumgarten (9), no particular trends were found with respect to changing sheet structure, though large variations in Poisson ratio between specimens were cited. This biaxial tester was employed recently in an investigation of three kraft linerboard samples (11). Poisson ratio ranges were 0.16-0.18 and 0.36-0.52 for ν_{xy} and ν_{yx}, respectively.

Z-DIRECTION

Investigations of mechanical properties of paper seldom include the Z-direction. In a few studies, measurements have been made of thickness changes

upon machine or cross-machine tensile straining (7,9,12). In recent work, Z-direction load-elongation curves were obtained (13).

Ranger and Hopkins (7) found that the apparent thickness of sulfate handsheets generally increased with increasing tensile strain. One-half inch diameter anvils were used to monitor sheet thickness. The degree of thickness increase was reduced as the pulps were beaten. An initial decrease in thickness was observed for the most highly beaten handsheet. When 1/8-inch diameter anvils were used, an initial decrease in thickness was typically found. This was followed by a series of relative thickness increases and decreases.

Ohrn (12) studied thickness variations of a flat kraft paper using a tensile tester equipped with a roller and flat plate for measuring paper thickness. Paper thickness was found to increase continuously and nearly linearly upon stretching up to the point of failure. Z-direction strains of 10% at failure were typical. Initial thickness decreases were observed in a few cases. Ratios of maximum Z-direction strain (thickness increase) to maximum tensile strain (at failure) ranged between -0.7 to 6.3 for the samples tested.

Ohrn argued that lateral contraction is not necessary for the thickness to increase upon stretching. Instead, Ohrn conceived paper as a woven structure and argued for a mechanism whereby fibers aligned in the direction of tensile loading straighten out when loaded. This in turn would result in a lifting of perpendicularly aligned fibers and, consequently, a thickness increase.

Gottsching and Baumgarten (9) measured Z-direction deformation with anvils of 1 cm^2 area. Results were reported in terms of one of the out-of-plane Poisson ratios, ν_{zx}. For spruce groundwood and bleached spruce sulfite hand-

sheets, ν_{zx} values fell in the ranges of 0.25-0.59 and 0.15-1.19, respectively. In both cases, ν_{zx} increased with the degree of pulp refining. Poisson ratios between 0.74 and 0.93 were found for a series of spruce sulfite handsheets of varying clay content. A series of handsheets made from different pulps yielded ν_{zx} values between 0.36 and 1.05. Negative Poisson ratios were found as well. These latter Poisson ratios were for calendered printing paper, machine finished newsprint, and printing paper made from synthetic fibers.

In this work, thickness usually decreased at first during tensile loading, passed through a minimum, and then increased, frequently to values above the initial thickness. If the thickness did not decrease at the beginning of the elongation, its increase was first slight and became steeper only with increasing elongation. Both shapes of curves suggest that multiple processes are involved in thickness changes.

Recently Van Liew (13) has studied the Z-direction load-elongation behavior of western hemlock bleached sulfite handsheets. Circular specimens were bonded between and onto two 1-inch diameter cylinders. As the tensile loads were applied, cylinder separation was measured at three points on the periphery. Several difficulties were encountered. Nonparallel separation of the cylinder surfaces was typical, indicating nonuniform strain over the specimen area. Failure occurred for strains in the range 0.25-0.7%. The load-elongation curves were almost immediately nonlinear.

Van Liew calculated Z-direction tensile moduli between 20 and 60 kg/mm^2 for the handsheets tested. These moduli are roughly 1/10th of the in-plane moduli. It was concluded that intrafiber deformation was the principle mechanism of response only at very low strains. At higher strains, the nonuniform fibrous structure results in early onset of fiber bond failure.

The Z-direction experimental results cited above are inconclusive. A valid method for measuring Z-direction strains mechanically has not been demonstrated. Indeed, this may not be possible because of local thickness and basis weight variations which are typical of paper sheets.

SONIC MEASUREMENT OF PAPER ELASTICITY

Sonic determinations of elastic parameters reported in the literature involve the measurement of velocities of longitudinal and shear waves propagated through the material. Sonic (or ultrasonic) elastic waves travelling through solids constitute propagation of stress and strain. For longitudinal waves, the points (particles) within the material are displaced parallel to the propagation direction. For shear wave propagation, particle displacement is perpendicular to the propagation direction.

These two types of waves are depicted in Fig. 1a and 1b (see page 31). These waves propagate through bulk materials, which are large in all three dimensions. The waves shown in these figures are pure longitudinal and pure shear waves since the particles are displaced exactly parallel and exactly perpendicular, respectively, to the direction of propagation. In the general case (see Fig. 1c), the wave motion has both longitudinal and transverse (shear) components. In the present work, the longitudinal and shear wave designations will be employed for waves in bulk materials and in plate materials at low frequencies.

LOW FREQUENCY

Though there are several sonic techniques for measuring wave velocities (14-17), the pulse propagation technique has been used almost exclusively

for measurements on paper. With this technique, wave propagation velocities are easily calculated from measurements of transit time at different transducer separations.

The Morgan Dynamic Modulus Tester (18), a commercial instrument, has been used in several experimental investigations of paper properties. The instrument employs ceramic piezoelectric transducers which resonate at about 10 kHz.

Attached to the transducers are small round-tipped probes which made essentially point contact with the paper. The electronic circuitry generates triangular pulses at a repetition rate of 60 Hz, which excite the transmitting transducer to resonate. As the propagated disturbances are received by the receiving transducer, the transit time of the pulse through the paper is measured and registered on a chart recorder. Both longitudinal and shear waves can be propagated and detected. Since the wavelengths at 10 kHz are always much longer than the paper thickness, the sonic pulse propagation technique is considered a low frequency technique.

Craver and Taylor (19,20) were the first to use the sonic pulse technique in the nondestructive measurement of paper elasticity. The authors presented a theoretical treatment of wave propagation in paper, which is considered a planar material. In this case, Z-direction stresses are assumed to be zero. For isotropic planar materials, the following relationship was given:

$$E = \rho V_L^2 (1-\nu^2), \qquad (1)$$

where E = Young's modulus

ρ = material density

V_L = velocity of longitudinal wave

ν = in-plane Poisson ratio

Craver and Taylor approximate Young's modulus by ρV_L^2, which is then called the sonic modulus. This approximate sonic modulus can be determined from a single velocity measurement.

Considering anisotropic machine-made paper to exhibit orthotropic behavior, Craver and Taylor presented the theoretical relationships between the four orthotropic planar stiffness coefficients and various wave velocities. By determining the velocity of longitudinal waves propagated in directions 0°, 45°, and 90° from the machine direction, and the shear velocity along the machine or cross-machine direction, one can determine all of the planar elastic constants for paper.

Sonic pulse data, rapidly and easily obtained, is independent of specimen size. In addition, sonic velocities can be measured continuously. A disadvantage of this technique is that it cannot easily measure the imaginary component of the complex Young's modulus.

Craver and Taylor used the sonic pulse technique in several studies (19-21). The anisotropy of unbleached kraft wrapping paper was measured as the ratio of the machine and cross-machine direction sonic moduli (19). Close agreement was found with both tensile moduli and tensile strength anisotropy factors. High correlation between tensile modulus and sonic modulus was found for handsheets made from several different pulps.

A study of the effects of fiber orientation and external directional stresses during drying showed that drying constraints have a pronounced effect on the anisotropy factor (20). Craver and Taylor, by varying the basis weight of bleached kraft softwood handsheets, demonstrated that the measured sonic

velocities were independent of sheet thickness. A basis weight effect was observed, though this was attributed to real moduli differences.

In a later study of wet-strength paper (21), various liquids were found to reduce the sonic velocity to different extents upon saturation. In other work, Chatterjee (22) measured wicking in paper using the Morgan instrument. Back and Didriksson (23), by monitoring modulus changes with temperature, were able to detect four secondary transition temperatures and the glass transition temperature of cellulose. In their work, paper sheets were subjected to 4 sec of thermostating at various nip temperatures prior to testing.

In a recent experimental investigation using kraft linerboard samples, Bornhoeft (11) measured in-plane Poisson ratios both sonically and mechanically and found reasonably good agreement.

Several investigations have demonstrated that paper strength properties, particularly tensile strength, correlate well with sonic modulus (19,24,25). It has been suggested that the sonic pulse technique could be adapted for use on paper machines. The value of such a continuous on-line monitor in terms of quality control would be great. Yastrebov and Kundzich (26) describe a version of the sonic pulse apparatus developed in Russia. They as well are interested in predicting strength on a moving web. Papadakis (27) has reviewed the problems associated with the development of such an on-line instrument. Recently, work at The Institute of Paper Chemistry, under Project 3332, has resulted in the development of a promising on-line instrument.

PLATE WAVE RESONANCE

Luukkala, et al. (28) have reported propagating waves through paper using a contactless, plate wave resonance method. In this method, plate waves are excited in paper directly from air.

When sound waves having a velocity in air of V_{air} impinge upon paper, making an angle α with the normal, a wave is excited in the paper. This wave will partially reradiate into the air on the other side of the paper. In essence, part of the incident wave energy is reflected, part is absorbed, and part is transmitted.

Paper is a plate material, having a small yet finite thickness. As a plate material, paper exhibits dispersive behavior at high frequencies. When the frequency of the incident wave increases, the wavelength decreases. As the wavelength approaches the plate thickness, the plate waves must travel slower in order to maintain certain boundary conditions. It has been found that at a given frequency, only certain wave modes are allowed (29-31). The phase velocities of these modes are functions of frequency.

With the plate wave resonance method, plate wave velocities can be measured, for a given frequency, by changing the angle of incidence α until the transmitted sound is at a maximum. A maximum in the received signal implies a resonance condition. At resonance, the velocity of the plate wave, V_p, is given by $V_{air}/\sin \alpha$. By systematically changing frequency and locating the resonance angles, one can construct experimental dispersion curves, i.e., V_p vs. frequency.

With the plate wave resonance technique, it is the phase velocity which is measured. This is evident from the fact that continuous waves are employed. With pulse techniques, it is the group velocity which is normally measured.

The group velocity is the propagation velocity of the pulse. As will be shown later, however, it is possible to measure phase velocities using pulse propagation techniques.

Luukkala, et al. (28) employed this method on several commercial papers. Limiting themselves to the machine and cross-machine directions, they treated paper as two different isotropic plates in these two directions. They then applied isotropic plate wave theory to paper. Luukkala, et al., had difficulty interpreting their data. Eventually they extrapolated their data to zero frequency and were able to calculate anisotropy factors which correlated with ones determined using the Morgan instrument.

The main disadvantage of the method is that the measurement and calculation procedures are quite complex. There are other limitations as well. Papadakis (27) discusses the limitations and problems associated with the employment of this technique on a paper machine.

COMPARISON OF SONIC AND MECHANICAL YOUNG'S MODULI

The measurement of Young's modulus should be independent of the testing method. With paper, however, discrepancies are found between sonic and mechanical techniques. In comparing sonic and mechanical moduli, it is important to clarify what is meant by these terms. The mechanical Young's modulus is an approximation to the real component of the complex Young's modulus, usually taken as the initial slope of a load-elongation curve. Viscoelastic effects faster than the test itself will reduce the measured modulus.

The sonic modulus, as defined by Craver and Taylor (19), is only a rough approximation to Young's modulus. Young's modulus itself can be determined

sonically by measuring both longitudinal and shear velocities. Neglecting viscoelastic effects, one would expect the sonic Young's modulus to agree well with the mechanical modulus.

The available experimental data suggest that the sonic modulus is up to 30% greater than the mechanical modulus (11,19,24,25,32). The reported discrepancies include a real Poisson effect which is typically 5-10%.

Various possibilities have been suggested to explain the remaining discrepancies between the two techniques. The techniques differ in two important ways. For sonic stress wave propagation, strain levels are very small. At the same time, the high sonic frequencies afford little time for creep or other time-dependent effects to be manifested.

Perhaps the most obvious discrepancy between mechanical and sonic measurements is seen as different dependencies on moisture content. Nissan (33) has reviewed available mechanical modulus *vs.* moisture content data from several investigations. The mechanical moduli were found to decrease exponentially at a rate consistent with Nissan's hydrogen bond theory. Sonic data (19,32,34, 35) indicate that the sonic modulus does not decrease nearly as fast. Part of this difference could be accounted for, if the in-plane Poisson ratios increased with moisture content.

Austin (32) has recently investigated the differences between sonic and mechanical Young's moduli. The machine direction of a bond paper was examined. The sonic modulus was measured at about 60 kHz using Morgan instrument transducers. In-plane Poisson ratios, also measured sonically, were used to determine a sonic Young's modulus. The mechanical Young's modulus was determined using an Instron.

After several possible causes for the observed discrepancies were investigated, it was concluded that the differences result primarily from viscoelastic effects. The slower mechanical testing method permitted stress relaxation effects to occur which reduce the measured modulus. This conclusion was supported by Instron data obtained at very high strain rates. A strain rate of 500 inches/min was realized using an optical recorder. At 15% and 50% R.H. the higher strain rate narrowed the observed discrepancy from 20 to 6%.

WAVE PROPAGATION THROUGH HETEROGENEOUS MATERIALS

For years ultrasonics has been an important tool in investigating the anisotropy of single crystals. By propagating longitudinal and shear modes in different crystalline directions, one may examine the directional properties. More recently ultrasonic techniques have been successfully employed in studying the elastic properties of many heterogeneous materials.

Early investigations in the textile industry of polymeric materials involved wave propagation through fibers and films (36,37). Later, yarn assemblies were studied. Zorowski and Murayama reported on wave propagation along continuous filament twisted yarns (38). It was found that the sonically determined modulus varied with twist angle as predicted from static extension theory, assuming a constant-volume deformation process. The reduction in modulus with increasing twist angle was attributed solely to a geometric effect. It was concluded that waves propagate through continuous filament yarns as one-dimensional longitudinal plane waves in a linear elastic medium.

Eden and Felsenthal (39), using 150 and 750 kHz ceramic transducers, studied the transmission of ultrasonic waves through packs of spherical and nonspherical particles. For glass spheres, actual transmission was detected only when suffi-

cient external pressure was applied, or when the particles cohered. The measured velocities varied with frequency.

Peck and Gurtman (40), in presenting a theoretical analysis of transient stress waves in linearly elastic laminated composites, discuss the problem of geometric dispersion. The heterogeneous structure of composite materials causes stress waves to change their shape as they propagate. This process is called geometric dispersion. For sufficiently long pulses, this effect may be small and the composite can be considered homogeneous. For sinusoidal waves geometric dispersion manifests itself in a dependence of phase velocity on frequency.

Development of composite fibrous materials containing strong uniaxial fibers in a low modulus resin has produced a class of materials which may have a tensile strength comparable with the best of the high quality steels, while having only 1/5th the density. By their very nature, these materials are highly anisotropic. The longitudinal to transverse stiffness ratio can be as great as 25:1. The simplest elastic symmetry which conforms to the properties of unidirectionally aligned composites is hexagonal. Such a medium is transversely isotropic and possesses five independent elastic constants.

Zimmer and Cost measured the hexagonal elastic constants for a unidirectional glass fiber reinforced epoxy using an ultrasonic pulse transmission technique (41). Quartz transducers were used. Specimens were cut from an original sheet such that the fibers made various angles with the specimen faces which were polished flat and parallel. It was reported that in all measurements attenuation was quite high, although the pulse waveform was relatively undistorted. Attenuation was lower at lower frequencies. An operating frequency of 5 MHz was chosen so that the wavelengths would be much greater than the fiber

diameter, thus reducing interactions which occur when the wavelength is nearly equal to the fiber diameter.

In general, Zimmer and Cost (41) found self-consistency with respect to the hexagonal wave theory. A discrepancy was found, however, in the propagation velocities of shear waves propagated in the layer plane and polarized parallel and perpendicular to the fibers. It was argued that one of the shear velocities was erroneously high due to dispersion.

Markham (42) used an immersion technique in a similar investigation of the properties of a carbon fiber-epoxy resin composite. The use of an ultrasonic immersion tank permitted measurements over a wide range of orientations for thin sheets of the composite. Markham assumes that the composite material is an elastic continuum and that the measured velocities are those relating to infinite plane waves on an unbounded medium. It is stated that the degree to which these conditions are approximated in a fiber composite depends on the magnitude of the wavelength relative to the fiber diameter and to the overall specimen dimensions. The wavelength should be large compared with the fiber diameter, but small compared with the dimensions of the specimen.

Dean and Turner (43), using the immersion pulse transmission technique developed by Markham (42), investigated various carbon fiber reinforced epoxy samples covering a range of fiber fraction. The five independent hexagonal elastic stiffness coefficients were determined. A theory of interpreting composite properties in terms of phase properties, concentration and geometry was used to analyze the experimental results. A close fit to the experimental data was obtained.

Reynolds and Wilkinson (44) surveyed studies of ultrasonic wave propagation in flat carbon fiber reinforced plastics and reported on their own work with two- and three-ply laminates and sandwich structures. Part of the earlier work included propagating longitudinal waves through uniaxial rods over the frequency range 0.5-1.25 MHz. For isotropic materials there is a sharp increase in velocity as the ratio of rod diameter to wavelength approaches unity. With the reinforced plastic the only velocity change was a slight increase at a diameter/wavelength ratio of about 0.2. The smallness of the velocity increase was attributed to the high degree of anisotropy.

Felix (45) investigated the attenuation and dispersion characteristics of various plastics in the frequency range 1-10 MHz. Little dispersion was detected for the resins tested, while significant frequency-dependent attenuation was found. Stress pulse distortion was quite significant after propagating only a few centimeters. It was concluded that the pulse distortion observed in plastic matrix composite materials may not be attributed to geometric dispersion and attenuation alone.

Finally, in a recent study (46), extruded polypropylene and polyethylene terephthalate were tested at 10 MHz using quartz transducers. The five hexagonal elastic constants were determined by propagating longitudinal and shear waves in three directions, 0°, 45°, and 90° to the extrusion direction. Anisotropy was found to be mainly due to orientation of the polymer. Pulse attenuation was high. In addition, for the 45° specimens, pulse distortion and extraneous signals were observed. These were thought to be due to diffraction and/or scattering effects, since both longitudinal and shear modes are excited. This difficulty affected only the determination of one of the stiffness coefficients.

As discussed above, ultrasonic techniques can be used to determine the elastic properties of heterogeneous materials. The validity of these techniques seems to depend strongly on the size or spacing of the heterogeneity relative to the ultrasonic wavelength employed. In general, such materials should obey the wave theories for homogeneous continuous elastic materials whenever the wavelength is much larger than the irregularities. Pulse attenuation is relatively high for heterogeneous materials. It is concluded, however, that dispersion related to pulse attenuation is negligible.

Paper differs from the other heterogeneous materials cited above in its high porosity. The mechanism of pulse propagation is not likely to be similar to that in a continuous polymeric film.

Paper consists of bonded and unbonded fibers in air. Because of the high acoustical mismatch of an air/fiber interface, direct propagation through fiber and void space in series is not possible. Instead, energy is transmitted through the solid material via stretching of intermolecular and intramolecular bonds. Fiber orientation affects the actual transmission path length (20).

With the exception of the work of Luukkala, et al. (28), all applications of ultrasonic techniques to paper have been at low frequencies, typically 10 kHz. At this frequency, longitudinal waves in paper have wavelengths which fall in the range of 10 to 40 cm. Fibers are generally less than 0.2-cm long and less than 0.002 cm in width. The large ratios of wavelength to fiber size permit paper to be considered as continuous. Consequently, wave theory for continuous elastic materials should apply to paper at these low frequencies. Longitudinal waves are expected to interact with fibers when the wavelength

approaches the fiber length, however. This corresponds to a frequency of about 1 MHz. This interaction may or may not significantly affect the velocity measurements.

THEORY OF WAVE PROPAGATION IN PAPER

ORTHOTROPIC MODEL FOR PAPER

It will be assumed that paper behaves as a continuous elastic material obeying Hooke's Law. Hooke's Law states that in an elastic solid the strain is proportional to the stress. The law applies to small strains only.

Consider a cube of material whose edges are parallel to rectangular coordinate axes. In general, there are three possible stresses acting on each face of the cube. In total there are three normal stresses (σ_{11}, σ_{22}, and σ_{33}) and six shear stresses (σ_{12}, σ_{13}, σ_{23}, σ_{21}, σ_{31}, and σ_{32}). The subscripts 1, 2, and 3 correspond to the coordinate directions X, Y, and Z, respectively. In paper, the X, Y, and Z directions correspond to the machine direction, cross-machine direction, and thickness direction, respectively. The first subscript in the stress notation indicates the direction normal to the plane of action. The second subscript indicates the direction of the stress. Under equilibrium conditions, the net force and the net moment on the cube are both zero, in which case $\sigma_{ij} = \sigma_{ji}$.

The deformation of the cube can be expressed in terms of a displacement vector field $\vec{U}(x,y,z)$. The vector $\vec{U}$ is the difference between a particle's location after deformation and its original location with respect to a fixed coordinate system. Strains are then defined in terms of the displacement vector components as follows:

$$e_{11} = \partial u_x/\partial x \tag{2}$$

$$e_{22} = \partial u_y/\partial y \tag{3}$$

$$e_{33} = \partial u_z/\partial z \tag{4}$$

$$e_{12} = e_{21} = (\partial u_x/\partial y + \partial u_y/\partial x) \tag{5}$$

$$e_{13} = e_{31} = (\partial u_x/\partial z + \partial u_z/\partial x) \tag{6}$$

$$e_{23} = e_{32} = (\partial u_y/\partial z + \partial u_z/\partial y) \tag{7}$$

When Hooke's Law is obeyed, each stress can be represented as a linear combination of the strains. It is convenient to redefine the stress components as follows:

$$\begin{aligned} \sigma_{11} &= \sigma_1 & \sigma_{23} &= \sigma_4 \\ \sigma_{22} &= \sigma_2 & \sigma_{13} &= \sigma_5 \\ \sigma_{33} &= \sigma_3 & \sigma_{12} &= \sigma_6 \end{aligned} \tag{8}$$

The strains are redefined similarly. In matrix notation, the stress components are given as follows:

$$(\sigma) = (C)(e) \tag{9}$$

The elastic stiffness matrix, C, is a 6 x 6 matrix. The elastic compliance matrix, S, is the inverse of the stiffness matrix.

With orthotropic elasticity there are three mutually perpendicular symmetry axes. It takes nine independent elastic constants to completely characterize the elastic behavior of orthotropic materials. The stiffness matrix has the following form:

$$\begin{bmatrix} \sigma_1 \\ \sigma_2 \\ \sigma_3 \\ \sigma_4 \\ \sigma_5 \\ \sigma_6 \end{bmatrix} = \begin{bmatrix} C_{11} & C_{12} & C_{13} & 0 & 0 & 0 \\ C_{12} & C_{22} & C_{23} & 0 & 0 & 0 \\ C_{13} & C_{23} & C_{33} & 0 & 0 & 0 \\ 0 & 0 & 0 & C_{44} & 0 & 0 \\ 0 & 0 & 0 & 0 & C_{55} & 0 \\ 0 & 0 & 0 & 0 & 0 & C_{66} \end{bmatrix} \begin{bmatrix} e_1 \\ e_2 \\ e_3 \\ e_4 \\ e_5 \\ e_6 \end{bmatrix} \tag{10}$$

Finally, the engineering elastic constants are given in terms of the compliance and stiffness coefficients as follows:

$$E_{11} = \frac{1}{S_{11}} = \frac{C_{11}C_{22}C_{33}+2C_{12}C_{13}C_{23}-C_{11}C_{23}^2-C_{22}C_{13}^2-C_{33}C_{12}^2}{C_{22}C_{33}-C_{23}^2} \tag{11}$$

$$E_{22} = \frac{1}{S_{22}} = \frac{C_{11}C_{22}C_{33}+2C_{12}C_{13}C_{23}-C_{11}C_{23}^2-C_{22}C_{13}^2-C_{33}C_{12}^2}{C_{11}C_{33}-C_{13}^2} \tag{12}$$

$$E_{33} = \frac{1}{S_{33}} = \frac{C_{11}C_{22}C_{33}+2C_{12}C_{13}C_{23}-C_{11}C_{23}^2-C_{22}C_{13}^2-C_{33}C_{12}^2}{C_{11}C_{22}-C_{12}^2} \tag{13}$$

$$G_{44} = \frac{1}{S_{44}} = C_{44} \tag{14}$$

$$G_{55} = \frac{1}{S_{55}} = C_{55} \tag{15}$$

$$G_{66} = \frac{1}{S_{66}} = C_{66} \tag{16}$$

$$\nu_{12} = -\frac{S_{12}}{S_{22}} = \frac{C_{12}C_{33}-C_{13}C_{23}}{C_{11}C_{33}-C_{13}^2} \tag{17}$$

$$\nu_{13} = -\frac{S_{13}}{S_{33}} = \frac{C_{13}C_{22}-C_{12}C_{23}}{C_{11}C_{22}-C_{12}^2} \tag{18}$$

$$\nu_{23} = -\frac{S_{23}}{S_{33}} = \frac{C_{23}C_{11}-C_{12}C_{13}}{C_{11}C_{22}-C_{12}^2} \tag{19}$$

$$\nu_{21} = -\frac{S_{12}}{S_{11}} = \frac{C_{12}C_{33}-C_{13}C_{23}}{C_{22}C_{33}-C_{23}^2} \tag{20}$$

$$\nu_{31} = -\frac{S_{13}}{S_{11}} = \frac{C_{13}C_{22}-C_{12}C_{23}}{C_{22}C_{33}-C_{23}^2} \tag{21}$$

$$\nu_{32} = -\frac{S_{23}}{S_{22}} = \frac{C_{23}C_{11}-C_{12}C_{13}}{C_{11}C_{33}-C_{13}^2} \tag{22}$$

The equations above apply to three-dimensional orthotropic materials. With thin materials such as paper, it is convenient to neglect all thickness direction stresses. In this way, the in-plane elastic properties of thin orthotropic materials are fully defined by four independent constants.

This approach has been used by Craver and Taylor (19,20) in their sonic investigations of paper anisotropy. Craver and Taylor relate the four planar orthotropic stiffness coefficients to four sonic velocities. Measurements of longitudinal and shear velocity were then made at various orientations in the sheet for several machine-made papers and oriented handsheets. The planar orthotropic theory was used to predict how these velocities varied with orientation. It was concluded from the close agreement of experimental data with theory that paper is orthotropic in the plane of the sheet.

Horio and Onogi (3), using the vibrating reed technique, found that Young's modulus at angle θ from the X-direction, E_θ, was given by the simple relationship:

$$1/E_\theta = \cos^2 \theta/E_{11} + \sin^2 \theta/E_{22} \tag{23}$$

This expression implies a special relationship between the planar orthotropic constants, known as Campbell's relationship (47), which effectively reduces the number of independent constants to three. Craver and Taylor's sonic data

(19,20) showed that Campbell's relationship between elastic constants was only approximately true for typical well-bonded paper (20).

Jones (8) also investigated the in-plane elastic behavior of paper, employing various mechanical measurement techniques. Shear modulus and Young's modulus were measured using a torsion pendulum and a table model Instron, respectively. Poisson ratios were determined by measuring the lateral contraction of glass beads affixed to loaded paper strips.

Jones found that the orthotropic model accurately described variations of both shear modulus and Young's modulus in the plane of the sheet. Contrary to Campbell's relationship, but as in the work of Kubat and Lindbergson (4), the shear modulus was found to vary with orientation.

It can be concluded from these two investigations, then, that the in-plane elastic properties can be accurately described using an orthotropic model.

From the limited thickness direction data available (7,9,12,13,48), it is quite evident that the thickness direction differs markedly in its elastic behavior from either in-plane direction. The simplest elastic model which would describe the elastic behavior of paper in all directions is the three-dimensional orthotropic model.

ELASTIC WAVES IN AN INFINITE ORTHOTROPIC MATERIAL

The general laws of elastic waves propagated in crystalline media are well known (49). The treatment of elastic waves in anisotropic media which follows was taken from published works of Borgnis (50) and Musgrave (51).

In infinite crystalline media, plane elastic waves can be propagated in any direction. These plane elastic waves are called bulk waves when speaking of real, finite, bulk materials. Let $\vec{U}$ be the particle displacement vector field and $\vec{K}$ the wave vector normal to planes of constant phase. The elastic wave motion is described by the following expression:

$$\vec{U} = \vec{U}_0 \exp(i(\omega t \pm \vec{K}\cdot\vec{r})) \tag{24}$$

where ω = angular frequency

t = time

$\vec{r}$ = position vector of any point in the medium

The displacement vector $\vec{U}$ has certain specified directions, which, in general, are not parallel to the wave vector $\vec{K}$. An equivalent expression is:

$$\vec{U} = \vec{U}_0 \exp \frac{2\pi i(lx+my+nz - Vt)}{\lambda} \tag{25}$$

where V = phase velocity

λ = wavelength

l,m,n = direction cosines of $\vec{K}$

The theory of wave propagation through infinite anisotropic media reveals that for any given direction of the wave vector $\vec{K}$, there are three possible displacement vectors $\vec{U}$, which are functions of the direction of $\vec{K}$. These three displacement vectors are independent of each other and form a mutually orthogonal set. These three vectors, then, belong to three independent plane waves propagated, in general, with three different velocities in the direction $\vec{K}$. If one of the three displacement vectors coincides with $\vec{K}$, it follows that the other two must lie in a plane perpendicular to $\vec{K}$. In this case, the wave-triplet consists of one purely longitudinal and two purely transverse waves.

In general, $\vec{U}$ can always be decomposed into a longitudinal and a transverse component. These components, however, are not independent of each other.

Hooke's Law for orthotropic elastic material is given as follows:

$$\sigma_1 = C_{11}\frac{\partial u_x}{\partial x} + C_{12}\frac{\partial u_y}{\partial y} + C_{13}\frac{\partial u_z}{\partial z} \tag{26}$$

$$\sigma_2 = C_{12}\frac{\partial u_x}{\partial x} + C_{22}\frac{\partial u_y}{\partial y} + C_{23}\frac{\partial u_z}{\partial z} \tag{27}$$

$$\sigma_3 = C_{13}\frac{\partial u_x}{\partial x} + C_{23}\frac{\partial u_y}{\partial y} + C_{33}\frac{\partial u_z}{\partial z} \tag{28}$$

$$\sigma_4 = C_{44}\left(\frac{\partial u_z}{\partial y} + \frac{\partial u_y}{\partial z}\right) \tag{29}$$

$$\sigma_5 = C_{55}\left(\frac{\partial u_z}{\partial x} + \frac{\partial u_x}{\partial z}\right) \tag{30}$$

$$\sigma_6 = C_{66}\left(\frac{\partial u_y}{\partial x} + \frac{\partial u_x}{\partial y}\right) \tag{31}$$

The equations of motion are:

$$\frac{\partial \sigma_1}{\partial x} + \frac{\partial \sigma_6}{\partial y} + \frac{\partial \sigma_5}{\partial z} = \rho \frac{\partial^2 u_x}{\partial t^2} \tag{32}$$

$$\frac{\partial \sigma_6}{\partial x} + \frac{\partial \sigma_2}{\partial y} + \frac{\partial \sigma_4}{\partial z} = \rho \frac{\partial^2 u_y}{\partial t^2} \tag{33}$$

$$\frac{\partial \sigma_5}{\partial x} + \frac{\partial \sigma_4}{\partial y} + \frac{\partial \sigma_3}{\partial z} = \rho \frac{\partial^2 u_z}{\partial t^2}\,, \tag{34}$$

where ρ is the material density.

Upon substitution of Equations (26)-(31) into Equations (32)-(34), a set of three simultaneous differential equations is obtained. When a plane wave

solution is sought of the form of Equation (24), then the following three equations are obtained:

$$(A-\rho V^2)u_{0x} + (D)u_{0y} + (E)u_{0z} = 0 \tag{35}$$

$$(D)u_{0x} + (B-\rho V^2)u_{0y} + (F)u_{0z} = 0 \tag{36}$$

$$(E)u_{0x} + (F)u_{0y} + (C-\rho V^2)u_{0z} = 0, \tag{37}$$

where

$$A = l^2C_{11} + m^2C_{66} + n^2C_{55} \tag{38}$$

$$B = l^2C_{66} + m^2C_{22} + n^2C_{44} \tag{39}$$

$$C = l^2C_{55} + m^2C_{44} + n^2C_{33} \tag{40}$$

$$D = lm(C_{12}+C_{66}) \tag{41}$$

$$E = nl(C_{13}+C_{55}) \tag{42}$$

$$F = mn(C_{23}+C_{44}) \tag{43}$$

The condition for nonzero solutions of $\vec{U}_0$ is:

$$\begin{vmatrix} A-\rho V^2 & D & E \\ D & B-\rho V^2 & F \\ E & F & C-\rho V^2 \end{vmatrix} = 0 \tag{44}$$

The resulting expression from Equation (44) can now be used to determine phase velocities of the three independent plane waves propagated in the direction $\vec{K}$. Equations (35)-(37) can then be used to determine the corresponding displacement vectors.

Orthotropic plane wave theory results will be represented by considering wave propagation in the X-Y plane. In this case, $n = 0$, $l^2 + m^2 = 1$. The angle

between $\vec{K}$ and the X-axis is given by $\theta = \cos^{-1}(1)$. Letting $c = \cos\theta$ and $s = \sin\theta$, Equations (38)-(43) become:

$$A = c^2C_{11} + s^2C_{66} \tag{45}$$

$$B = c^2C_{66} + s^2C_{22} \tag{46}$$

$$C = c^2C_{55} + s^2C_{44} \tag{47}$$

$$D = cs(C_{12}+C_{66}) \tag{48}$$

$$E = 0 \tag{49}$$

$$F = 0 \tag{50}$$

The roots of Equation (44) are given by the following equations:

$$(c^2C_{11}+s^2C_{66}-\rho V^2)(c^2C_{66}+s^2C_{22}-\rho V^2)-c^2s^2(C_{12}+C_{66})^2 = 0 \tag{51}$$

$$c^2C_{55} + s^2C_{44} - \rho V^2 = 0 \tag{52}$$

The three roots are given as follows:

$$\rho V_1^2 = \tfrac{1}{2}(Q+P) \tag{53}$$

$$\rho V_2^2 = \tfrac{1}{2}(Q-P) \tag{54}$$

$$\rho V_3^2 = c^2C_{55} + s^2C_{44}\ , \tag{55}$$

where

$$Q = c^2C_{11} + s^2C_{22} + C_{66} \tag{56}$$

$$P = [(c^2(C_{11}-C_{66}) + s^2(C_{66}-C_{22}))^2 + 4c^2s^2(C_{12}+C_{66})^2]^{\frac{1}{2}} \tag{57}$$

The particle displacements for the wave with velocity V_3 turn out to be perpendicular to the X-Y plane. This wave is a transverse wave, and is designated the out-of-plane shear wave.

The displacement vectors for the other two waves both lie in the X-Y plane. Let ψ be the angle between the displacement vector $\vec{U}_0$ and the X-axis. Then, from Equations (35) and (36),

$$\tan \psi_1 = (\rho V_1^2 - A)/D \tag{58}$$

$$\tan \psi_2 = (\rho V_2^2 - A)/D \tag{59}$$

It can be shown that ψ_1 and ψ_2 always differ by 90°. Usually, ψ_1 is approximately equal to θ. This implies that the wave associated with V_1 is nearly longitudinal. The velocity V_2 is then associated with an in-plane shear wave.

For propagation along the principle axes, these waves represent purely longitudinal and shear modes. In general, the normal modes in orthotropic materials are not pure. These modes can be thought of as combinations of longitudinal and shear waves, with one or the other dominant. These phenomena are illustrated in Fig. 1 for wave propagation in the X-Y plane. $\vec{K}$ gives the direction of wave propagation in each case, while $\vec{U}$ gives the direction of particle displacement. Points on the grid which are in phase with one another are indicated. It is seen that these points lie along lines. In three dimensions, there are planes of constant phase. The normal mode depicted in Fig. 1c has a small transverse component to its particle displacement vector.

There are other directions for which the vectors $\vec{U}$ and $\vec{K}$ are parallel or perpendicular. For propagation in the X-Y plane there is only one other direction. If ψ_1 in Equation (58) is set equal to θ in Equation (53), the following expression is obtained:

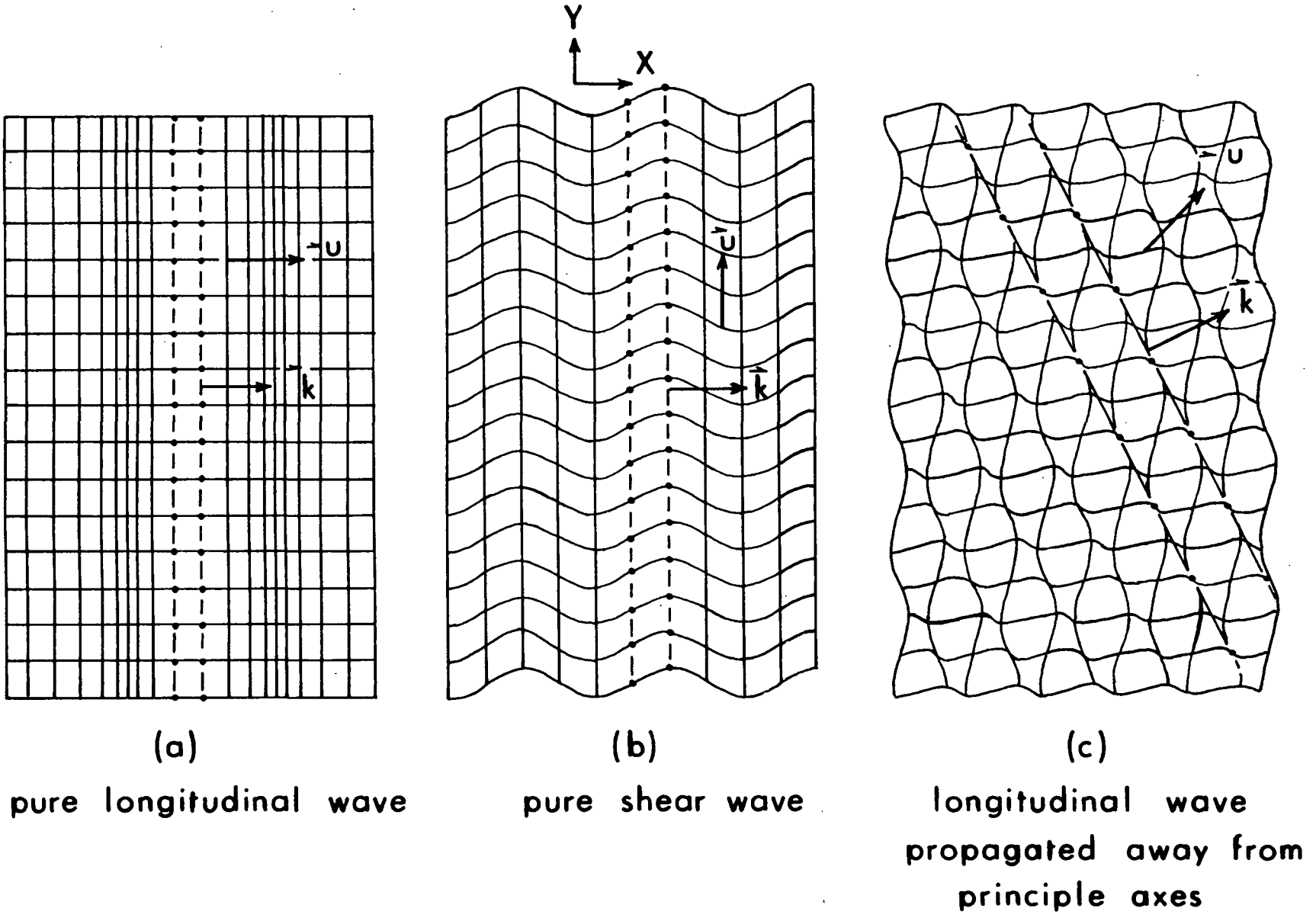

Figure 1. Wave Patterns for X-Y Plane Propagation in an Orthotropic Material

$$\tan \phi = [C_{11}+C_{12}/C_{22}+C_{12}]^{\frac{1}{2}}, \tag{60}$$

where ϕ = angle between this special direction and the X-direction.

The velocities along this direction are determined by substituting Equation (60) into Equations (53) and (54). The result of doing this is as follows:

$$\rho V_L^2 = C_{12} + C_{66} + \frac{C_{11}C_{22}-C_{12}^2}{C_{11}+C_{22}+2C_{12}} \tag{61}$$

$$\rho V_S^2 = \frac{C_{11}C_{22}-C_{12}^2}{C_{11}+C_{22}+2C_{12}} \tag{62}$$

It can be shown that $\partial/\partial\theta(\rho V_S^2)$ is zero at $\theta = \phi$. Therefore, Equation (62) gives the minimum (or maximum) shear velocity which occurs at this special angle ϕ.

In transforming the stiffness matrix for rotation in the X-Y plane, it is found that the transformed coefficient C_{36} is zero only when θ equals 0° or 90°. It follows that when $\theta = \phi$, shear wave propagation will result in a finite Z-direction normal stress. This is also true at all angles other than 0° and 90°.

Equations similar to (53)-(62) can be derived for plane wave propagation in the X-Z and Y-Z planes. In addition, more complicated expressions can be derived to predict wave propagation in directions oblique to all three orthotropic planes. In principle, by measuring a number of wave velocities using ultrasonic techniques, one can determine all nine independent orthotropic elastic constants. As pointed out by Markham (42), however, the degree to which waves propagated in real bulk materials approximate plane waves depends upon the size of the specimen relative to the wavelength.

It can be seen, then, that orthotropic plane wave theory has limited application to thin materials like paper. Only waves propagated in the thickness direction can be considered bulk waves. As such, only C_{33}, C_{44}, and C_{55} can be determined using standard techniques.

ORTHOTROPIC PLATE WAVE THEORY

In conjunction with IPC Project 3332 and this investigation, plate wave theory was developed for the orthotropic case (52). Such a development had not been found in the literature, and was needed for the treatment of wave propagation in paper.

DESCRIPTION

For bulk materials there are three normal modes of oscillation. In orthotropic materials along the principal directions, these waves represent pure modes. In all propagation directions, the wave propagation velocities are independent of frequency. Since group and phase velocities are equal in the absence of dispersion, one can measure bulk velocities using pulse propagation techniques.

For elastic wave propagation in plates, which have two boundary surfaces, two sources of complexity arise. First, multiple reflections of waves between the boundary surfaces occur. Second, mode conversion of P and SV type waves occurs. P is the designation given to the longitudinal type of bulk wave. SV refers to a shear wave which is polarized in the vertical plane, perpendicular to the plane of the plate. A third type of wave, designated SH, is a shear wave polarized in the plane of the plate.

These three types of waves are depicted in Fig. 2a and b. The SH waves are shown separately, since they do not couple with either P or SV waves upon reflection in the isotropic case. This greatly simplifies the mathematical description of isotropic plate waves. The larger arrows in Fig. 2b show the direction of particle displacement for the SV waves.

In the orthotropic case, SH waves do not couple only for propagation along the principal directions. Consequently, in order to avoid excessive mathematical complexity, consideration of plate wave propagation in orthotropic materials will be restricted to the two principal in-plane directions.

Along the principal orthotropic axes, the lowest order SH mode is nondispersive, and propagates with the velocity of the transverse bulk wave. This pure SH mode propagates while satisfying the zero stress boundary conditions. Higher order SH modes also exist (30). These modes are dispersive and will not be further considered.

Mathematical formulation of plate waves involves describing all normal plate wave modes. The desired description gives the phase velocity of the various modes as a function of the thickness, density, and elastic properties of the plate, and the frequency.

Analytical solutions to orthotropic plate wave propagation can be obtained using the method of partial waves. Solie and Auld (53) have done this for plates having cubic symmetry. In this method, plate wave solutions are constructed from the simple P, SH, and SV partial waves, which reflect back and forth between the boundaries of the plate. From this point of view, plate waves are seen as travelling waves in the propagation direction, and as standing

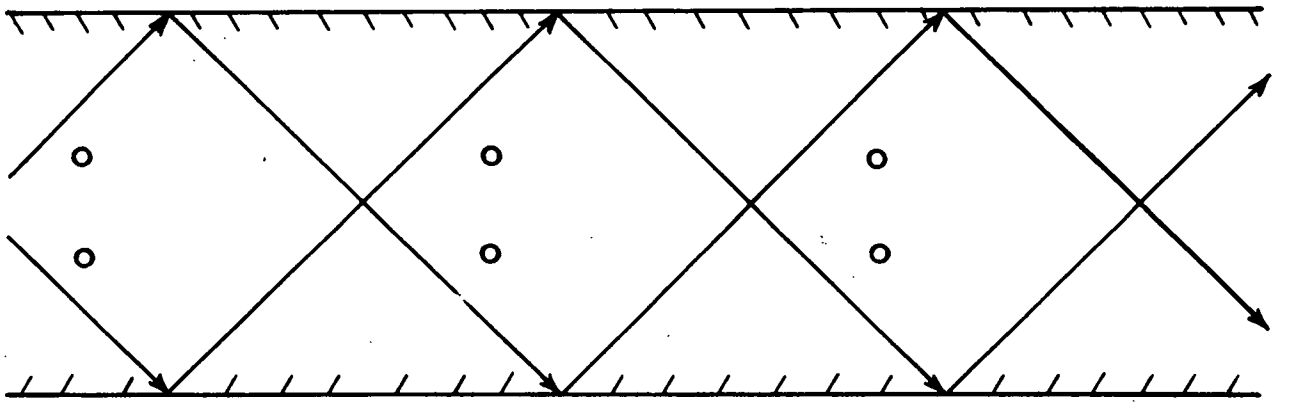

(a) SH partial waves

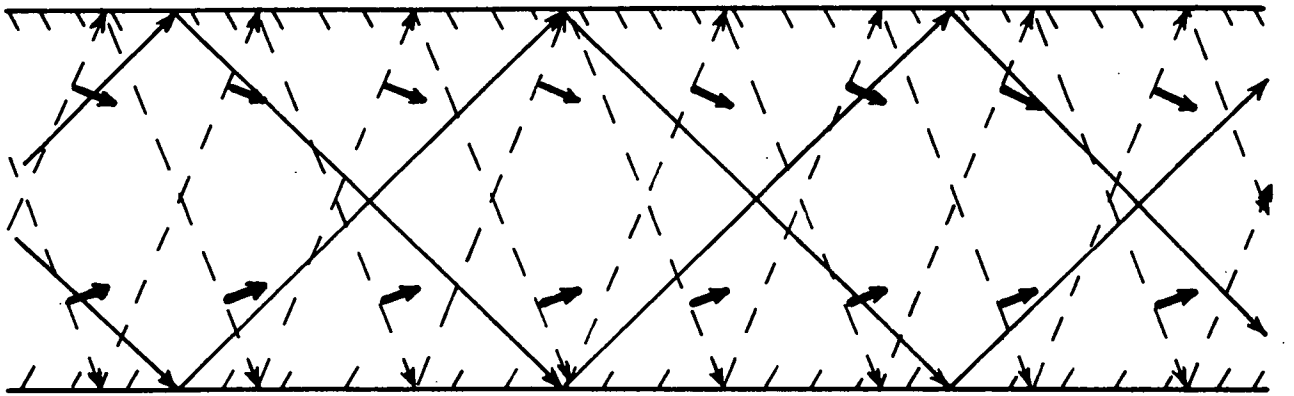

(b) SV partial waves ----
P " " ——

Figure 2. Six Partial Waves Used to Construct Plate Waves

waves in the plate thickness direction. Plate wave solutions are found by imposing the condition of zero normal and shear stresses at the plate surfaces.

A basic principle of the partial wave method is that the partial waves are coupled to each other by reflections at the plate boundaries. Every partial wave must have the same vector component in the propagation direction. This is depicted in Fig. 3 for X-direction propagation.

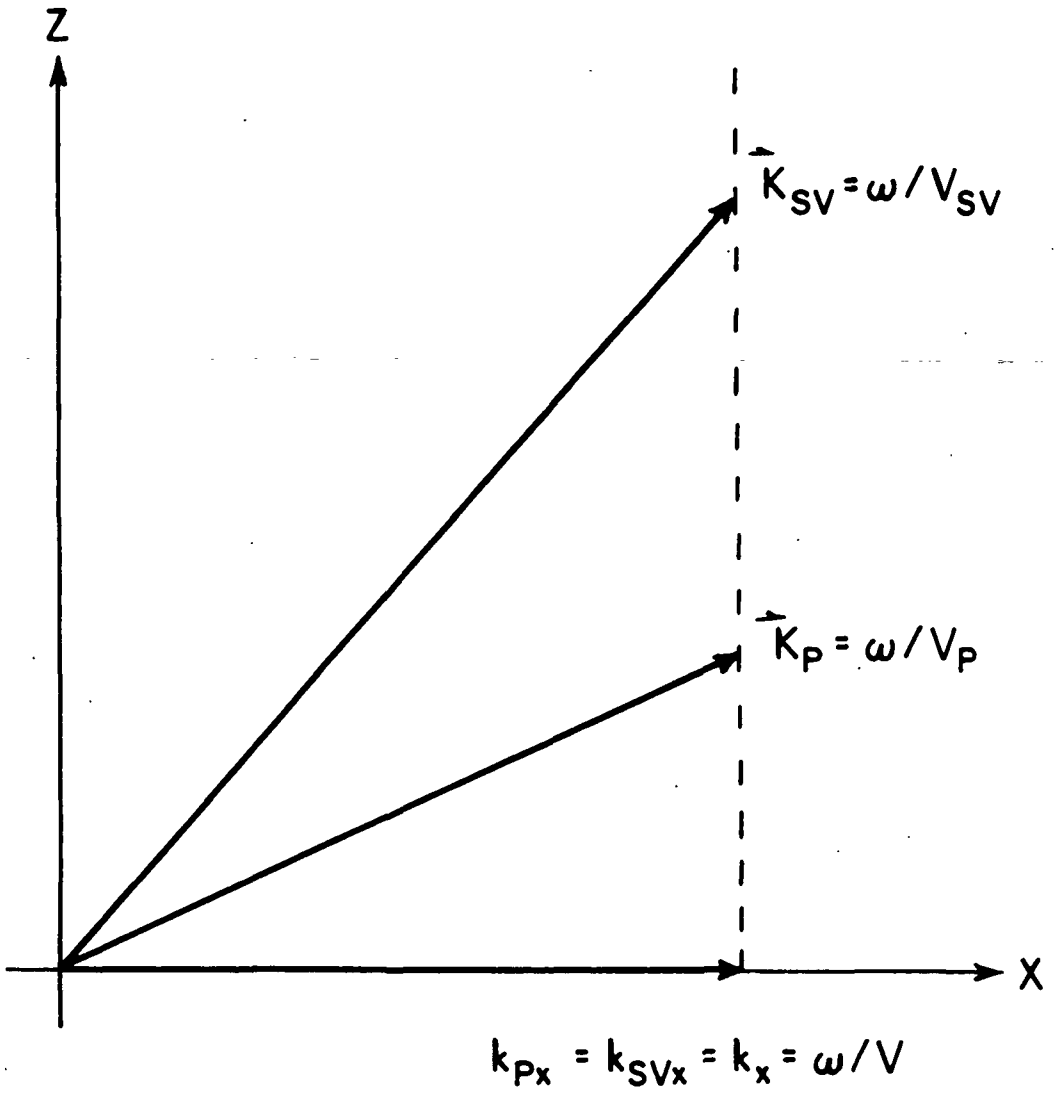

Figure 3. Wave Vectors for Longitudinal (P) and Shear (SV) Partial Waves Showing Requirement that Components of Wave Vectors in the Propagation Direction (X) be the Same

For propagation along the principal directions in orthotropic plates, the free boundaries couple the P and SV waves. In this case, a total of four partial waves, two P and two SV waves, are required to construct the normal plate wave modes. The magnitudes and directions of these bulk waves are chosen so that the free boundary conditions are met at the plate surfaces. The transverse components of the wave vectors are positive for one P and one SV wave, and negative for the other two. As is seen in Fig. 3, the slower SV wave propagates in a direction which is nearer to the plate normal (Z-direction).

As frequency is changed, corresponding changes in the direction and magnitude of the partial waves are required in order to satisfy the boundary conditions. This gives rise to the dispersive character of plate wave modes. A set of dispersion curves can be constructed which depicts the dependency of phase velocity on frequency for the various plate modes. Plate waves can be described as either symmetric or antisymmetric modes, depending on the symmetry about the midplane of the particle displacements along the direction of propagation.

THEORETICAL DEVELOPMENT

In the following analysis the discussion is limited to the X-Z plane. Plate wave propagation is in the X-direction. Results for Y-direction propagation can be obtained by changing the appropriate elastic constants.

The equations of motion for mechanical disturbances have been presented in Equations (32)-(34). In order to construct plate waves in the principal direction, it is necessary to first find plane wave solutions to Equations (32)-(34). For bulk waves propagating in the X-Z plane, u_y and all derivatives

with respect to y must be zero. Using Equations (26)-(31) to express the stress components in terms of the displacements, Equations (32) and (34) become:

$$\rho \frac{\partial^2 u_x}{\partial t^2} = C_{11}\frac{\partial^2 u_x}{\partial x^2} + C_{13}\frac{\partial^2 u_z}{\partial x \partial z} + C_{55}\left(\frac{\partial^2 u_x}{\partial z^2} + \frac{\partial^2 u_z}{\partial x \partial z}\right) \tag{63}$$

$$\rho \frac{\partial^2 u_z}{\partial t^2} = C_{33}\frac{\partial^2 u_z}{\partial z^2} + C_{13}\frac{\partial^2 u_x}{\partial z \partial x} + C_{55}\left(\frac{\partial^2 u_x}{\partial x \partial z} + \frac{\partial^2 u_z}{\partial x^2}\right) \tag{64}$$

Requiring that the solutions represent plane waves means that

$$u_x = u_{0x} \exp(i(k_x x + k_z z - \omega t)) \tag{65}$$

$$u_z = u_{0z} \exp(i(k_x x + k_z z - \omega t)) \tag{66}$$

Equations (63) and (64) then become:

$$\rho u_{0x}\omega^2 = C_{11}u_{0x}k_x^2 + (C_{13}+C_{55})u_{0z}k_x k_z + C_{55}u_{0x}k_z^2 \tag{67}$$

$$\rho u_{0z}\omega^2 = C_{55}u_{0z}k_x^2 + (C_{13}+C_{55})u_{0x}k_x k_z + C_{33}u_{0z}k_z^2 \tag{68}$$

Eliminating u_{0x} and u_{0z}, it is found that k_z^2 must satisfy the following quadratic equation:

$$(C_{13}+C_{55})^2 k_x^2 k_z^2 = (\rho\omega^2 - C_{11}k_x^2 - C_{55}k_z^2)(\rho\omega^2 - C_{55}k_x^2 - C_{33}k_z^2) \tag{69}$$

Given a value of k_z, u_{0z}/u_{0x} can be determined as follows:

$$u_{0z}/u_{0x} = (\rho\omega^2 - C_{11}k_x^2 - C_{55}k_z^2)/(C_{13}+C_{55})k_x k_z \tag{70}$$

For $k_x^2 = 0$, Equation (69) permits two possible values of k_z^2. One of these is $k_z^2 = \omega^2/C_{33}$. For this value of k_z^2, u_{0z}/u_{0x} is found from Equation (70) to be infinity. This is a longitudinal wave travelling in the Z-direction with velocity $V = (C_{33}/\rho)^{\frac{1}{2}}$. The other solution is a transverse wave in the Z-direction with velocity $V = (C_{55}/\rho)^{\frac{1}{2}}$. If $k_z^2 = 0$, Equation (69) yields two

other solutions. These are longitudinal and transverse waves in the X-direction. It is seen, then, that orthotropic bulk waves travelling in the principal directions are like isotropic bulk waves for which particle displacements are always either parallel or normal to the propagation direction.

For waves oriented at an angle to the principal axes ($k_x \neq 0$, $k_z \neq 0$) the polarizations of the two wave solutions are neither normal nor parallel to the direction of travel. In this more general case, the two solutions of k_z^2 from Equation (69) are given as follows:

$$k_{z\pm}^2 = k_x^2(-B\pm(B^2-4D)^{\frac{1}{2}})/2 \tag{71}$$

where

$$B = (-\rho V^2(C_{33}+C_{55})-C_{13}(C_{13}+2C_{55})+C_{11}C_{33})/C_{33}C_{55} \tag{72}$$

$$D = (\rho V^2-C_{55})(\rho V^2-C_{11})/C_{33}C_{55} \tag{73}$$

$$V = \omega/k_x \tag{74}$$

For a given frequency, ω, and component of the wave vector in the X-direction, k_x, Equation (71) establishes the four possible values of k_z for orthotropic bulk waves. Equation (70) can then be used to find the polarization of the disturbance. These waves are nondispersive, but the velocity and the angle between the wave vector and the polarization depend on the direction of propagation.

Plate waves will now be constructed from combinations of these bulk (partial) waves. The X-direction plate modes must be plane waves along the machine direction. As shown above, for any X-direction component of the wave vector, there are four bulk plane waves. Since any combination of these four bulk waves is a plane wave in the X-direction, sums of these bulk waves are

sought which meet the free boundary conditions. It will turn out that solutions exist only for certain combinations of ω and k_x. Since the plate velocity is equal to ω/k_x, dispersion curves relating frequency to velocity can then be constructed from the permissible combinations of V and k_x.

The $z = 0$ plane is taken to be at the center of the plate. The plate, of thickness T, has boundaries at $z = \pm T/2$.

The possible plate wave solutions have the following form:

$$u_x = e^{i(k_x x-\omega t)}(Me^{ik_{z+}z}+Ne^{-ik_{z+}z}+Pe^{ik_{z-}z}+Qe^{-ik_{z-}z}) \tag{75}$$

$$u_z = e^{i(k_x x-\omega t)}(\tan\psi_+(Me^{ik_{z+}z}-Ne^{-ik_{z+}z}) + \tan\psi_-(Pe^{ik_{z-}z}-Qe^{-ik_{z-}z})), \tag{76}$$

where $\tan\psi_+$ and $\tan\psi_-$ are defined as the values of u_{0z}/u_{0x} when $k_{z\pm}$ are inserted into Equation (70).

The boundary conditions which must be met at $z = \pm T/2$ are as follows:

$$\sigma_3 = C_{33}\frac{\partial u_z}{\partial z} + C_{13}\frac{\partial u_x}{\partial x} = 0 \tag{77}$$

$$\sigma_5 = C_{55}\left(\frac{\partial u_z}{\partial x} + \frac{\partial u_x}{\partial z}\right) = 0 \tag{78}$$

Substituting u_x and u_z from Equations (75) and (76) into Equations (77) and (78), imposes the following four conditions on M, N, P, and Q:

$$\begin{bmatrix} G_+e^{\frac{1}{2}ik_{z+}T} + G_+e^{-\frac{1}{2}ik_{z+}T} + G_-e^{\frac{1}{2}ik_{z-}T} + G_-e^{-\frac{1}{2}ik_{z-}T} \\ G_+e^{-\frac{1}{2}ik_{z+}T} + G_+e^{\frac{1}{2}ik_{z+}T} + G_-e^{-\frac{1}{2}ik_{z-}T} + G_-e^{\frac{1}{2}ik_{z-}T} \\ H_+e^{\frac{1}{2}ik_{z+}T} - H_+e^{-\frac{1}{2}ik_{z+}T} + H_-e^{\frac{1}{2}ik_{z-}T} - H_-e^{-\frac{1}{2}ik_{z-}T} \\ H_+e^{-\frac{1}{2}ik_{z+}T} - H_+e^{\frac{1}{2}ik_{z+}T} + H_-e^{-\frac{1}{2}ik_{z-}T} - H_-e^{\frac{1}{2}ik_{z-}T} \end{bmatrix} \begin{bmatrix} M \\ N \\ P \\ Q \end{bmatrix} = 0 \tag{79}$$

where
$$G_{\pm} = C_{33}k_{z\pm}\tan\psi_{\pm} + C_{13}k_x \tag{80}$$
$$H_{\pm} = k_{z\pm} + k_x \tan\psi_{\pm} \tag{81}$$

There are nonzero solutions for $\vec{U}$ only if the determinant of the matrix in Equation (79) is zero. This requirement reduces to:

$$[\tan(\tfrac{1}{2}k_{z+}T)/\tan(\tfrac{1}{2}k_{z-}T)] = [H_-G_+/H_+G_-]^{\pm 1} \tag{82}$$

When Equations (70)-(73) are used to eliminate $\tan\psi_{\pm}$ and $k_{z\pm}$, Equation (82) becomes a relationship between ω and V that must be satisfied if a plate wave is to exist. This equation is the orthotropic plate wave dispersion equation. This equation can be put into the following alternative form:

$$\left[\frac{\tan(\tfrac{1}{2}\sqrt{Z}_+k_xT}{\tan(\tfrac{1}{2}\sqrt{Z}_-k_xT}\right]^{\pm 1} = \frac{\sqrt{Z}_+}{\sqrt{Z}_-}\left[\frac{a+bZ_-}{a+bZ_+}\right]\left[\frac{c-dZ_+}{c-dZ_-}\right], \tag{83}$$

where
$$Z_+ = k_{z+}^2/k_x^2$$
$$Z_- = k_{z-}^2/k_x^2$$
$$a = \rho V^2 - C_{11}$$
$$b = C_{13}$$
$$c = a + C_{13}(C_{13}+C_{55})/C_{33}$$
$$d = C_{55}$$

One can find the particle motion of a particular mode by choosing values of ω and V that satisfy Equation (82), finding M, N, P, and Q from Equation (79), and then substituting into Equations (75) and (76) to find $\vec{U}$ as a function of x, z, and t (time). The plate wave solutions to Equation (82) can be classified by the symmetry of motion in the sheet direction. The plate waves corresponding to the +1 exponent in Equations (82) and (83) are called symmetric modes.

The antisymmetric modes are those with a -1 exponent. For symmetric modes M = N, and P = Q, while antisymmetric modes have M = -N and P = -Q.

Equation (83) is transcendental, and therefore solutions must be found with numerical techniques. The wave vector components depend, for a given material, on phase velocity and frequency. However, the wave vector components for both directions are proportional to frequency. Hence, Z_+ and Z_-, which are given in terms of the ratios of these components, are independent of frequency.

This fact can be used to simplify the numerical determination of solutions to Equation (83). A computer program has been written to do this. A listing of the program is presented in Appendix I, along with an explanation of the parameters. Generally, the program is capable of finding all solutions of Equation (83) over a given frequency range and for any given phase velocity.

A set of dispersion curves is shown in Fig. 4. These are for an orthotropic plate 0.679-mm thick. The X to Z-direction stiffness ratio is 2:1. Each mode is identified by a letter, A or S, indicating either a symmetric or antisymmetric mode, and by a number indicating the order of the mode. It is seen that all modes tend to approach a common velocity at high frequencies. Theory predicts that this is indeed the case, with the limiting velocity being that of a Rayleigh wave. A Rayleigh wave is a surface wave which propagates along the surface of a semiinfinite material. At higher and higher frequencies plate wave motion becomes more and more localized at the plate surfaces, the condition for surface wave propagation.

A second computer program, listed and described in Appendix II, has been written for the purpose of graphically representing the plate deformations.

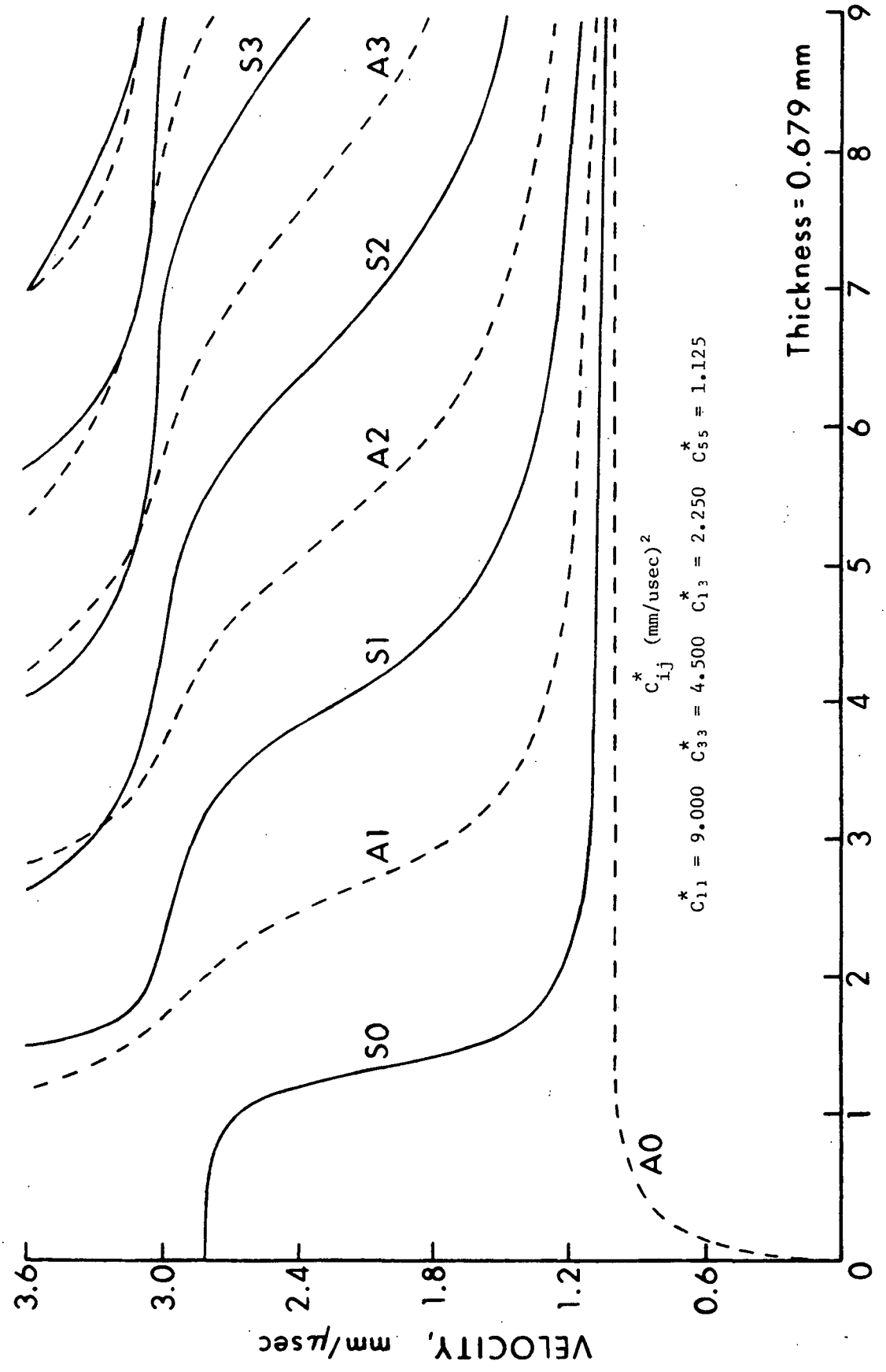

Figure 4. Theoretical Dispersion Curves for an Orthotropic Plate

The program computes particle displacements, u_x and u_z, for any mode at any frequency.

LOW FREQUENCY SYMMETRIC MODE

At low frequencies the zeroth order symmetric mode is nondispersive. A plateau region exists for which phase velocity is essentially independent of frequency. This plateau region is evident in Fig. 4. This plateau region has been expanded in Fig. 5. It is seen here that the SO mode is very flat up to at least 900 kHz. It is also seen that the AO curve begins to level off at about this frequency.

The limiting velocity at zero frequency can be related to the orthotropic stiffness coefficients by using Equation (83). The left side of Equation (83) approaches:

$$\tfrac{1}{2}\sqrt{Z}_+ k_x T / \tfrac{1}{2}\sqrt{Z}_- k_x T = \sqrt{Z}_+ / \sqrt{Z}_- \tag{84}$$

as $k_x = 2\pi f/V$ approaches zero, where f is the frequency. At zero frequency, then, Equation (83) becomes:

$$(a+bZ_+)(c-dZ_-) = (a+bZ_-)(c-dZ_+) \tag{85}$$

The next step is to expand Equation (85) in terms of the C_{ij}'s, ρ, and V. After considerable algebraic manipulation, the following simplification is obtained:

$$\rho V_{SOx}^2 = C_{11} - C_{13}^2/C_{33} \tag{86}$$

where V_{SOx} = SO velocity in the limit of zero frequency for propagation in the X-direction. In terms of the engineering constants, Equation (86) has the following form:

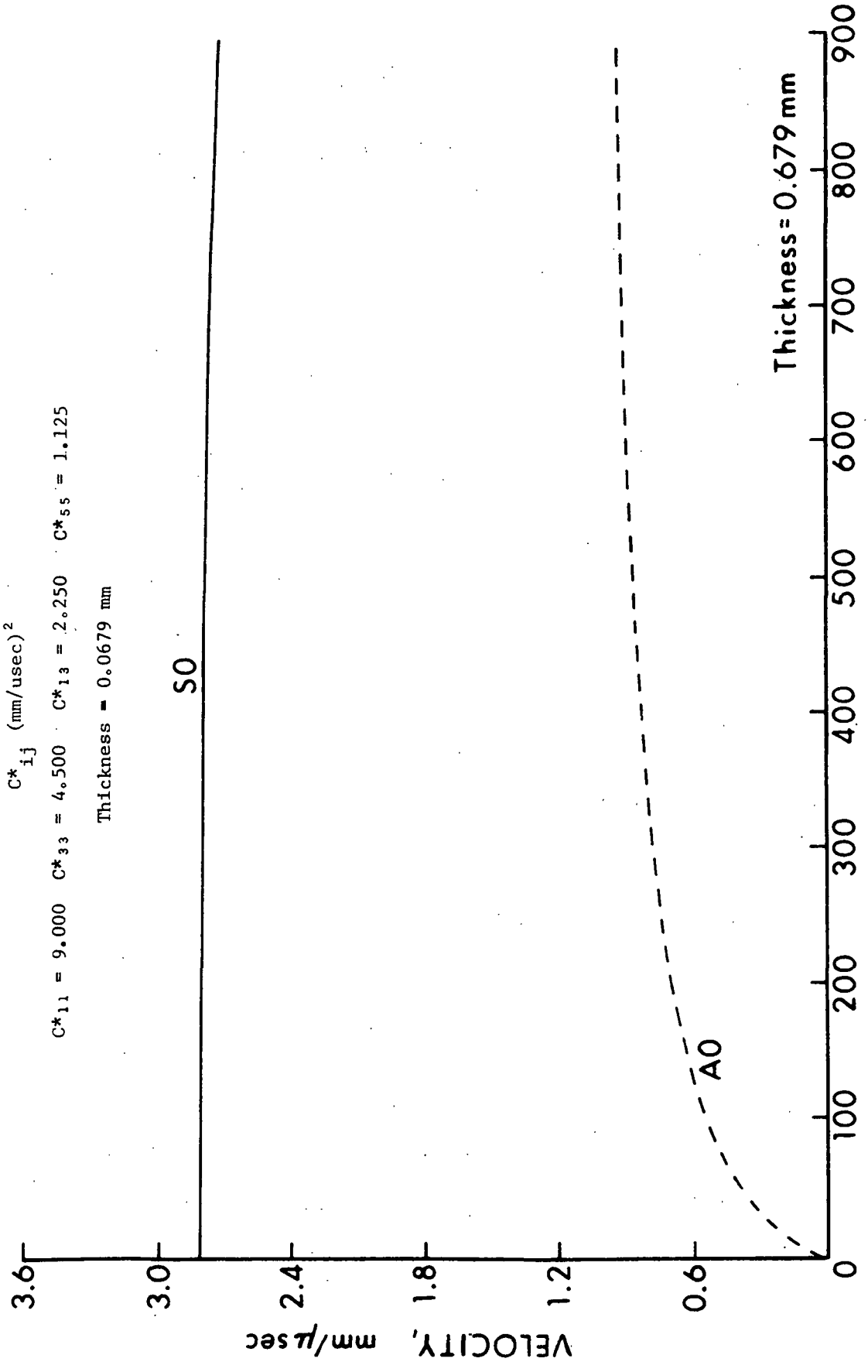

Figure 5. Theoretical Dispersion Curves for an Orthotropic Plate Showing Nondispersive Low Frequency Region for the S0 Mode

$$\rho V^2_{SOx} = E_{11}/(1-\nu_{12}\nu_{21}) \tag{87}$$

Since Equation (87) involves only in-plane elastic constants, the low frequency zeroth order symmetric mode velocity, V_{SOx}, does not depend directly on Z-direction properties. Upon examination of Equations (75) and (76), it is found that as f approaches zero, $u_z(max)/u_x(max)$ approaches zero. In the limit, then, there is no Z-direction motion and the wave velocity should not depend on Z-direction properties.

Paper is sometimes treated as a planar material. This means that Z-direction stresses are assumed to be zero and Z-direction motion is ignored. In this case, it is easily shown that the longitudinal velocity is also given by Equation (87). Therefore, in the limit of zero frequency, the planar assumption is valid and is expected to provide the correct velocity. As the frequency increases, however, Z-direction motion begins and the plate mode becomes dispersive.

Treating orthotropic materials as planar materials reduces the number of elastic constants from 9 to 4. While compliance coefficients and engineering constants remain numerically unchanged, in this case, the assumption of zero Z-direction stresses will necessitate redefining the stiffness coefficients. The numerical difference in the stiffness coefficients in the two cases can be understood by recalling how C_{11} is determined. The coefficient C_{11} is determined by straining the plate in the X-direction while preventing Y and Z-direction displacements. The restraint on the plate effectively increases its stiffness in the X-direction depending upon the Z-direction properties. The zero stress assumption essentially removes the restraint, with a resulting decrease in stiffness.

The four planar stiffness coefficients, denoted by primes, are given in terms of the three-dimensional constants as follows:

$$C'_{11} = C_{11} - C_{13}^2/C_{33} \tag{88}$$

$$C'_{22} = C_{22} - C_{23}^2/C_{33} \tag{89}$$

$$C'_{12} = C_{12} - C_{13}C_{23}/C_{33} \tag{90}$$

$$C'_{66} = C_{66} \tag{91}$$

Equation (86) can then be written as follows:

$$\rho V_{S0x}^2 = C'_{11} \tag{92}$$

This equation, giving the low frequency limit to the zeroth order symmetric mode velocity, is simply Equation (53) for $\theta = 0°$ with planar constants substituted for bulk constants. It is found, then, that the equation for bulk longitudinal waves is valid for planar materials when the planar constants are substituted for the bulk constants. Of course, these equations will be approximate except in the limit as frequency goes to zero. Since $C'_{11} \neq C_{11}$, the low frequency longitudinal velocity in the planar case will differ from the longitudinal bulk velocity by some small amount.

In the case of shear wave propagation in the X-Y plane, there will be no velocity difference between the planar and bulk materials when $\theta = 0°$ or $90°$. This is because $C'_{66} = C_{66}$. Consequently, the bulk shear modulus C_{66} can be measured on thin specimens by propagating shear waves along the X or Y-directions.

The bulk and planar shear velocities will differ, however, for propagation in the X-Y plane which is not along either principal axis. Equation (54) gives these shear velocities as a function of angle, θ. Again, bulk or planar shear velocities are obtained by using bulk or planar stiffness coefficients,

respectively. The inequality of these two velocities away from the principal axes can be appreciated by recalling that shear wave propagation in the X-Y plane of a bulk orthotropic material will result in a finite Z-direction normal stress for all angles except 0° and 90°. In the planar case, this Z-direction stress vanishes, and it follows that the shear wave velocity must be different.

BULK LONGITUDINAL VELOCITY

In a later section, the propagation of plate waves through single thicknesses of paper at the bulk velocity will be discussed. In order to propagate these waves, it will be necessary to predict the frequencies for which the symmetric modes have plate wave velocity equal to the bulk longitudinal velocity. For X-direction propagation the bulk longitudinal velocity is given by:

$$V = (C_{11}/\rho)^{\frac{1}{2}} \tag{93}$$

When this relationship is substituted into Equations (72) and (73), it is seen from Equation (71) that k_{z-}^2 becomes zero. It can also be demonstrated that for plate wave velocities greater than the bulk longitudinal velocity, both k_{z+}^2 and k_{z-}^2 are positive. In a region below the bulk velocity, k_{z+}^2 remains positive, while k_{z-}^2 becomes negative. Eventually, k_{z+}^2 becomes negative as well.

For symmetric modes, Equation (83) has the following form:

$$\tan(\tfrac{1}{2}Yk_xT) = \left[\frac{Y(c-dY^2)}{a+bY^2}\right]\left[\frac{a+bX^2}{c-dX^2}\right]\left[\frac{\tan(\tfrac{1}{2}Xk_xT)}{X}\right], \tag{94}$$

where $Y = Z_+$

$X = Z_-$

$a = \rho V^2 - C_{11}$

$b = C_{13}$

$c = \rho V^2 - C_{11} + C_{13}(C_{13}+C_{55})/C_{33}$

$d = C_{55}$

Now, when $V = (C_{11}/\rho)^{\frac{1}{2}}$, $X = 0$, but $Y > 0$. Therefore, in the limit as X approaches 0,

$$\lim_{X \to 0} \tan(\tfrac{1}{2}Yk_xT) = \left[\frac{C_{13}+C_{55}-C_{55}Y}{C_{33}Y \quad C_{13}}\right]\left[\frac{0}{C_{13}(C_{13}+C_{55})/C_{33}}\right]\left[\lim_{X\to 0} \frac{\tan(\tfrac{1}{2}Xk_xT)}{X}\right] \tag{95}$$

Since

$$\lim_{X\to 0} \frac{\tan(\tfrac{1}{2}Xk_xT)}{X} = \frac{(\sec^2\tfrac{1}{2}Xk_xT)\,(X\,\partial k_x/\partial x + k_x)T/2}{1}\bigg|_{X=0} = \tfrac{1}{2}k_xT \neq 0 \tag{96}$$

it is seen that

$$\lim_{X\to 0} \tan(\tfrac{1}{2}Yk_xT) = 0 \tag{97}$$

Therefore, the following must be true:

$$\tfrac{1}{2}Yk_xT\,\Big|_{X=0} = \sqrt{Z}_+ \frac{2\pi fT/2}{V}\Big|_{X=0} = \sqrt{Z}_+\Big|_{X=0} \frac{\pi\, ft}{\sqrt{C_{11}}} = n\pi \tag{98}$$

or

$$f_n = \frac{\sqrt{C_{11}}}{T}\frac{n}{\sqrt{Z}_+\;\;X=0} = n\frac{\sqrt{C_{11}}}{T}\left[\frac{C_{33}C_{55}}{C_{13}(C_{13}+2C_{55})+C_{11}C_{55}}\right]^{\frac{1}{2}} \tag{99}$$

$$= n\frac{V_{Lz}}{T}\left[\frac{1}{\frac{1 + C_{13}(C_{13}+2C_{55})}{C_{11}C_{55}}}\right]^{\frac{1}{2}} \qquad (100)$$

where f_n = crossover frequency of the nth symmetric mode

V_{Lz} = bulk longitudinal velocity in the Z-direction

Now, since T is the plate thickness, V_{Lz}/T is the reciprocal of the transit time of a longitudinal wave propagated through the plate.

APPLICABILITY OF WAVE PROPAGATION THEORIES: EXPERIMENTAL ASPECTS

The primary objective of this thesis is to test the validity of wave propagation theories as applied to paper. In particular, orthotropic wave theories are to be tested, since it is known that the elastic properties of machine-made paper differ along each of the three principle axes. The main consideration here is whether or not wave theories developed for continuous homogeneous materials apply to fibrous networks which contain more or less discrete elements in a porous heterogeneous structure.

A useful approach commonly adopted in such investigations is to make more than a sufficient number of ultrasonic velocity measurements and to then analyze the velocity data, using the assumed theory, for self-consistency. A different approach will be used in this investigation.

Paper will first be treated as a bulk material. Bulk velocity measurements will be made and some of the stiffness coefficients will be determined. These coefficients will then be used to predict theoretical plate wave dispersion curves. Finally, actual plate wave velocities in dispersive regions will be measured, and compared with the theoretical predictions. Close agreement

between theoretical and experimental data will constitute sufficient proof that the wave theories for bulk and plate waves are valid for paper.

It was first necessary to investigate the propagation of waves through paper in some detail. Much of this work consisted of developing techniques for measuring various bulk and plate wave velocities.

SAMPLE DESCRIPTION

The main part of the experimental work was conducted with four board samples. Much of the early developmental work was done with chipboard. The main advantage of using chipboard was its immediate availability. The chipboard was homogeneous throughout its thickness, but was made from a heterogeneous fiber furnish. Chipboard results will not be reported below in much detail.

Thick samples were selected for two basic reasons. First, thick sheets simplify the construction of three-dimensional paper specimens. Second, the thicker samples will permit more of the plate wave dispersion curves to be detected.

The other three board samples, made on fourdrinier machines using kraft pulp, consisted of two unbleached linerboards and a fully bleached milk carton stock. The milk carton stock was supplied by Champion Papers, and was made on a single headbox machine. The milk carton stock had an average basis weight of 107.8 lb/1000 ft^2. Data for the two linerboard samples, supplied by the manufacturers, are presented in Table I. Both linerboards were made on double headbox machines.

SEM photomicrographs were taken for these three board samples. These are presented in Appendix III. A pronounced difference between felt and wire sides is observed for both linerboard samples. The wire side is more open and the

fibers show a high degree of orientation in the machine direction. Fibers on the felt side appear better bonded and do not exhibit any preferred orientation. A pronounced two-sidedness is not observed with the milk carton stock. A small amount of filler material is apparent. The edge view shows a much denser structure relative to the linerboard samples.

TABLE I

DATA FOR TWO LINERBOARD SAMPLES

Sample	#1	#2
Manufacturer	MacMillan Bloedel	Union Camp
Average basis weight (lbs/1000 ft^2)	87.3	88.4
Top layer		
% by weight	20	20
Kappa number	75	
C.S.F. (mL)	400	300
Furnish	90% pine	70% pine
	10% hardwood	30% hardwood
Bottom layer		
% by weight	80	80
Kappa number	85	
C.S.F. (mL)	650	650
Furnish	90% pine	65% pine
	10% hardwood	10% hardwood
		25% waste

The two linerboard samples were received in web form and immediately cut up into 14 inch by 28 inch specimens. These specimens were then placed under constant conditions of 73°F and 50% RH.

The milk carton stock was received as 14 inch by 28 inch specimens. These were placed in a low humidity environment (about 22% RH) for 48 hours before being placed in a 73°F, 50% RH environment.

Most of the measurements, including all of the velocity measurements, were made at 73°F and 50% RH. Transport of specimens between conditioned rooms was accomplished with the samples in air-tight polyethylene bags.

The average thickness of each sample was determined using a Schopper micrometer. About 40 thickness measurements were made for each sample. The micrometer was calibrated according to TAPPI Standard 411. These results appear in Table II.

TABLE II

AVERAGE BASIS WEIGHT, THICKNESS, AND DENSITY FOR THREE BOARD SAMPLES

	90 lb. Linerboard		Milk Carton
	No. 1	No. 2	Stock
Basis weight (g/cm^2)	0.0426	0.0432	0.0526
Apparent thickness (mm)	0.682	0.625	0.679
Apparent density (g/cm^3)	0.625	0.691	0.775

PRELIMINARY INVESTIGATIONS

MORGAN INSTRUMENT

The initial experimental work was with the Morgan Dynamic Modulus Tester. The main purposes for this work were to become acquainted with low frequency wave propagation in paper in general, and with the Morgan instrument in particular.

During this time the only auxiliary equipment used in conjunction with the self-contained Morgan instrument was an oscilloscope. With this set-up the basic operation of the instrument was ascertained. A high voltage triangular-shaped pulse of approximately 300 μsec duration and 60 Hz repetition rate is fed to the sending transducer. The electrical pulse is such as to cause the ceramic transducer to resonate at about 10 kHz. These oscillations attenuate rapidly between pulses.

The sending transducer probe rests on the paper and displaces in a direction parallel to the plane of the sheet. The receiving transducer is oriented along or perpendicular to this direction for longitudinal or shear wave propagation, respectively. The receiving transducer converts particle motion back to an electrical signal and in this way senses the propagated pulse. When the transducers are positioned far from the sheet edges, reflections which arrive at the receiving transducer will be attenuated and delayed in time. This is seldom a problem since only the very first portion of the received signal is used to determine pulse transit times.

The circuitry of the Morgan instrument determines transit time using an internal counter. The start pulse is coincident with the high voltage triangular pulse. A separate circuit provides the stop pulse by triggering on the initial slope of the received signal. The trigger voltage level is set by the operator. A small systematic error results from this method whenever the initial slope changes with transducer separation distance. This error should be less than 1%.

The Morgan instrument employed, Model PPM-5, was equipped with a chart recorder which would continuously display the total pulse delay time. The variability in the recorder reading was very large, and was attributed to both

the recorder and the paper. Variations of elastic properties within the sheet were found to be quite large. Consequently, accurate characterization of a particular sheet required a large number of transit time measurements over a large area. The overall accuracy of the velocity measurement has been estimated to be about ±1%.

In general, the dry, essentially point contact that the transducers make with the paper was found to be quite efficient. It was also found that the backing material onto which the paper is placed has no significant effect on the received signal.

MEASUREMENT SYSTEM

It was apparent at the outset that the Morgan instrument would not be suitable for measuring wave velocities at other than these low frequencies. A more versatile measuring system was therefore sought. The initial intent was to make velocity measurements on paper at higher frequencies where attenuation would be high and where the waves might be dispersive.

In highly dispersive or attenuating materials the echo or pulse overlap techniques (14,16,17,54) may be impractical due to pulse distortion or an inability to observe echos. In addition, the pulse echo technique is applicable only at frequencies sufficiently high that the width of the pulse can be made small compared to the transit time through the sample.

The pulse through-transmission technique may be used on highly dispersive and attenuating materials by measuring the time of flight of a pulse on a single pass through the specimen. The measuring system depicted in Fig. 6 was eventually assembled, and the pulse through-transmission technique was used exclusively.

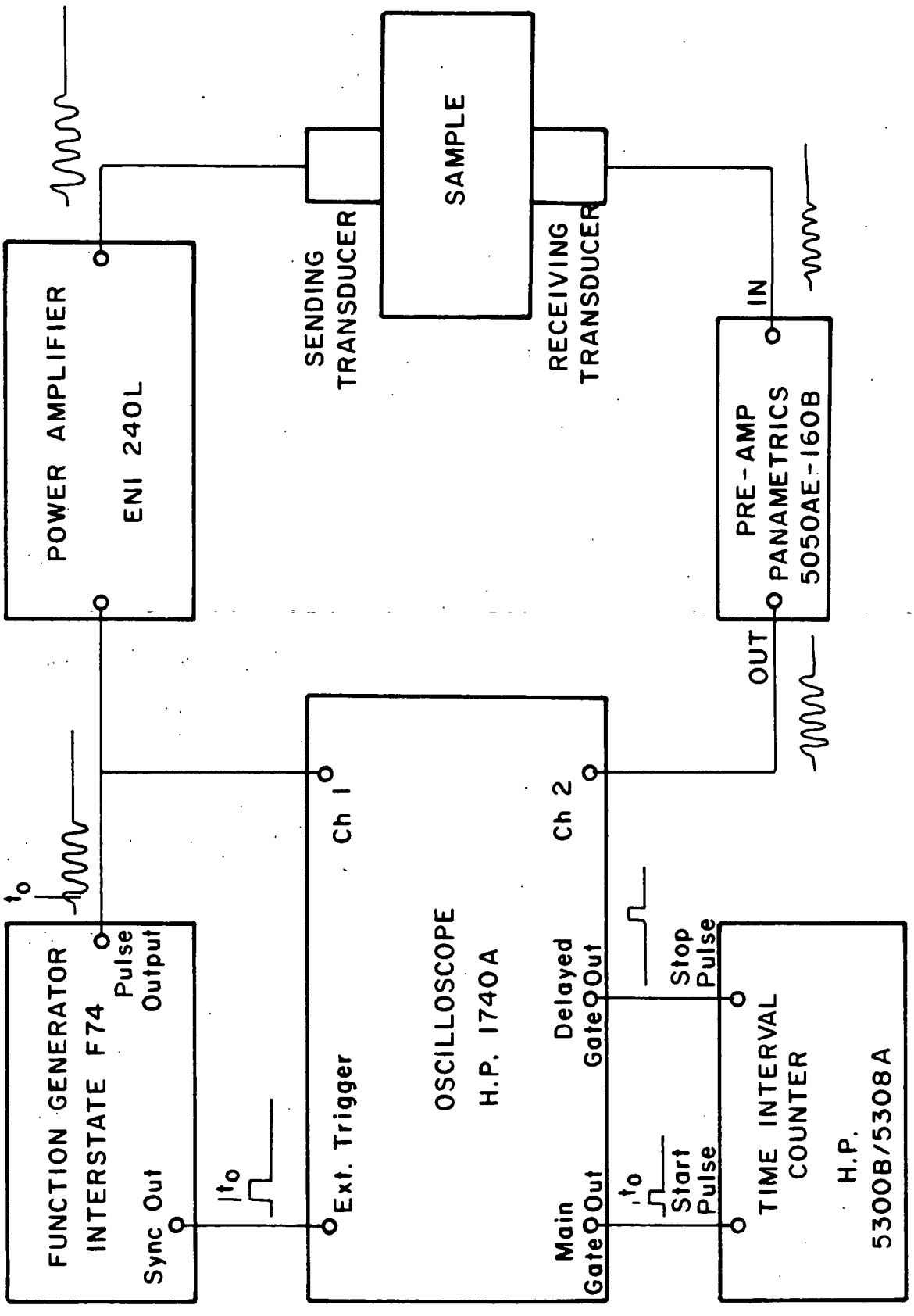

Figure 6. System for Making Through-transmission Velocity Measurements

Appreciable versatility was designed into this system. For instance, the function generator is capable of producing both continuous waves and pulses of varying width and repetition rate. The direct current to 20 MHz generator can produce bursts of sine waves, particularly useful in the through-transmission technique, and can also sweep frequency while in the continuous wave mode of operation. The H.P. 1740A oscilloscope has two time bases. When used in conjunction with the time interval counter, the oscilloscope can be used to measure delay times to the nearest nanosecond.

The operation of this system is as follows. The input pulse waveform is amplified and fed to the sending transducer. The positive slope of the SYNC OUT square pulse is coincident with the first positive peak in the generator output, and is used to trigger the main time base on the oscilloscope. At the same time, the oscilloscope main GATE OUT starts the counter. The receiving transducer picks up the attenuated signal, which is amplified and displayed on the oscilloscope.

The instant of triggering of the second time base is controlled by the operator. When automatic triggering is chosen, the measuring system acts like a sophisticated Morgan instrument. Greater accuracy is obtained by manually adjusting the delay time multiplier knob on the scope. The scope is designed to provide visual representation of the point of triggering of the delayed time base. For instance, it is possible to trigger on any peak or crossover point. Generally, it is advantageous to trigger somewhere toward the middle of the burst of sine waves, where the waveform will be least distorted.

Finally, coincident with the triggering of the delayed time base, is the delayed GATE OUT which stops the counter. The counter gives a continuous digital display of the measured delay time. The number of time periods

averaged by the counter is selectable. The counter can also be used as a frequency counter to calibrate the function generator.

With the time interval counter, the measuring system depicted in Fig. 6 is capable of making delay time measurements to the nearest nanosecond. To calculate a velocity from this delay time measurement, however, it is necessary to account for the time delays through the various electronic components as well as through the transducers. Also, transducer separation must be determined. In general, these latter considerations limit the accuracy of the pulse through-transmission technique.

CONTACT TRANSDUCERS

With the objective of investigating high frequency wave propagation in paper, it was necessary to obtain appropriate transducers. Commercially available piezoelectric contact transducers were found to operate at these high frequencies.

The contact transducer consists of a slab of piezoelectric ceramic material attached to a wear plate, and enclosed in a cylindrical-shaped housing. A special backing material behind the ceramic material controls the damping behavior of the transducer. A highly damped transducer will result in less wear plate displacement for a given applied voltage. However, the highly damped transducer will be broadbanded. Low damped transducers are more sensitive, but over a smaller frequency range.

Three matching pairs of contact transducers were used in the experimental work. A pair of 1 MHz immersion transducers was obtained from Dapco Industries. These were highly damped longitudinal transducers. The immersion transducers have epoxy wear plates of 1/2-inch diameter, which acoustically match

the transducers to water. The epoxy wear plates vibrate in a direction normal to the plate surface, parallel to the axis of the cylindrical transducer.

The other two pairs were obtained from Panametrics, Inc. One of these were 5 MHz longitudinal transducers of 1-inch diameter. The other were 1 MHz shear transducers of 1/2-inch diameter. Both pairs have the higher impedance wear plate. The faces of the shear transducers vibrate in a direction perpendicular to the axis of the cylindrical transducer.

Initially, attempts were made to propagate waves in the Z-direction of heavy board materials. It was quickly learned that signal losses resulting from poor transducer-specimen contact were severe. It was discovered that an intimate contact was required. Even the roughness of a smooth calendered paper surface was prohibitive. The displacements of contact transducers are extremely small.

Of the contact aids which were tried, vacuum grease worked best. The vacuum grease could be applied in small amounts and yet sufficiently fill in the surface irregularities, thereby acting as a bridge between the transducer and individual fibers in the sheet.

Penetration of the vacuum grease into the fibrous structure does occur. Penetration is a slow function of time, and is affected by the initial amount of grease applied and by the degree of contact pressure. Vacuum grease penetration affects both transit time and signal amplitude measurements. A slight signal decrease has been observed with time as the grease penetrates, thereby altering the nature of the transducer-specimen bond. This change is so small as to be insignificant.

The effect on the transit time measurement can be substantial. Longitudinal waves propagating in the X-Y plane, transit times and transducer separations are both large, and the effect of the grease penetrating a few mils is negligible. The grease does not affect the fibrous structure other than to fill some of the void space. Since longitudinal waves travel slower in the grease than in the paper, the net effect will be a slight decrease in the wave velocity in the regions of grease penetration. Generally, this effect is negligible for propagation in the X-Y plane.

In the case of Z-direction propagation, however, grease penetration is no longer negligible. The Z-direction longitudinal velocity in paper turns out to be considerably less than that in the grease. The effect of the grease is to decrease the measured transit time, yielding an erroneously high Z-direction longitudinal velocity.

The extent of grease penetration has been approximated by examining various paper specimens under the microscope. Areas on the specimens which have made contact with vacuum grease are darker. It was found that the depth of this discoloration was only a couple mils.

Z-direction measurements can be made with little vacuum grease applied to the transducers. The precise techniques which were developed to minimize the effect of grease penetration are discussed later.

Vacuum grease, like most nonsolids, does not transmit shear motion. A special shear wave coupling material is required. It was found that honey serves this purpose quite well. Honey did partially penetrate the fibrous structure, but as with the vacuum grease, penetration effects were negligible for propagation in the X-Y plane, and have been minimized for Z-direction propagation.

SPECIMEN-TRANSDUCER CONFIGURATIONS

Studies were made of various specimen-transducer configurations in order to determine possible means for measuring the velocities of waves in paper. Unlike the Morgan instrument probes, the contact transducers have large active areas. Z-direction wave propagation is straightforward enough. The transducers are simply coupled to opposite surfaces on single specimens. Propagation in the X-Y plane is more difficult.

The Morgan instrument is capable of propagating low frequency longitudinal waves in the X-Y plane. Using contact transducers, it was desired to propagate bulk longitudinal waves in the X-Y plane. The bulk velocities are somewhat higher than the corresponding Morgan velocities. Both types are needed for calculating some of the elastic constants, the out-of-plane Poisson ratios in particular.

One scheme for measuring these bulk velocities consists of constructing stacks made of paper. The stacks of paper were compressed in a special clamping apparatus, and two opposite faces of the stacks were smoothed on a belt sander. The transducers are bonded to these smooth surfaces. The stacks were typically 1 1/2 inches in width (between transducers), 1 1/2 inches in depth, and 3 inches in length. Stack widths were always in the range of 1/2 to 2 inches.

The most accurate way to measure propagation velocities is to measure the total delay time for two identical stacks of different widths. For each stack, the total delay time includes the following:

1. actual transit time through the fibrous material;
2. extraneous time delays occurring at the transducer-specimen interfaces; and

3. time delays in the transducers and associated electronic equipment.

Everything being the same, the difference between the two total delay times corresponds to the actual transit time through a hypothetical stack having a width equivalent to the difference between the original stack widths. This measuring technique assumes that the two paper stacks are identical in all respects except their widths.

It has been shown that sanding the opposite faces of the stacks changes the fibrous structure only slightly. The affected regions are very narrow, perhaps a couple mils into each surface. The above technique would cancel out even this small effect, since presumably the effect on measured delay time would be the same for each stack.

The stack widths are never small relative to the transducer diameter, as is the case for Z-direction propagation. The transducers are neither point sources nor infinite plane sources. Strictly speaking, then, these bulk waves are not plane waves. It has been found that the above transducer-specimen arrangement approximates plane wave propagation remarkably well, though care must be taken to insure that the transducers are directly opposite one another.

An interesting experiment was conducted using this stack configuration. Four stacks of Mountie Offset printing paper were constructed using different orientation schemes, as follows:

1. all sheets were oriented with X-direction parallel to the propagation direction;
2. every third sheet was oriented in the Y-direction;
3. every other sheet was oriented in the Y-direction; and

4. all sheets were oriented with Y-direction parallel to the propagation direction.

Eight stacks were constructed, two for each orientation scheme. For each pair the difference in widths was approximately 50 mm. Delay times were measured for longitudinal wave propagation through each stack, and velocities were calculated.

Elasticity theory predicts that for a layered arrangement, Young's moduli add in a series fashion. Since the bulk longitudinal velocity squared is very nearly proportional to Young's modulus, it was expected that the V_L^2 values would vary linearly with the proportion of sheets oriented in the X-direction. The results of the experiment are given in Fig. 7.

The linear plot in Fig. 7 gives support to the general validity of the ultrasonic technique. This specific result seems reasonable when one compares the wavelength with the thickness of the individual Mountie Offset sheets. This experiment was conducted at 1 MHz. The wavelengths ranged, then, between 2.7 and 3.8 mm. Each sheet was only about 2.5 mils, or 0.064 mm thick. With such a large wavelength-to-sheet thickness ratio, it is not surprising that the longitudinal wave would travel at the correct average velocity when layer orientation is mixed.

Other specimen-transducer configurations were studied. Another arrangement which proved acceptable involved single sheets. The transducers were affixed to opposite edges of the narrow specimens. The arrangement was essentially like the stack configuration. This technique is limited to fairly heavy board material of sufficient rigidity. The disadvantage of this technique is that signal levels are greatly reduced since very little of the

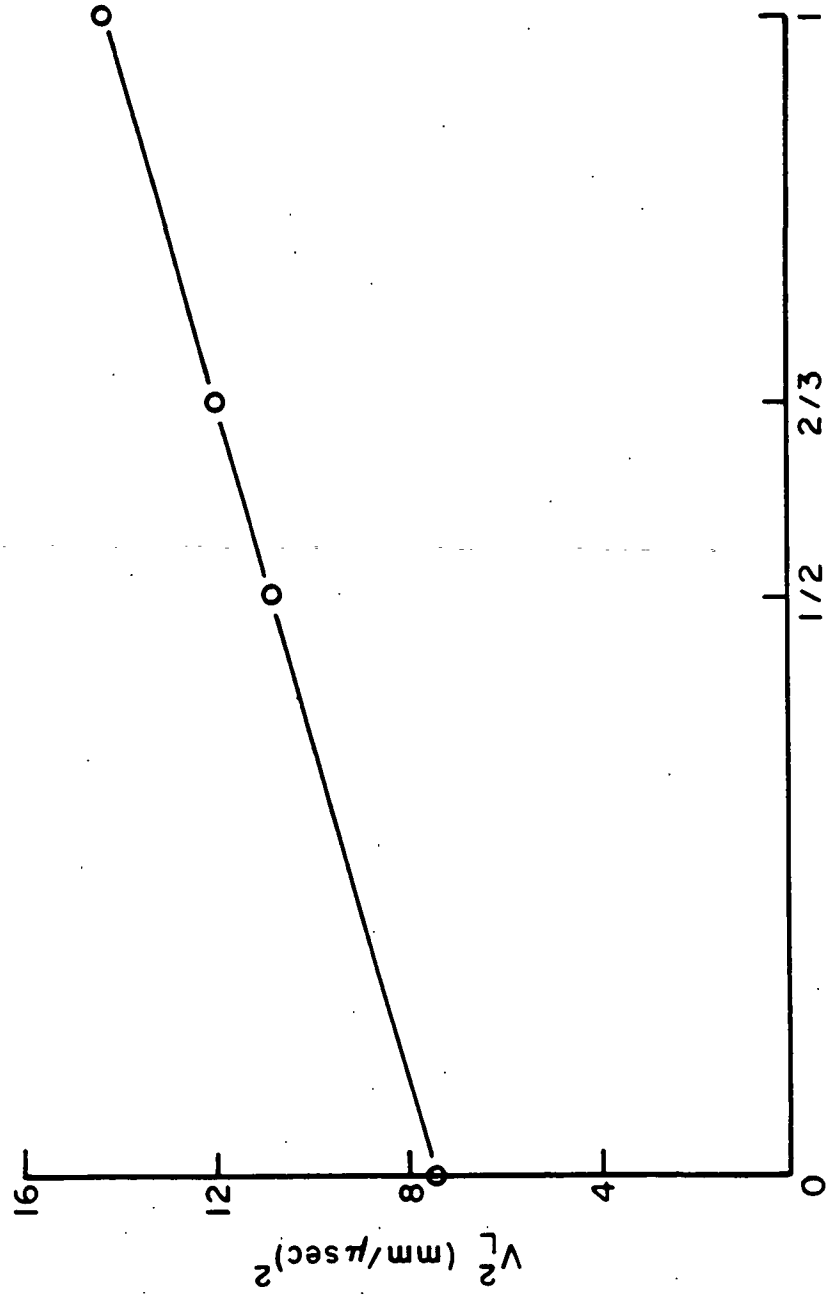

Figure 7. V_L^2 vs. Fraction of X-direction Orientation for Mountie Offset Compressed Stacks

transducer active area is in contact with the specimen. Also, plate waves, not bulk waves, are propagated with this arrangement.

ATTENUATION AND DISPERSION IN PAPER

Attenuation and dispersion phenomena are important to the measurement of elastic properties using ultrasonic techniques. A wave velocity which changes with frequency cannot be easily used to uniquely determine an elastic constant.

There are various types of dispersion. Basically they all stem from an interaction of the wave with some aspect of the material. With paper, three types of dispersion can be considered.

Plate wave dispersion is associated with the interaction of waves with the paper itself. In this case, the wavelength/plate thickness ratio has particular significance. This type of wave dispersion is characteristic of plate materials, and can be predicted theoretically from a knowledge of plate density, thickness, and elastic constants.

Ultrasonic waves will be attenuated in a viscoelastic material. This attenuation will result in dispersion. This effect is generally very small, and is negligible except when attenuation is extremely high.

The third type of dispersion, important for all fibrous systems, results from an interaction of the waves with the fibers. This type of dispersion can be thought of in terms of wave scattering or attenuation. In general, higher frequency waves will be attenuated more since wavelength decreases with frequency.

It was necessary at the outset to determine if this latter type of dispersion was significant at ultrasonic frequencies around 1 MHz. In propagating

longitudinal waves through Mountie Offset stacks of varying widths, it was observed that short 1 MHz pulses became increasingly distorted as they travelled through the stacks. The distortion was accompanied by considerable attenuation.

To quantify these effects, the shape of the received pulse was characterized for propagation through two stacks of different widths. These signals were compared using Fourier transform techniques. A computer program was written for this purpose. The original pulse was fairly wide, having Fourier frequency components which fell in a fairly narrow band centered around 0.94 MHz. Useful computer data was limited to the frequency range 0.80 to 1.08 MHz. As expected, it was found that the higher frequencies were attenuated more. It was also found that the velocity of the frequency components was essentially constant over this frequency range.

The quality factor, Q, is proportional to the number of wavelengths travelled by the wave before it is attenuated by a factor of 0.368 (= 1/e), and is defined as follows:

$$Q = \pi f(\Delta d)/V \ln(A.F.), \tag{101}$$

where f = frequency

V = phase velocity

A.F. = attenuation factor, ratio of signal amplitudes over distance Δd

Δd = distance over which attenuation factor applies

The quality factor depends on frequency and direction in the material.

From the data plotted in Fig. 8 it is seen that the log of attenuation factor increases linearly with the log of frequency, while the quality factor is essentially constant. The high Q value of about 15 implies that attenuation

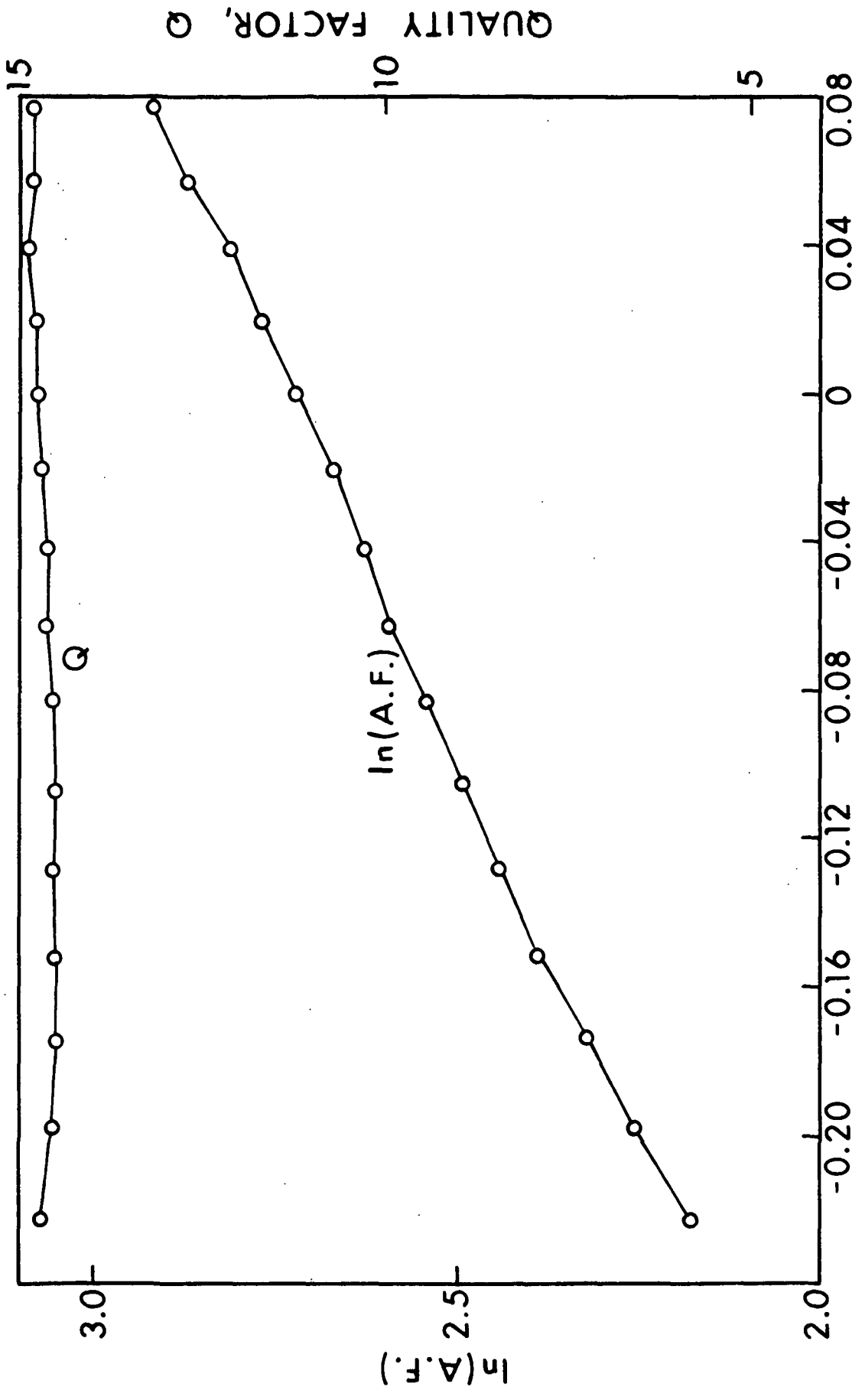

Figure 8. Computer Attenuation Data for Mountie Offset Stack

is not particularly severe. While attenuation is moderately high, the resultant dispersion is negligible.

Measurements at frequencies as high as 10 MHz have been made on other stacks. It was found that attenuation became increasingly severe above 1 MHz. Presumably, wave dispersion would be significant at higher frequencies. However, the severe attentuation precludes its measurement.

Z-direction velocities and attenuation have also been measured as functions of frequency. The Z-direction longitudinal velocity variations with frequency were always within experimental error. Wave attenuation is much more severe in the Z-direction compared with propagation in the X-Y plane. This is not surprising in view of the fact that the wavelengths are about 1/10 those in the X-Y plane.

In conclusion, it was found that wave attenuation increases with frequency, becoming severe above about 1 MHz. This attenuation is not associated with any measurable dispersion. Therefore, the velocities of ultrasonic bulk waves in paper should be independent of frequency below at least 2 MHz. This would be necessary in order for these velocities to relate directly to the elastic properties of paper.

EXPERIMENTAL TECHNIQUES

IN-PLANE BULK VELOCITY MEASUREMENTS

As stated previously, in order to measure all of the elastic constants for paper, it is necessary to make in-plane bulk velocity measurements. In order to predict the dispersion curves for plate wave propagation, it is necessary to determine the in-plane bulk longitudinal velocities. The thinness of paper makes it imperative to construct bulk paper specimens.

The most direct approach is to simply stack individual sheets to the desired overall thickness. With this approach it is necessary to compress the loose stack in order to effect good contact between sheets. The result is a layered structure which may or may not behave as a true bulk material. The criterion which must be applied to wave propagation through such a material is whether there is slippage between the layers. It is necessary that all stresses and strains be continuous across the interfaces between individual sheets. This will be true when surfaces are completely bonded. With a compressed stack, this may or may not be a good approximation to a bulk material.

Experimentally, it was found that the propagation velocity of longitudinal waves through compressed stacks increased slightly with compressive strain. An increase in longitudinal velocity of 1.4% was measured for a Mountie Offset stack when a 10% strain was applied. This increase could be the result of compressing the individual sheets, or the result of improving the contact between layers, or both. It is not possible to separate these effects. In conclusion, while the compressed stack permits an easy way to measure the bulk velocities, there exists uncertainty as to how closely these velocities approximate the true bulk velocities.

A second approach involves constructing stacks by gluing the individual sheets to each other with a rubber cement. This approach insures good contact between layers. However, the effect of the glue on the measured velocity must be ascertained. Experimental work with glued stacks will be discussed below. First, a discussion of the velocity measurement procedure will be given.

There are two basic ways to measure bulk velocities on loose or glued stacks. The simplest way, Method 1, is to measure the total delay time both with and without the specimen in place. A fairly long burst of sine waves

is propagated. Since a long wave train will have a narrow Fourier spectrum, any frequency dependent attenuation will not severely distort the pulse. It is generally found that distortion is limited to the initial and final few cycles in the wave train. Accurate phase velocities are therefore obtained when time measurements are made to a specific point within the pulse. A common practice used in the present experimental work was to measure the delay time out to the fourth or fifth peak. With this approach it is only necessary to measure the delay time out to corresponding points on each signal.

It has been found that this technique suffers from small frequency dependent errors. These errors are associated with apparent time delays which are associated with the transducer-transducer and transducer-specimen interfaces. The extraneous time delay, T_t, is defined as the total effective time delay occurring at the transducer-specimen interfaces. Various mechanisms have been considered which would account for this extraneous time delay. The transit time through the vacuum grease itself is about 15 nsec/mil. However, if the same amount of grease is used with and without the specimen, this would not contribute to T_t. Another possibility is the occurrence of phase changes at the various interfaces resulting from impedance mismatches. While mismatches certainly exist at these interfaces, phase shifts appear in pairs having opposite signs. These should cancel out. The origin of T_t has not been accounted for.

The preferred method, Method 2, uses two specimens of different widths and eliminates the error due to the extraneous delay time. In this case, the propagation velocity is given as follows:

$$V = (d_2-d_1)/(t_{d2}-t_{d1}), \tag{102}$$

where d = specimen width

t_d = total measured delay time

This method assumes the same average velocity through each stack. It can be shown that if this is not so, the calculated velocity will be either greater or less than the two true stock velocities. Consequently, this method is only accurate to the degree to which the two specimens are characterized by the same velocity.

The extraneous delay time can be evaluated by measuring the delay time through just the transducers, t_{do}, in addition to t_{d1} and t_{d2}. Then, T_t is given as follows:

$$T_t = t_{d2}-t_{do} - d_2(t_{d2}-t_{d1})/(d_2-d_1) \tag{103}$$

A very large chipboard stack was glued together in order to evaluate these two methods for calculating longitudinal velocities. Two applications of a rubber cement were made to each interface. The stack was compressed and then cut into two pieces, having the following final dimensions: length, 2.75 inches; height, 1.40 inches; width, d_2 = 33.48 mm and d_1 = 14.99 mm.

Delay times were measured for both specimens, and with the transducers together, as a function of frequency. This was done using both the 1 MHz and 5 MHz longitudinal transducers. From the delays, velocities were calculated using both methods. Also, it was possible to calculate the extraneous delay time at each frequency, using Equation (103). Results are shown plotted in Fig. 9. The difference between the two total delay times, i.e., $t_{d2}-t_{d1}$, is roughly 10 μsec.

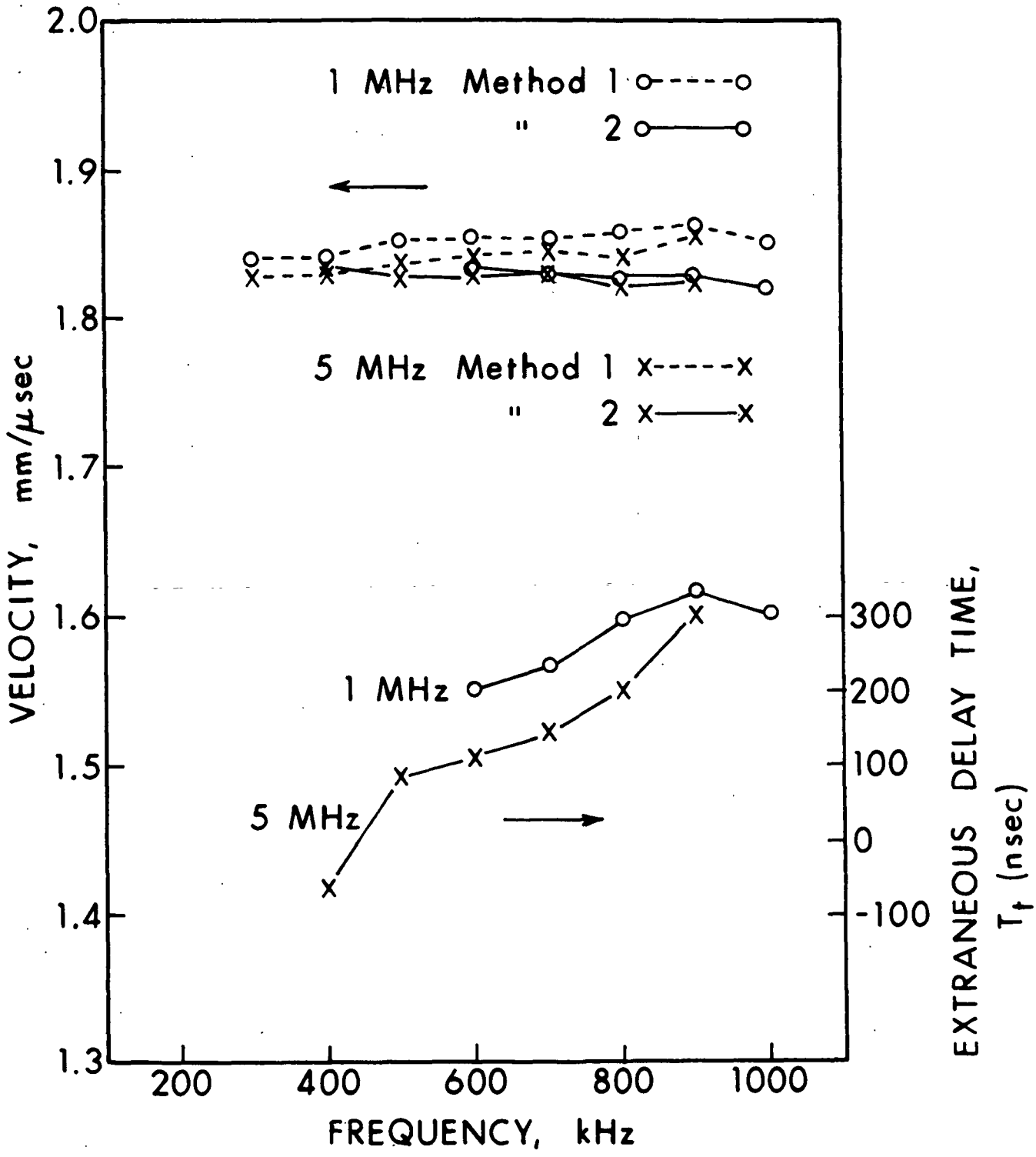

Figure 9. Velocity and Extraneous Delay Time vs. Frequency for Chipboard Stacks

The extraneous delay time is found to increase with frequency. Consequently, Method 1 has associated with it a slight frequency-dependent error. This error can be minimized by employing larger specimens if this is feasible. For the most accurate velocity measurements, however, the second method should be employed. The stacks should be constructed in a way that minimizes differences between the stacks.

The gluing of paper sheets into stacks is itself a source of potential error. The presence of glue alters the fibrous structure. The question here is whether the glued stack is representative of a single layer.

The stacks are constructed as follows:

1. one or more applications of glue are made to each sheet allowing time for drying;
2. sheets are compressed to roughly 100-200 psi for approximately 5 minutes;
3. opposite faces are sanded smooth and parallel; and
4. stacks are permitted to reach equilibrium with environment.

It was found that a single glue application often resulted in a bond as strong as the paper in the Z-direction.

Sanford's Grippit and Rubber Cement glue were used exclusively. According to the CRC Handbook of Chemistry and Physics (55), the bulk longitudinal velocity for gum rubber is 1.55 mm/μsec. This velocity is only slightly lower than for Y-direction propagation in paper. The effect of the glue will be greater for X-direction propagation, for which the bulk velocities are roughly twice the velocity through the gum rubber.

In the process of forming the stacks, particularly in compressing them, it is possible to permanently alter the structure. An actual weakening of the structure may occur due to bond breaking, or more likely, the stack may be permanently deformed. The very presence of the glue is expected to have some effect, since wave velocities in gum rubbers are slower. If the glue remains as separate layers, it is expected that the measured velocity would be reduced in proportion to the glue content. It is also possible that glue penetrates the surface structure of the individual fibrous sheets. This would result in an increase in stack density and might also strengthen the surface regions, thereby increasing the measured velocity.

A simple experiment was conducted to determine the total effect of the glue in the stack. Six chipboard stacks were constructed, three with only one glue application/layer, and three with three applications/layer. All six were compressed to about 125 psi, and machined carefully to nearly the same widths. X-direction bulk longitudinal waves were propagated through each of the stacks. The results of the experiment are summarized in Table III. It is seen that the difference in glue content of 4.1% resulted in a velocity difference of only 1.45%. The predicted velocity for the 6.0% glue content stack is 3.067 mm/μsec. This value is based on the measured velocity of 3.204 mm/μsec for the low glue content stack, and is obtained by assuming that the glue and paper moduli add in series. With this assumption, the measured value of 3.158 mm/μsec implies that at least two glue effects are operative, and that these effects are not all in the same direction. These results can be used to extrapolate back to 0% glue content, though not without some uncertainty.

TABLE III

V_{Lx} vs. GLUE CONTENT FOR CHIPBOARD STACKS

Average glue content	1.9%	6.0%
Longitudinal velocity (mm/μsec)	3.204	3.158

In a second experiment, the three low glue content stacks were subjected to varying amounts of Z-direction compression, each for three minute periods. Stack thickness and the X-direction bulk longitudinal velocities were remeasured after five days. The results are presented in Table IV. These velocity changes are within experimental error. It is concluded that pressures as high as 400 psi are insufficient to significantly alter the fibrous structure.

TABLE IV

IRRECOVERABLE STRAIN AND V_{Lx} FOR CHIPBOARD STACKS

vs. MAXIMUM PRESSURE FOR COMPRESSING STACK

	Pressure		
	0 psi	200 psi	400 psi
Irrecoverable strain	0%	1.2%	1.5%
Initial velocity (mmμsec)	3.186	3.208	3.218
Final velocity (mm/μsec)	3.198	3.202	3.215
Velocity change	0.4%	-0.2%	-0.1%

Later stack work was conducted using the heavy bleached kraft milk carton stock. Glued stacks having 3.3 and 5.2% glue were constructed. Two stacks with d_2 = 1.51 inches and d_1 = 0.90 inch were made for each glue content level. A fifth loose stack was also assembled. The longitudinal velocities were determined in each case. Over a large frequency range, no significant differences among the three glue contents (0, 3.3 and 5.2%) were detected.

It is concluded that both stack types, loose and glued, approximate bulk sheets under conditions of X-Y plane propagation. The gluing of stacks is definitely more time consuming. However, the uncertainty in the measured velocity is probably less for glued stacks.

For the purpose of making in-plane bulk velocity measurements, three glued stacks were constructed for each sample. Both longitudinal and shear waves were propagated through the stacks in the width direction. The three stacks were oriented along the X-direction, Y-direction, and at a 45° angle to the X-direction.

The actual stack construction procedure varied from sample to sample. For instance, more glue was needed for the milk carton stock stacks. The arrangement of individual sheets in the stacks was also varied. Typically, every other sheet was flipped over, leaving wire sides and felt sides of adjacent layers together. This was done in order to balance the internal stresses which were initially present in the heavy boards as evidenced by pronounced curvature.

Three delay time measurements were made on each stack at different locations on the smoothed surfaces. The delay time through the transducers was also measured. The velocities were calculated from delay times by estimating the extraneous delay time. Both longitudinal and shear velocities were measured in this way.

Z-DIRECTION BULK VELOCITY MEASUREMENTS

Z-direction bulk velocities are easier to measure than in-plane bulk velocities. The transducers are bonded to opposite surfaces of a single thickness

of paper using either vacuum grease or honey. It will be shown, however, that the accuracy of Z-direction velocities is substantially less.

In early work with the two 90-lb linerboard samples, fairly thick layers of vacuum grease were applied to the transducers in making longitudinal velocity measurements. With lesser amounts, the transducers would not remain affixed to the specimens, making it necessary to apply external pressure to the transducers. It was found that the measured delay time was quite sensitive to the applied pressure.

It was also observed that, with the transducers together, the measured delay time varied with the amount of grease between the transducers. Time measurements suggested a typical grease application of about 3 mils. Using feeler gages, the grease layer between transducers was found to be between 2 and 3 mils.

With the higher velocity through the vacuum grease, it became apparent that any grease penetration would give erroneously high velocities. It was estimated that significant grease penetration was occurring due to high initial contact pressure used to bond the transducers to the specimens.

The effect of grease penetration on the measured longitudinal velocity was determined by making velocity measurements with very small amounts of grease. The new method of making Z-direction measurements attempts to minimize the application of both grease and external pressure. As pressure is applied to the transducers, the signal on the scope is observed to increase in magnitude from no signal at all. As pressure is increased, the magnitude of the signal increases and the signal is shifted to shorter delay times (pulse is coming through board sooner). In making delay time measurements with the new method,

the applied pressure is increased just until a peak in the output signal can be distinguished. This method resulted in much slower velocities for both longitudinal and shear velocity measurements.

The effect of straining the material was investigated by measuring Z-direction longitudinal velocities as a function of Z-direction compressive strain. This was done for two specimens per sample. The results, plotted in Fig. 10, represent the averages. Though a couple of strong fingers could produce strains of up to 12%, these strains correspond to pressures well beyond what is necessary to make good contact. Nonetheless, these results indicated the sensitivity of Z-direction velocity measurements to Z-direction strain.

Three factors influence the accuracy of the Z-direction measurements. First, as discussed above, the amount of grease and pressure applied is very important. Second, it is not possible to determine the extraneous delay time, T_t, for Z-direction measurements, since only single thickness specimens can be used. This extraneous delay time has been estimated to lie between -100 and +100 nsec. This delay time error is relative to the total delay time, which depends greatly on the third factor, specimen thickness. For thicker specimens, having greater transit times, the delay time errors due to the first two factors will constitute less relative error. Error due to the uncertainty in the thickness measurement is also significant.

The three board samples investigated had thicknesses in the range of 24.4 and 26.9 mils. Transit times for longitudinal waves were between 2940 and 3245 nsec. Experimental accuracy for these velocity measurements has been estimated to be ±5%. This estimate applies to both longitudinal and shear velocity measurements for thick board materials.

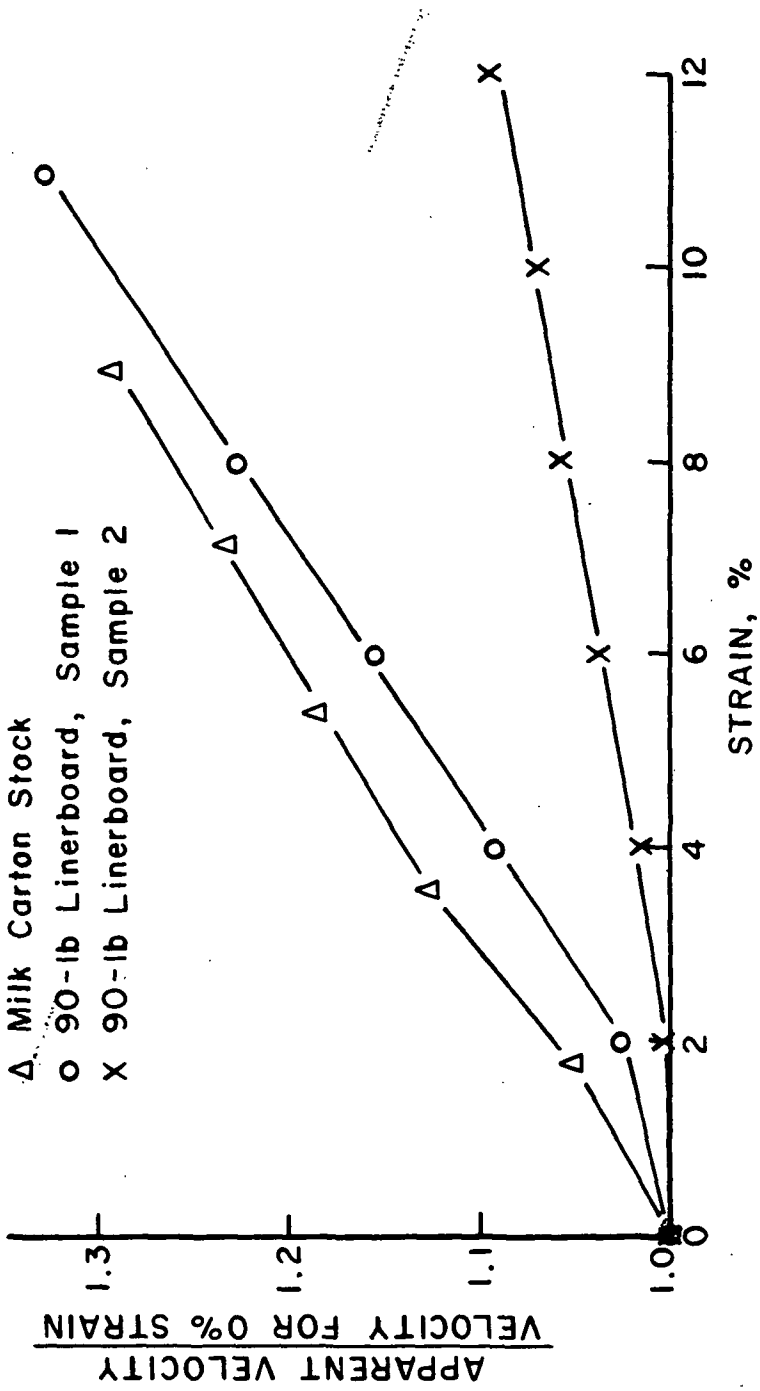

Figure 10. Change in Apparent Z-direction Longitudinal Velocity with Strain

The error associated with Z-direction measurements will obviously depend upon specimen thickness quite strongly. Another consideration is the large variation which exists from point to point within and between specimens. Twenty or more delay time and thickness measurements have to be made in order to obtain a good representative average.

The Z-direction bulk velocity measurements were made on small specimens. For convenience, inch-wide specimens were used. These strips were taken from several of the large specimens. The strips were marked off into 1 inch by 1 inch sections. Generally, longitudinal waves were propagated through 20 squares, and only 10 squares were tested for each shear wave polarization.

MORGAN VELOCITY MEASUREMENT

The errors associated with the measurement of the low frequency zeroth order symmetric mode velocity using the Morgan Dynamic Modulus Tester have been discussed previously. The error has been estimated to be about ±1%. The technique was modified to eliminate much of the error associated with measuring delay time.

In the original modification, only the Morgan instrument transducers were used. Eventually, even these were replaced with contact transducers. Using the Morgan transducers, the sending transducer is excited by a signal originating at the function generator. Complete control over both frequency and repetition rate is maintained. The measurement scheme depicted in Fig. 6 is employed.

The main advantage of this set-up is that it allows one to trigger off the same point on the received pulse waveform despite transducer separation distance. In this way, delay time measurements are much more accurate.

The pulse carrier frequency was typically in the range 40-60 kHz, despite the fact that the transducers had a center frequency of about 10 kHz. The response of the transducers at higher frequencies is strongly dependent on frequency. However, for certain frequencies in the 40-60 kHz range, strong signals were received.

The time period between peaks is substantially reduced at these higher frequencies. This in itself increases the sensitivity of the delay time measurements. Because attenuation is relatively low at these low frequencies, signal reflections from the specimen ends and sides eventually are detected by the receiving transducer. These extraneous signals superimpose on the original, straight-path, signal and distort the received pulse beyond a certain point. The length of the undistorted portion depends on transducer separation, the specimen dimensions, and the position of the transducers on the specimen. For any given transducer-specimen configuration, the number of undistorted wavelengths can be increased by increasing the frequency. This, then, is a second advantage of going to higher frequencies.

The new technique was found to work well. Delay times measured to peaks 1 and 2 gave the same results, indicating that pulse distortion was negligible.

A further modification of the low frequency technique involved doing away with the Morgan instrument transducers. Instead, the 5 MHz longitudinal transducers were used. In this case, the transducers were coupled to the edges of the board specimens, which were trimmed so that opposite sides were parallel. Also, specimens were generally longer than they were wide to preclude effects of side reflections. Vacuum grease was used to couple the transducers to the board specimens. A slight pressure maintained good transducer-specimen contact.

The 5 MHz transducers had a very strong response at about 50 kHz. While the received signal was less noisy for the contact transducers, the two types of transducers were found to measure the same velocities.

In Fig. 11, delay time is plotted versus transducer separation distance for a milk carton stock specimen. The 5 MHz transducers were used at 50 kHz. Each data point represents the average delay time for measurements at three locations within the specimen. Delay time measurements were made to Peaks 1 and 3. In order to enhance the comparison of the data, the Peak 3 data has been shifted to the left by subtracting from each Peak 3 delay time some constant, roughly two wave periods. This puts the two curves nearly together.

It is seen that for transducer separations above about 5 inches, both sets of data fall on the same straight line. Below 5 inches separation, the Peak 3 data becomes somewhat erratic. This behavior is explained in terms of end reflections which will superimpose on the third peak (before the first peak) as transducer separation is decreased.

In making transit time measurements, it is desirable to avoid making delay time measurements to portions of the signal which have been distorted. Using Peak 1, this usually means that transducer separation must be greater than about 2 inches.

A simplified procedure for making these velocity determinations has been tried, whereby delay times are measured at various locations for a specimen of given width and then the specimen is cut in half, and time delay measurements are made on each of the half-width pieces. Average delay times are then calculated for the two transducer separations. The difference between these two delay times represents the average transit time through half the original specimen width. This procedure is quicker and works equally well.

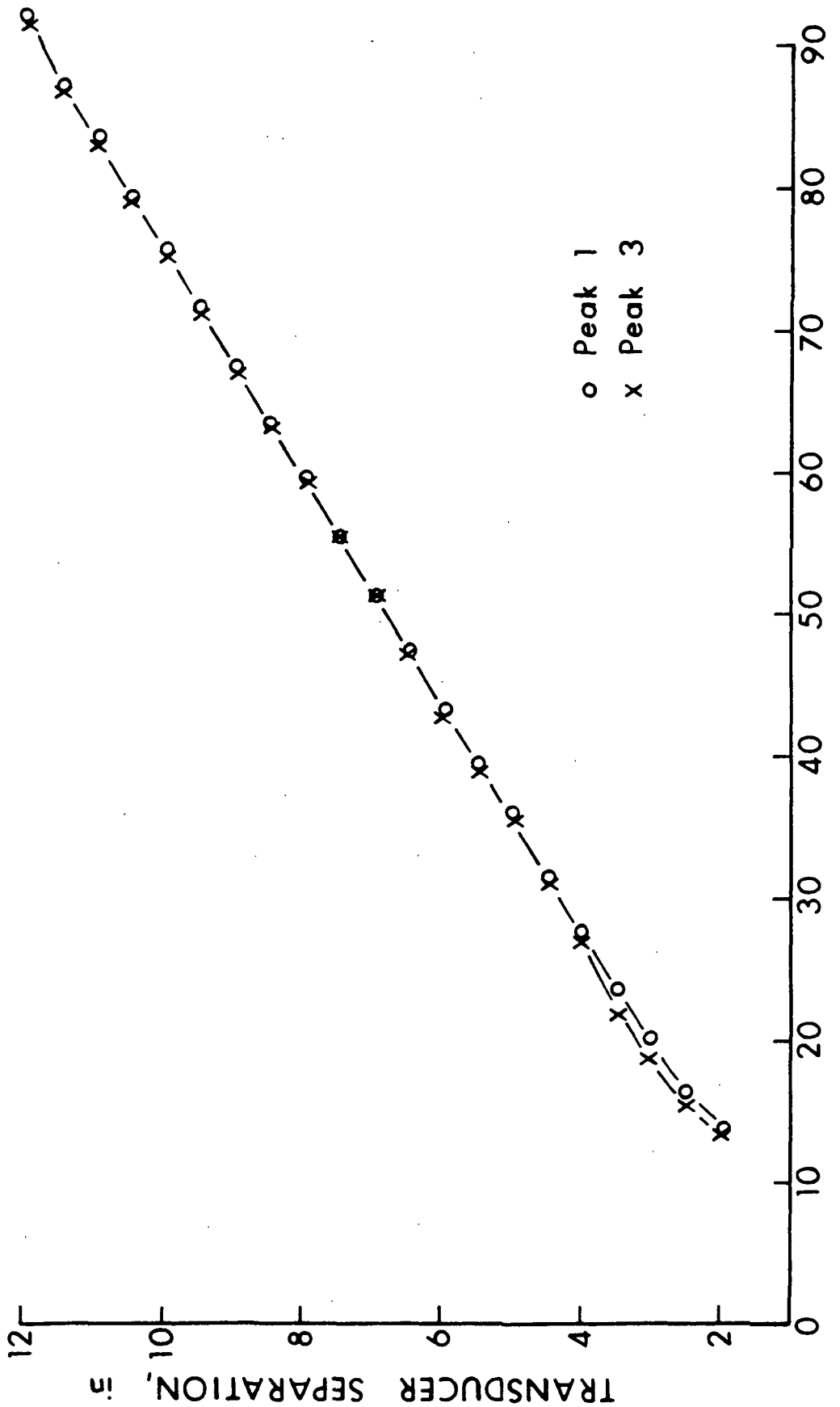

Figure 11. Transducer Separation vs. Delay Time Data for Milk Carton Stock, Peaks 1 and 3

The new techniques for measuring these low frequency velocities are much more accurate. This accuracy has been estimated to be about ±0.25%. This estimate is based on experience making numerous velocity measurements using several different techniques. The actual measurement accuracy is difficult to determine and is a function of the precise measurement procedure used.

PLATE WAVE RESONANCE TECHNIQUE

To test the predictions of the orthotropic plate wave theory, it was necessary to measure plate wave velocities. Since the zeroth-order symmetric mode is nondispersive at low frequencies, its velocity can be determined using an ultrasonic pulse technique. However, this straightforward procedure is not applicable in general. The only successful measurements of dispersive waves in paper have been achieved using an air-paper resonance technique (28). An adaptation of this plate wave resonance technique has been used here. The basic set-up is depicted in Fig. 12.

With the air-paper resonance technique, a large sheet of paper is mounted between an ultrasonic transmitter and receiver. The transducers are rigidly connected so that they always face each other, but can be rotated with respect to the plane of the sheet. As the transducers rotate, the wavelength of the disturbance along the sheet changes. At angles where the frequency and wavelength along the sheet correspond to those of a plate wave mode, optimum transfer of energy occurs. This results in a peak in the receiver signal. Therefore, the velocities of plate wave modes can be determined by recording peaks in the received signal *versus* angle curves at different frequencies. The plate wave velocities are given by the following equation:

$$V_p = V_{air}/\sin \alpha, \tag{104}$$

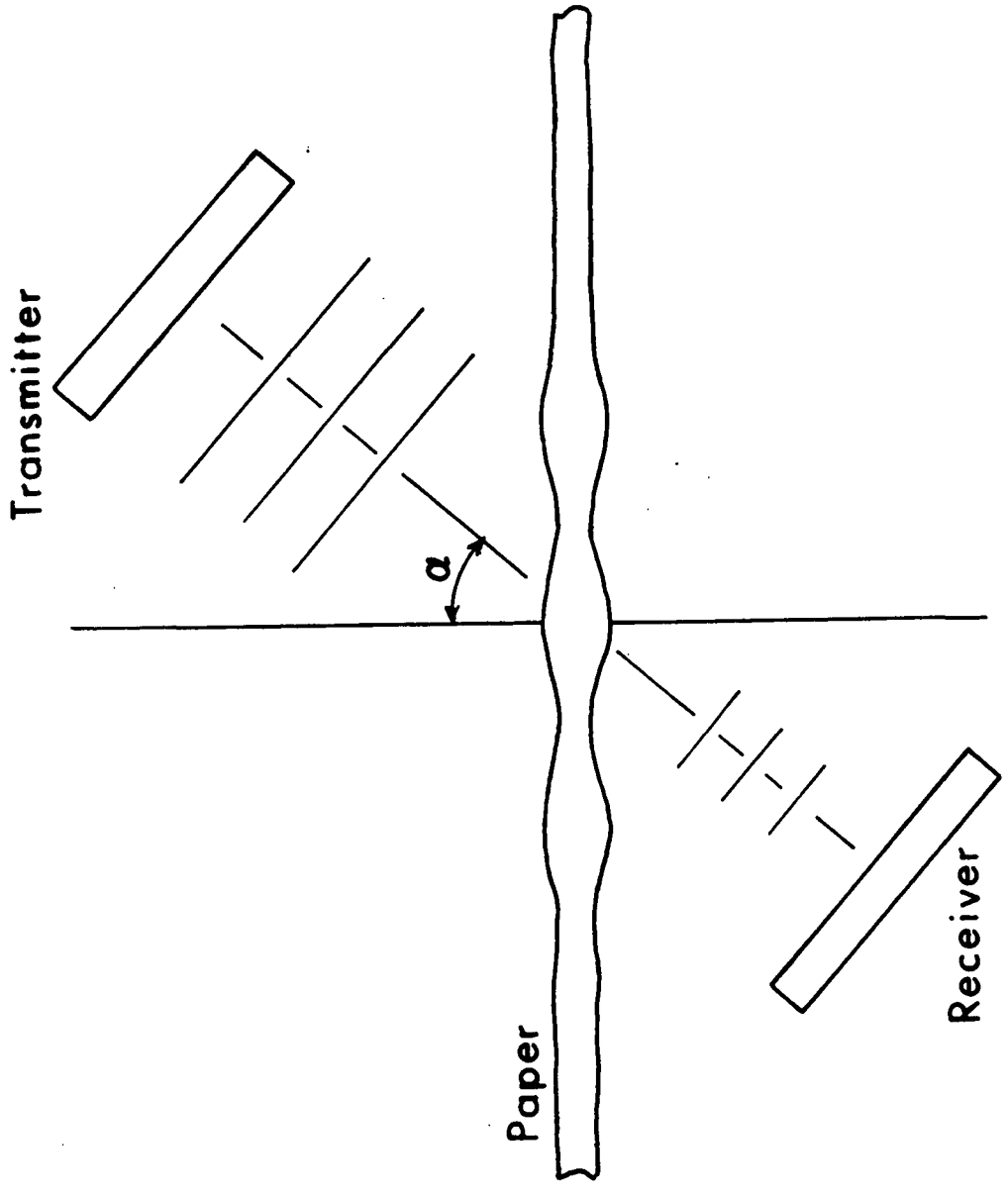

Figure 12. Basic Set-up of Plate Wave Resonance Technique

where V_p = plate wave velocity

V_{air} = velocity of wave in air

α = angle of wave incidence measured to plate normal

The technique used here differed from that described by Luukkala, et al. (28) in one important aspect. Instead of direct current biased electrostatic transducers, permanently polarized dielectric films were used as the active medium in the transducers. These films were made by voltage cycling 0.125 mm F.E.P. Teflon films as described by Curtis (56). These transducers were constructed as part of IPC Project 3332.

The specific apparatus was designed for rotating the paper relative to the transducers, which remained stationary. The 14-inch by 28-inch paper sheets were taped to an aluminum plate which had a 12-inch by 24-inch opening. The aluminum plate, mounted vertically, pivoted about a vertical axis which was 11.5 inches from the transmitter and 4.5 inches from the receiver. Two of the three transducers used had diameters of 1.75 inches. The third transducer had a diameter of 3.0 inches.

The plate wave resonance apparatus included a variable speed reversible motor for rotating the paper sheets, and a chart recorder. The received signal was amplified and rectified. The direct-current voltage was amplified and used to drive the chart recorder. A large corrugated box housed the rotating plate and the transducers. It was found that small air velocity, temperature and relative humidity fluctuations caused interference effects. The enclosure reduced the resulting noise considerably.

The portion of the dispersion curves that can be measured with this plate wave resonance technique is limited by a number of factors. First, attenuation of ultrasonic waves in air limits the frequency range to below about 400 kHz.

One result of this limitation is that a sheet must be fairly thick in order to excite plate waves by this technique. Paper thicknesses must be about 15 mils or more. Second, since the wavelength along the sheet is always greater than in the air, velocities below that of sound in air cannot be measured. With physical limitations of the apparatus, this limits the measurements to velocities above about 0.38 mm/μsec. Finally, resolution becomes increasingly poor as alpha is decreased. Consequently, there is a practical upper limit as well. In general, waves with velocities greater than about $5V_{air}$ cannot be resolved.

Plate wave velocities are obtained in the following manner. The function generator is set for continuous wave operation at some given frequency. The specimen is taped to the aluminum plate. The motor driven plate is positioned so that $\alpha = 70°$. With the chart recorder on, the motor is switched so that the plate starts to rotate. When $\alpha = 0°$, the motor drive is reversed. The plate reverses its rotation while the chart paper records the return path as well. This procedure is repeated at other frequencies.

A chart recorder tracing is shown in Fig. 13 for X-direction propagation through milk carton stock at 230 kHz. The two peaks correspond to two different modes which were detected at this frequency. The method of determining the angles associated with resonance conditions is indicated. The velocity of sound in air used in calculating the plate wave velocities, using Equation (104), is 344 m/sec.

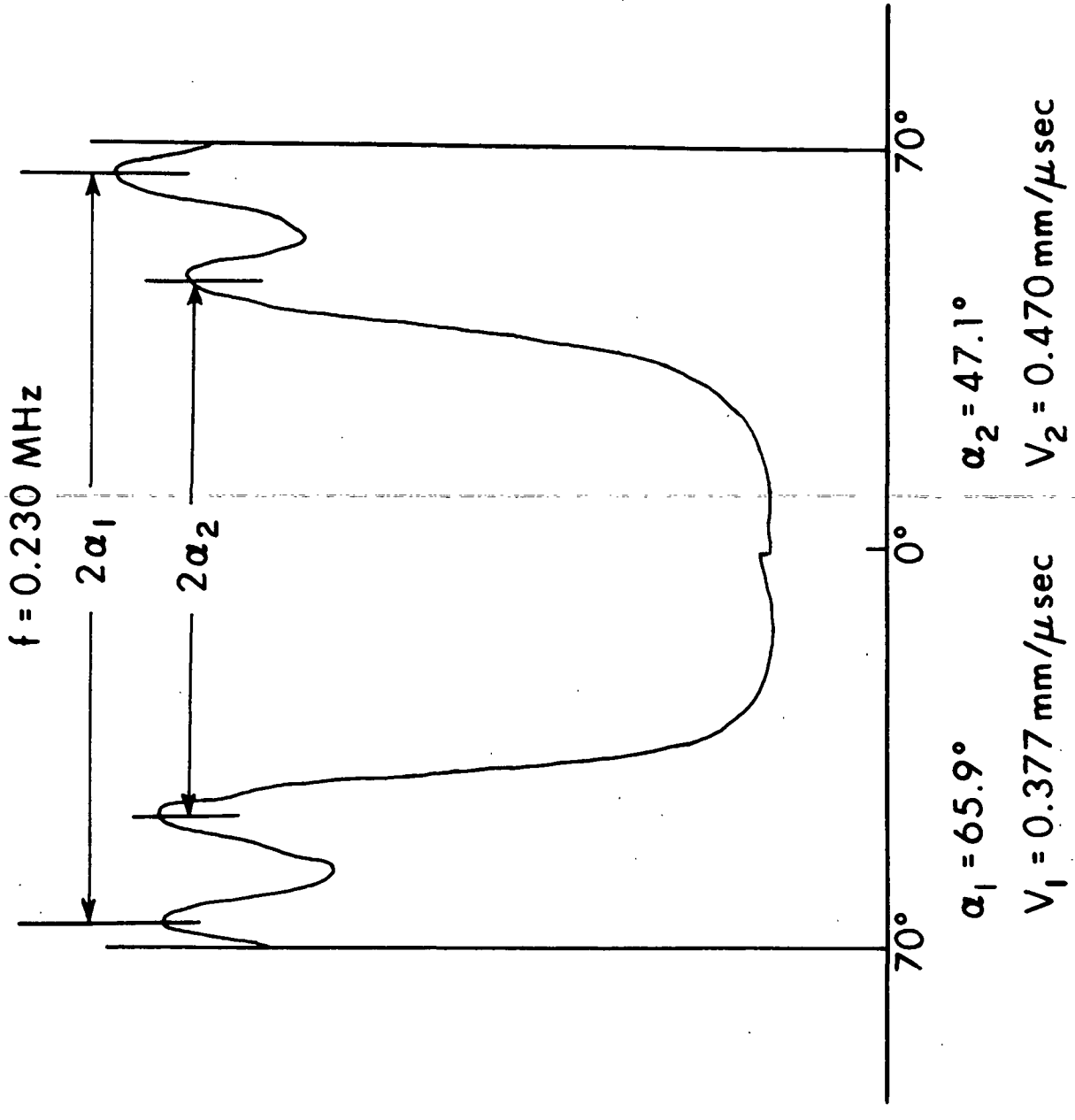

Figure 13. Chart Recorder Tracing Used with Plate Wave Resonance Technique to Determine Plate Wave Velocities

RESULTS AND DISCUSSION

EXPERIMENTAL RESULTS

STIFFNESS COEFFICIENTS

Several longitudinal and shear velocities were measured on the various specimens. The specific velocities which are needed to predict the dispersion curves for both X and Y-direction plate wave propagation are as follows:

V_{Lx} = bulk longitudinal velocity in the X-direction

V_{Ly} = bulk longitudinal velocity in the Y-direction

V_{Lz} = bulk longitudinal velocity in the Z-direction

V_{Sx-z} = bulk shear velocity in the Z-direction, polarization in the X-direction

V_{Xy-z} = bulk shear velocity in the Z-direction, polarization in the Y-direction

V_{SOx} = low frequency zeroth-order symmetric mode velocity in the X-direction

V_{SOy} = low frequency zeroth-order symmetric mode velocity in the Y-direction

These velocities for the three board samples are given in Table V. All velocities have units of millimeter/microsecond (= km/sec).

Seven of the nine independent orthotropic stiffness coefficients can be calculated from these velocities. Stiffness coefficient calculations are normalized with respect to density throughout this work, in order to avoid errors due to the uncertainty in the density. As presented, stiffness coefficients will have units of velocity squared, or millimeter squared/microsecond squared.

TABLE V

MEASURED VELOCITIES FOR THREE BOARD SAMPLES

Velocity (mm/μsec)	90 lb. Linerboard No. 1	90 lb. Linerboard No. 2	Milk Carton Stock
V_{Lx}	3.337	3.428	3.279
V_{Ly}	2.078	2.194	2.307
V_{Lz}	0.191	0.214	0.231
V_{Sx-z}	0.389	0.431	0.418
V_{Sy-z}	0.351	0.387	0.356
V_{SOx}	3.354	3.342	3.188
V_{SOy}	2.103	2.123	2.199

These seven normalized coefficients (indicated by asterisks) are determined, from Equations (53), (55), and (86), as follows:

$$C^*_{11} = V^2_{Lx} \tag{105}$$

$$C^*_{22} = V^2_{Ly} \tag{106}$$

$$C^*_{33} = V^2_{Lz} \tag{107}$$

$$C^*_{44} = V^2_{Xy-z} \tag{108}$$

$$C^*_{55} = V^2_{Sx-z} \tag{109}$$

$$C^*_{13} = \pm(C_{33}(C_{11}-V^2_{SOx}))^{\frac{1}{2}} \tag{110}$$

$$C^*_{23} = (C_{33}(C_{22}-V^2_{SOy}))^{\frac{1}{2}} \tag{111}$$

C^*_{13} and C^*_{23} are assumed to be given by the positive roots in Equations (110) and (111).

The coefficients for the three board samples are given in Table VI. All coefficients have units of square millimeter/square microsecond. Values for

C^*_{13} and C^*_{23} are not given for 90-lb linerboard Sample No. 1. From Equations (110) and (111) it is apparent that V_{Lx} and V_{Ly} must be greater than V_{SOx} and V_{SOy}, respectively. This was not found for this sample.

TABLE VI

SEVEN OF THE NINE ORTHOTROPIC STIFFNESS COEFFICIENTS FOR THE THREE BOARD SAMPLES

Stiffness Coefficient ($mm^2/\mu sec^2$)	90 lb. Linerboard No. 1	90 lb. Linerboard No. 2	Milk Carton Stock
C^*_{11}	11.134	11.750	10.750
C^*_{22}	4.318	4.814	5.322
C^*_{33}	0.0363	0.0458	0.0534
C^*_{13}	---	0.163	0.177
C^*_{23}	---	0.119	0.161
C^*_{44}	0.123	0.150	0.127
C^*_{55}	0.151	0.186	0.175

For all three samples, the bulk longitudinal and SO velocities are very nearly equivalent. This fact means that in general C^*_{13} and C^*_{23} will be difficult to accurately determine. Apparently, for Sample No. 1 these velocities are too close to each other to distinguish them.

DISPERSION CURVES

Dispersion curves for the milk carton stock are given in Fig. 14 and 15. The computer program described earlier and given in Appendix I was employed for this purpose. The parameters involved in predicting each set of curves are given at the tops of Fig. 14 and 15.

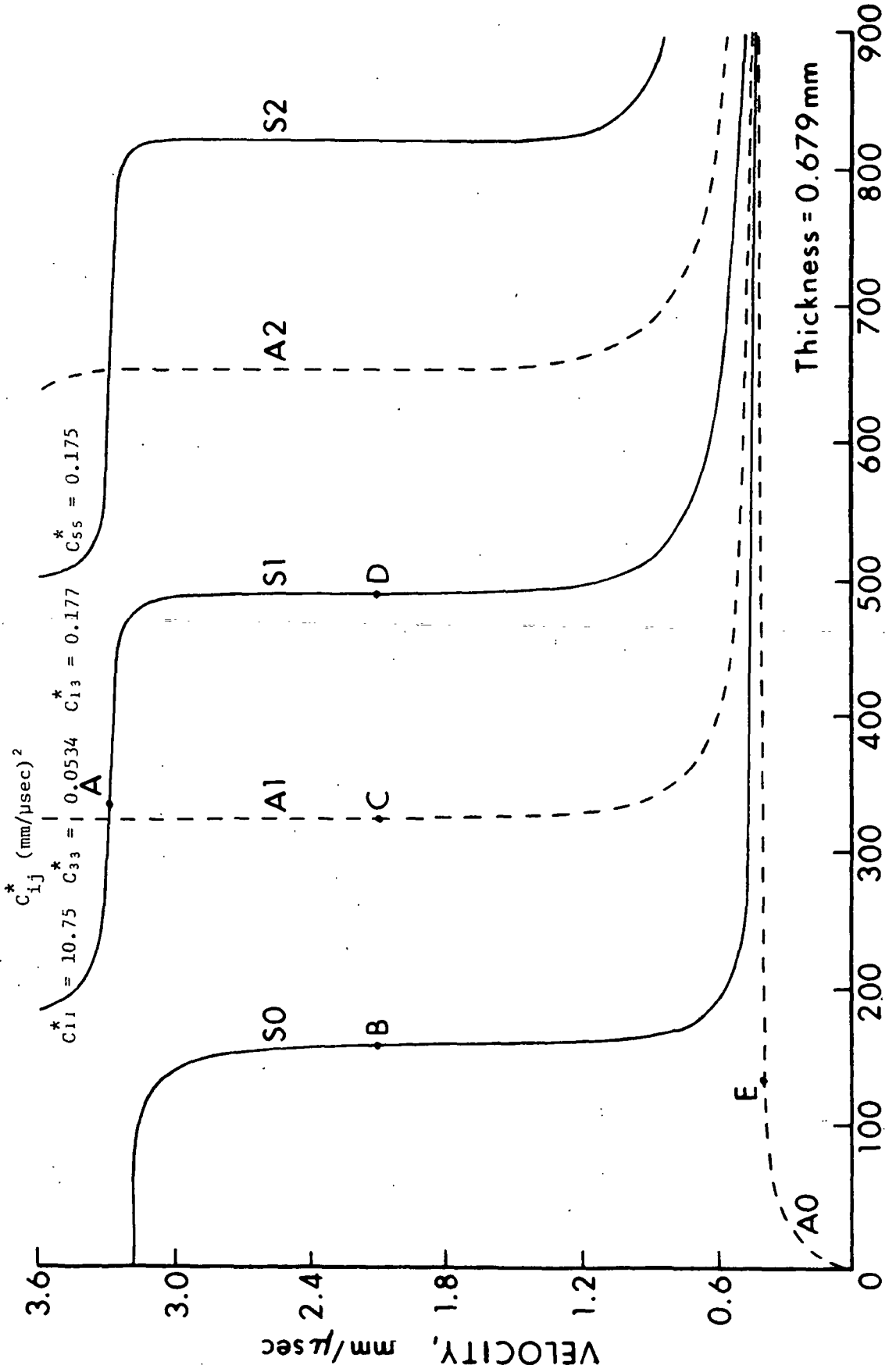

Figure 14. Theoretical Dispersion Curves for Milk Carton Stock, X-direction (Points A,B,C,D, and E Refer to Figure 17)

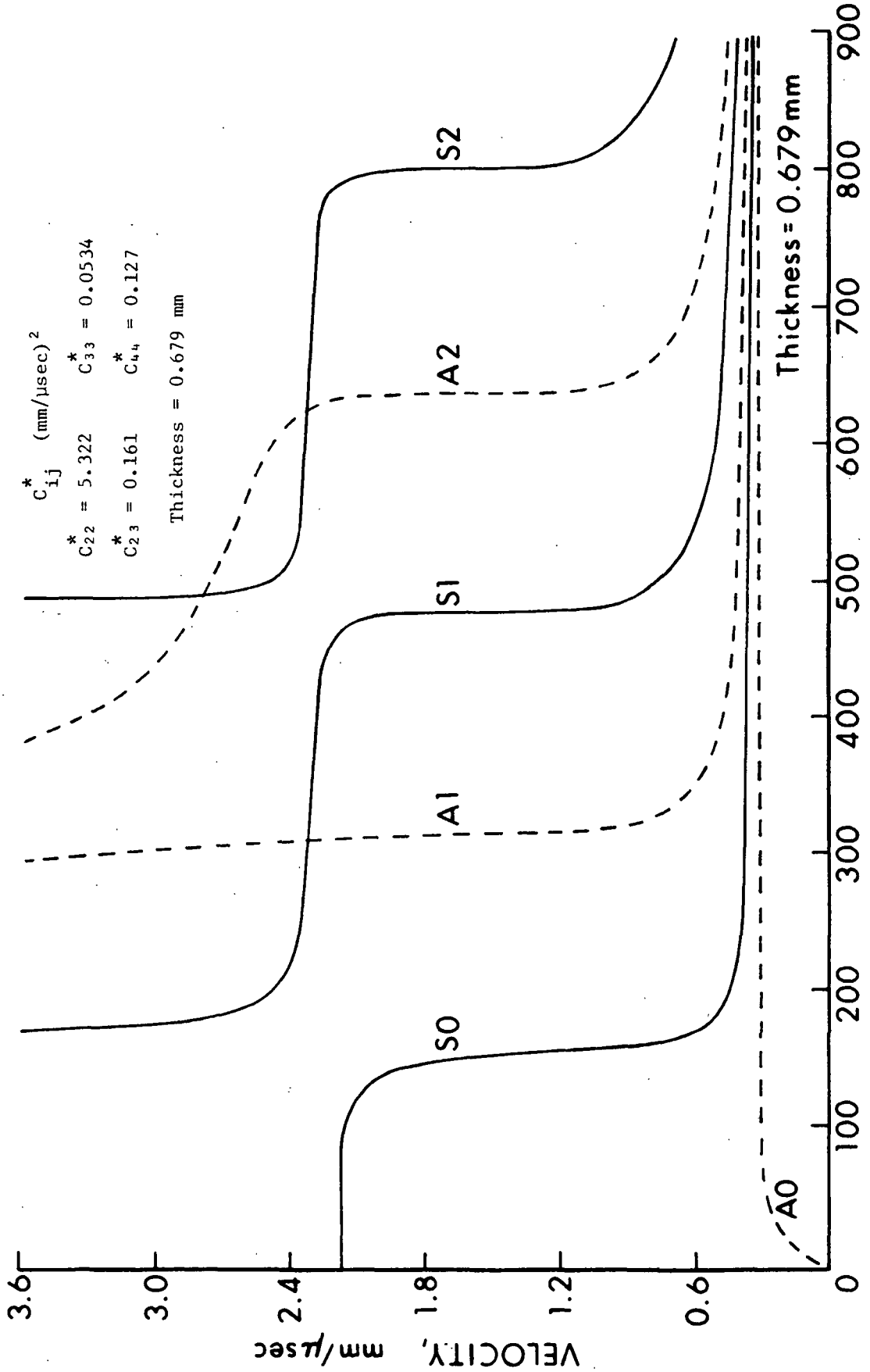

Figure 15. Theoretical Dispersion Curves for Milk Carton Stock, Y-direction Propagation

The milk carton stock dispersion curves are typical of all the board samples tested. In comparing Fig. 14 and 15 with Fig. 4, one notes several interesting features. Most obvious is a difference in the shape of the curves. For the milk carton stock, the curves are "sharper," having pronounced horizontal and vertical regions. Horizontal plateau regions are found for each of the symmetric modes. Comparing Fig. 14 and 15, it is seen that these plateau regions occur near the bulk longitudinal velocities. This velocity is higher in the case of X-direction propagation.

The nondispersive region of the SO mode is much shorter in the case of the milk carton stock. In fact, relative to Fig. 4, the dispersion curves for the milk carton stock are shifted considerably to lower frequencies. Evidence for this can also be seen in Equation (100). The velocity V_{Lz} is much lower for the milk carton stock. In essence, the low Z-direction modulus of the milk carton stock causes the SO mode to become dispersive at a relatively low frequency.

The AO mode becomes flat very quickly. The limiting velocity, very nearly equal to the Z-direction shear velocity, is much lower for the milk carton stock. The Z-direction bulk shear waves with polarization in the X and Y-directions have the same velocities as shear waves polarized in the Z-direction, propagating in the X and Y-directions, respectively. At higher frequencies, each mode approaches a surface wave. This is seen in Fig. 16, where three SO waves are depicted. As frequency increases, it is seen that the wave motion becomes increasingly localized at the surfaces.

Other waves are shown in Fig. 17 for X-direction propagation in the milk carton stock. These waves are identified in Fig. 14 by letters. The particle

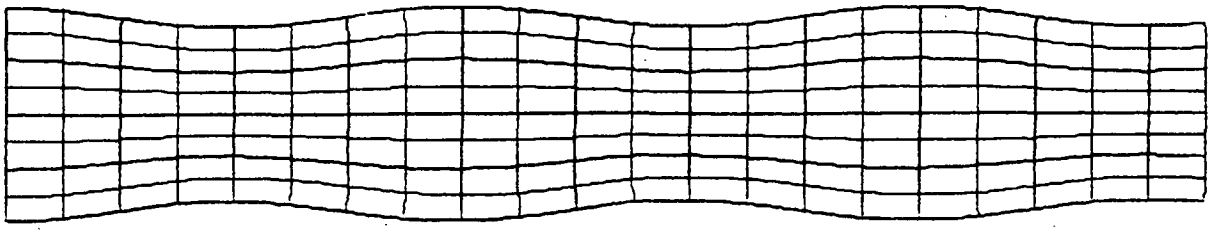

(a) A0 mode: v = 0.450 mm/usec, f = 0.276 MHz

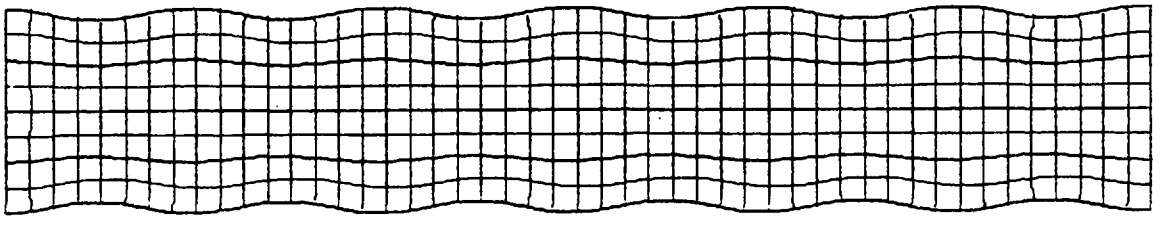

(b) A0 mode: v = 0.410 mm/usec, f = 0.602 MHz

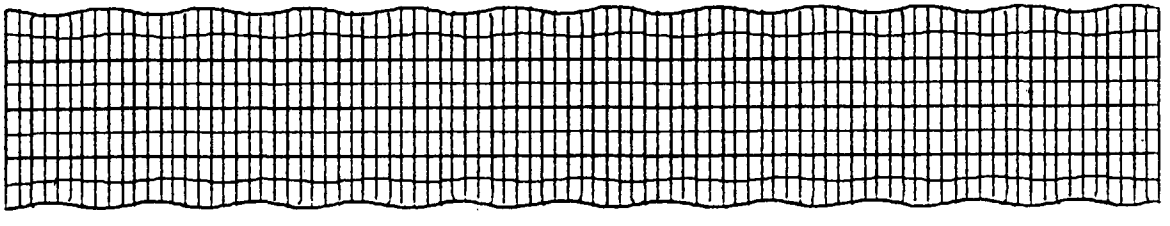

(c) A0 mode: v = 0.407 mm/usec, f = 1.114 MHz

Figure 16. A0 Plate Waves for Milk Carton Stock Showing Localization of Motion with Increasing Frequency

A

(a) S1 Mode: $V = V_{Lx}$
$= 3.279$ mm/usec

B

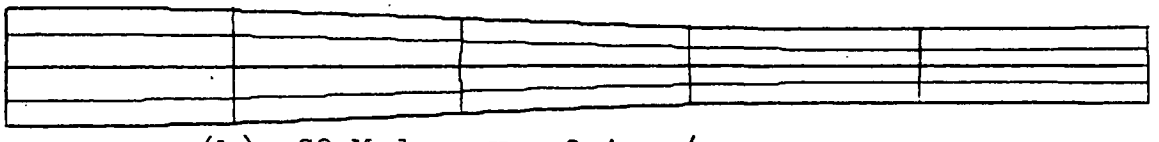

(b) S0 Mode: V = 2.1 mm/usec

C

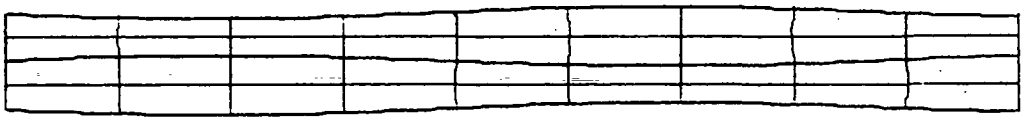

(c) A1 Mode: V = 2.1 mm/usec

D

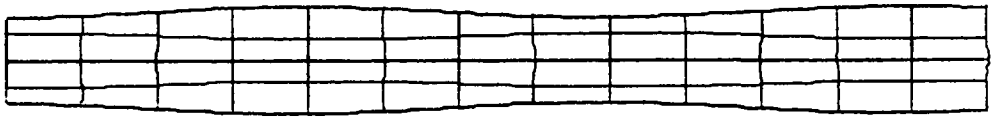

(d) S1 Mode: V = 2.1 mm/usec

E

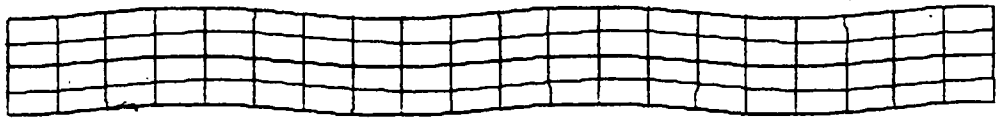

(e) A0 Mode: V = 0.38 mm/usec

Figure 17. Various Plate Waves for Milk Carton Stock (Refer to Figure 14 for Identification of These Waves on the Dispersion Curves)

displacements have been greatly exaggerated. In each case there are 8 vertical divisions per wavelength.

Wave A belongs to the S1 mode and travels at the bulk longitudinal velocity. Interestingly, the plate surfaces, in this case, do not move. Waves B, C, and D propagate at the same velocity (2.1 mm/μsec), yet constitute different modes of propagation. Several things are observed by comparing these three waves. First, the wavelength, given by V/f, decreases with increasing frequency. Second, higher order modes have more complicated displacement patterns. Third, symmetric modes have displacements which are symmetric about the midplane. Wave E belongs to the A0 mode and is sometimes called a flexural wave.

Wave patterns corresponding to those in Fig. 17 are presented in Fig. 18 for an isotropic plate ($\nu = 1/3$). The isotropic plate appears larger than the orthotropic plate in order to better show the detailed deformation. Comparing Fig. 17 and 18, one sees that, for a given location on the dispersion curves (e.g., Point A), the wavelength is longer in the case of the milk carton stock. The major difference, however, is that there is very little X-direction displacement with the milk carton stock. Motion in the Z-direction predominates.

In summary, the Z-direction properties of milk carton stock are seen to greatly affect the nature of both the dispersion curves and the displacement patterns.

EXPERIMENTAL PLATE WAVE DATA

The experimental plate wave data for the two linerboard samples and the milk carton stock are presented in Fig. 19 through 24. The plate wave resonance technique was capable of detecting only these three modes for the three heavy board samples tested because of the high signal attenuation at high frequencies.

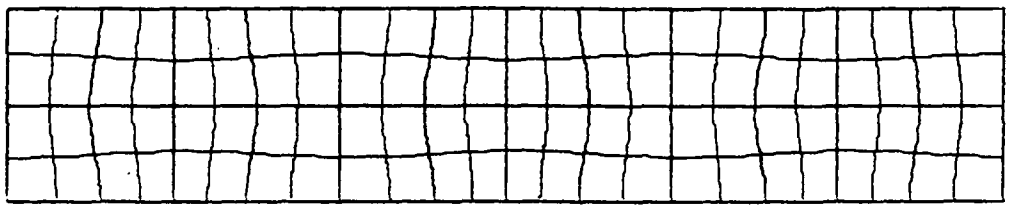

(a) S1 Mode: v = bulk longitudinal velocity
= 3.0 mm/usec

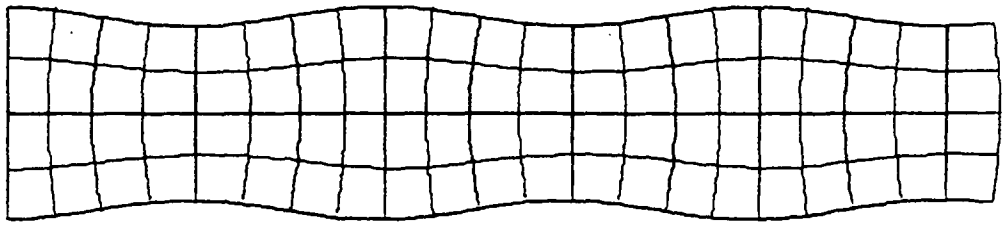

(b) S0 Mode: v = 2.1 mm/usec

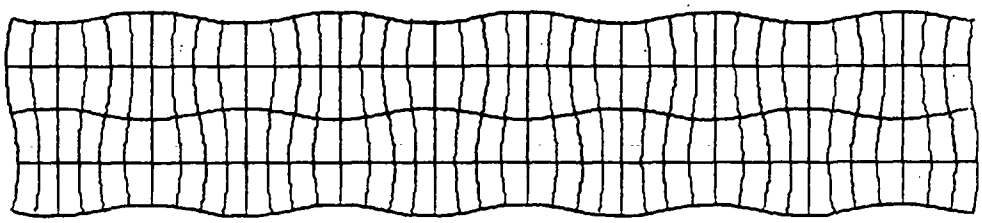

(c) A1 Mode: v = 2.1 mm/usec

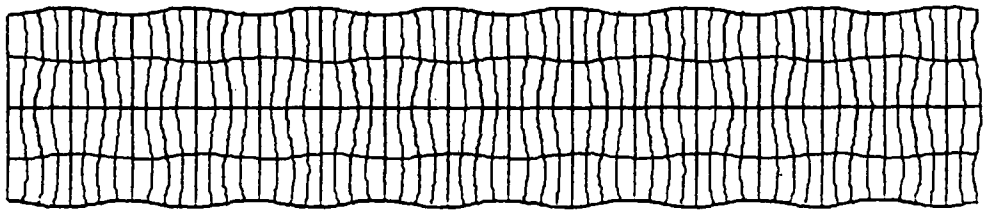

(d) S1 Mode: v = 2.1 mm/usec

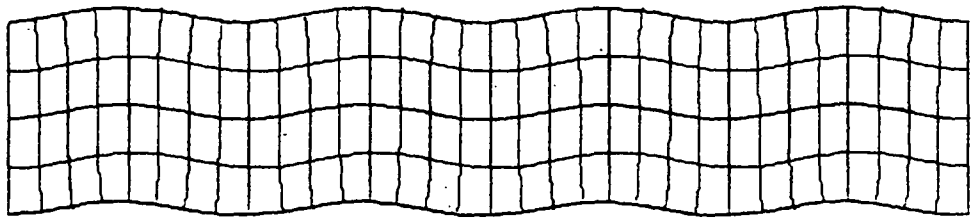

(e) A0 Mode: v = 1.3 mm/usec

Figure 18. Various Isotropic Plate Waves

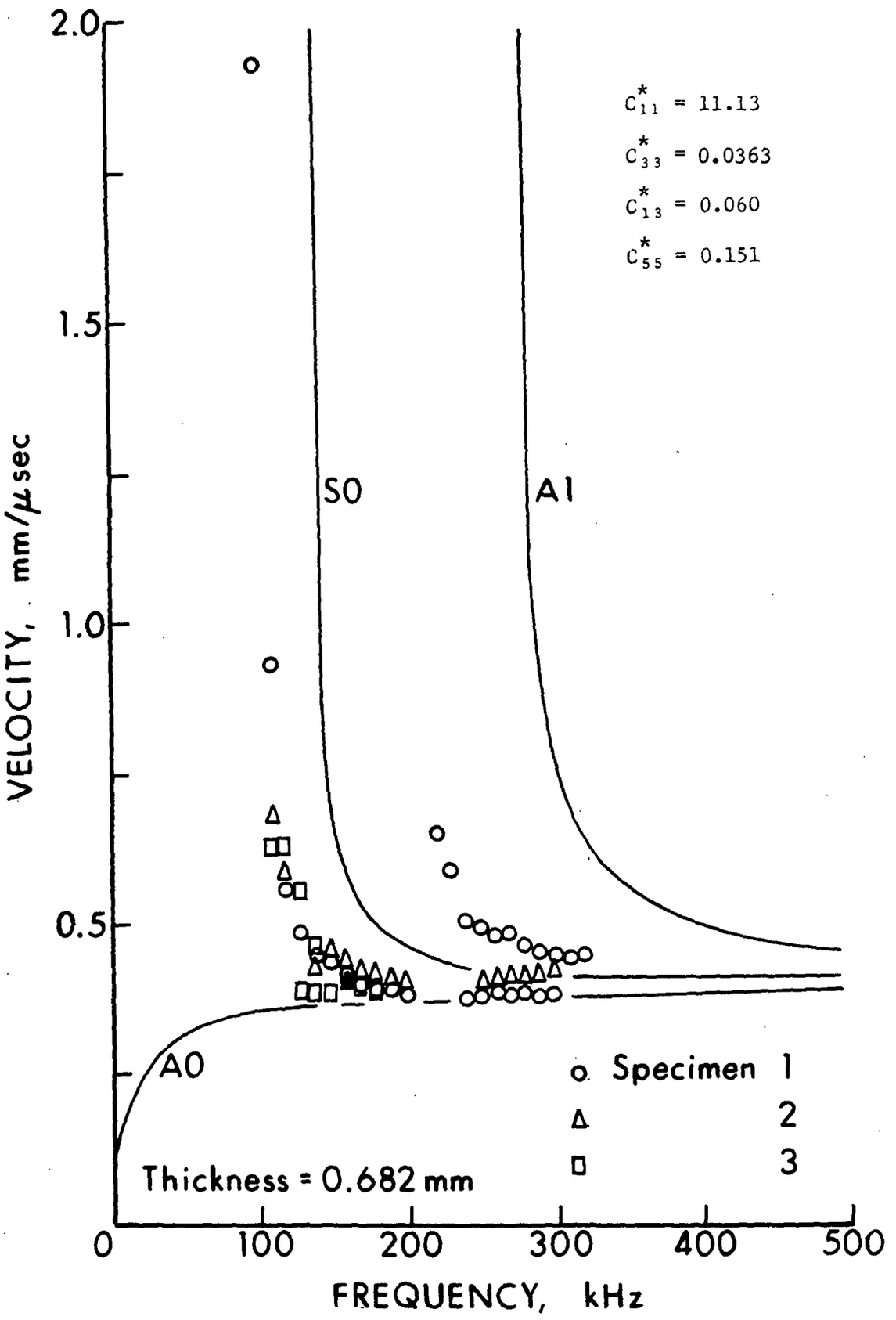

Figure 19. Theoretical and Experimental Dispersion Curves for 90 lb Linerboard Sample No. 1, X-direction Propagation

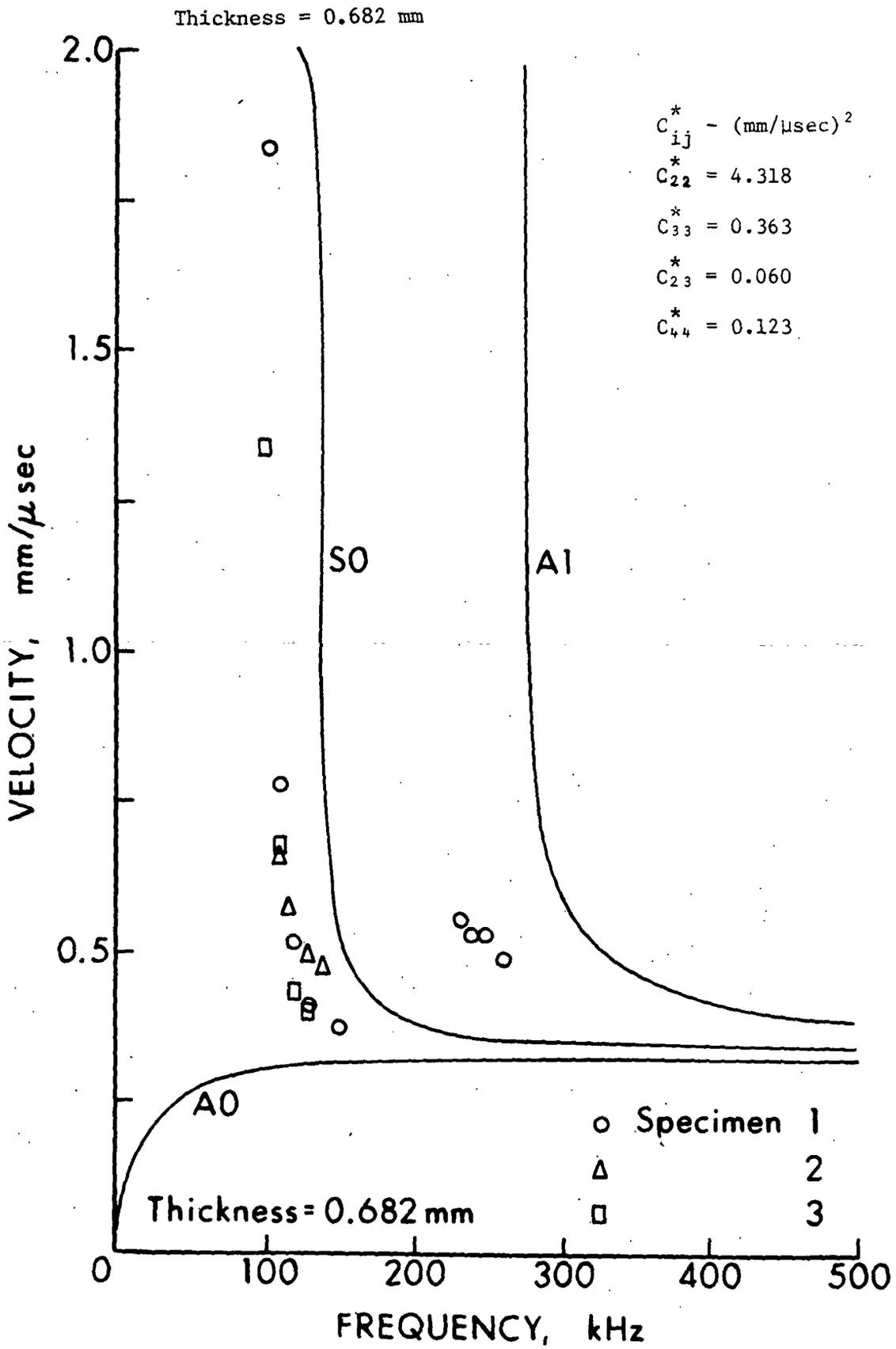

Figure 20. Theoretical and Experimental Dispersion Curves for 90 lb Linerboard Sample No. 1, Y-direction Propagation

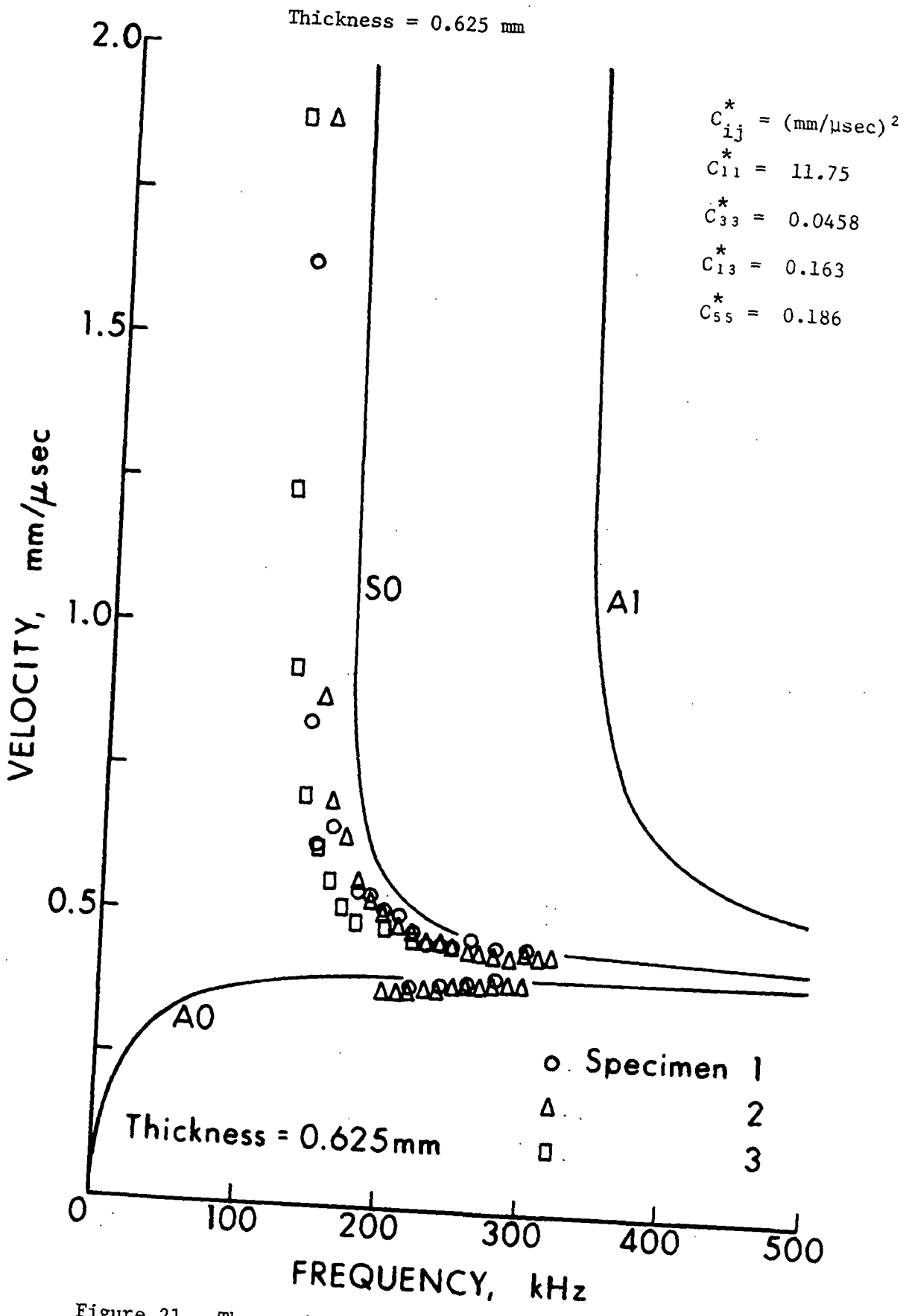

Figure 21. Theoretical and Experimental Dispersion Curves for 90 lb Linerboard Sample No. 2, X-direction Propagation

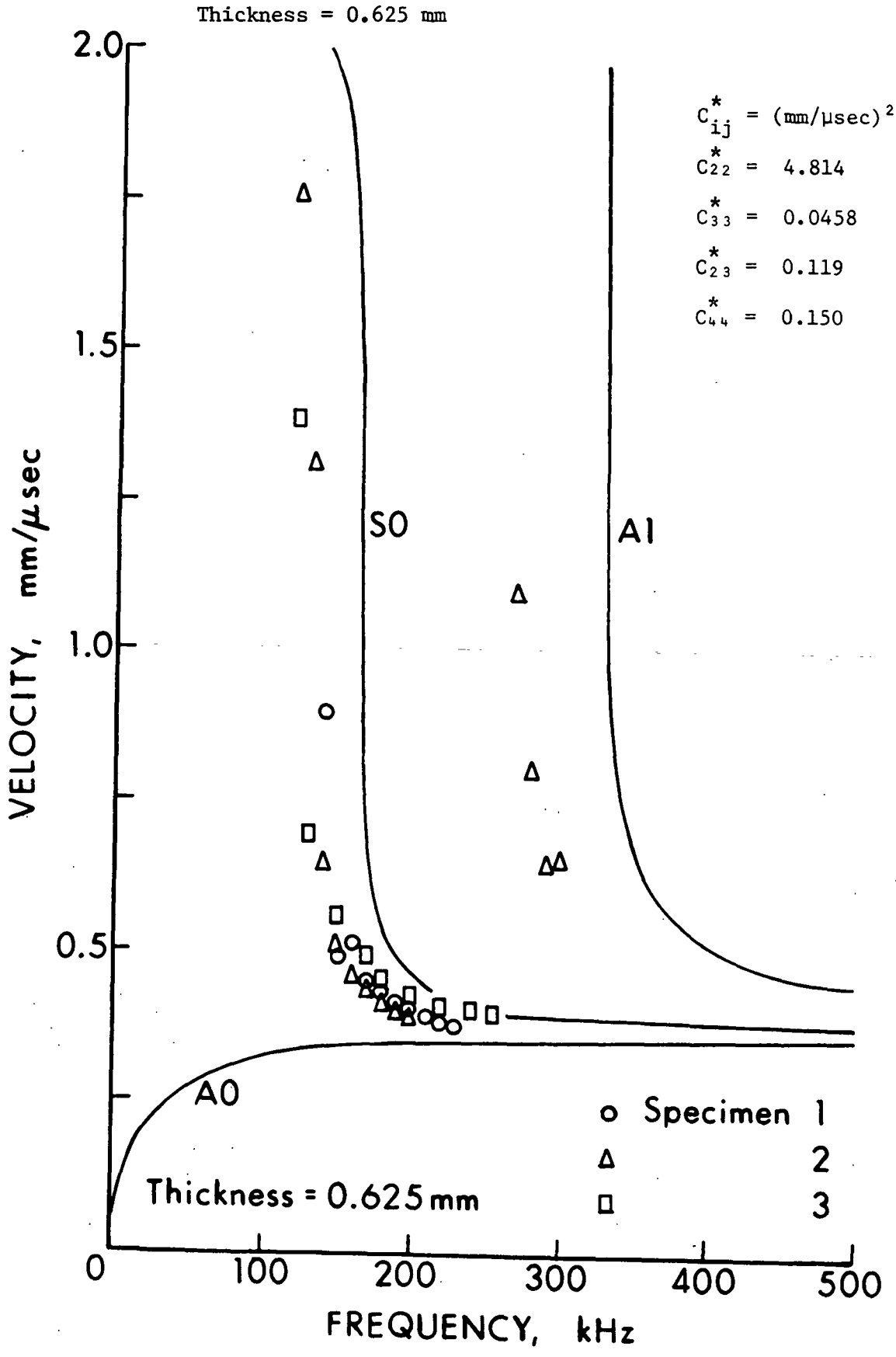

Figure 22. Theoretical and Experimental Dispersion Curves for 90 lb Linerboard Sample No. 2, Y-direction Propagation

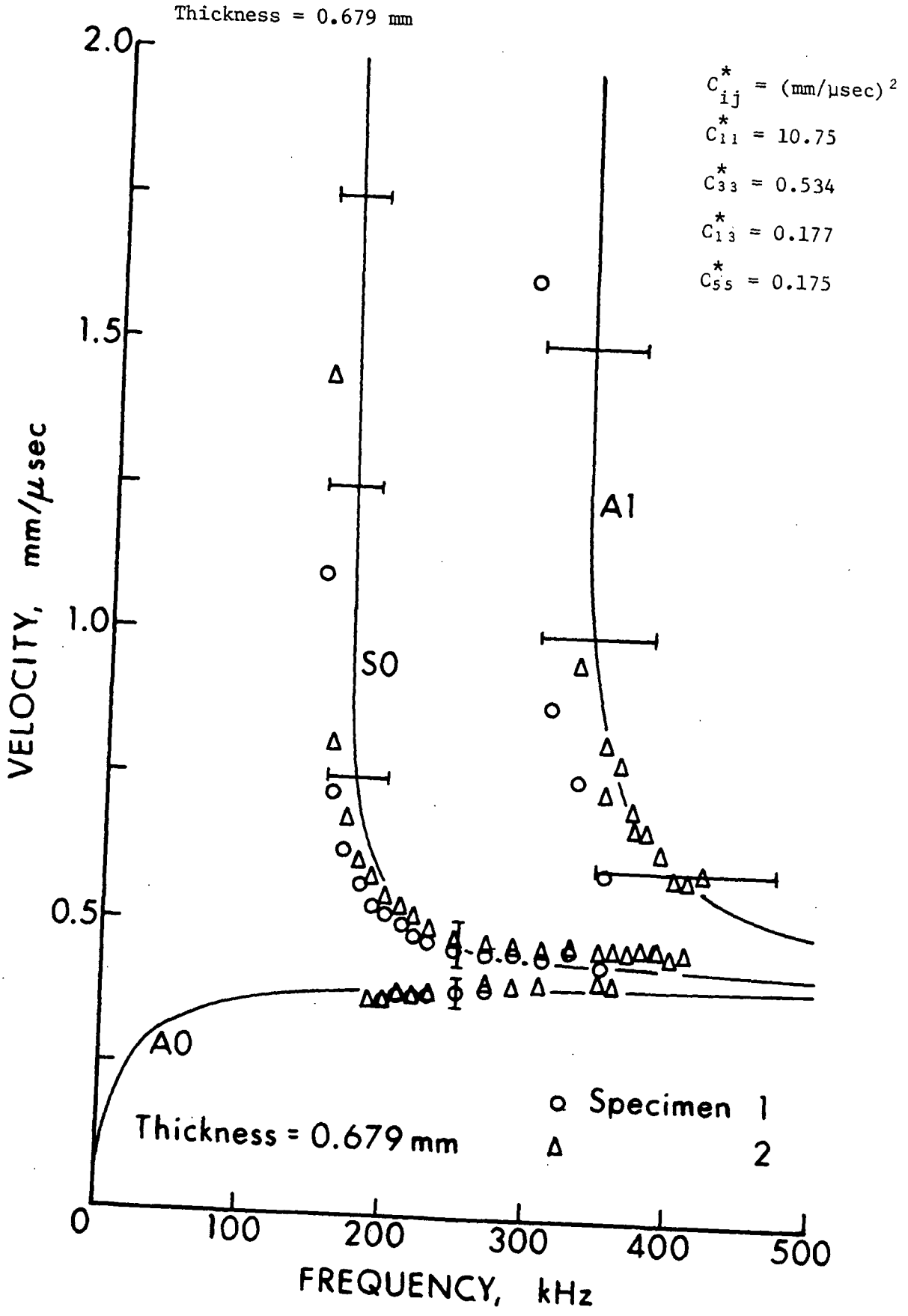

Figure 23. Theoretical and Experimental Dispersion Curves for Milk Carton Stock, X-direction Propagation

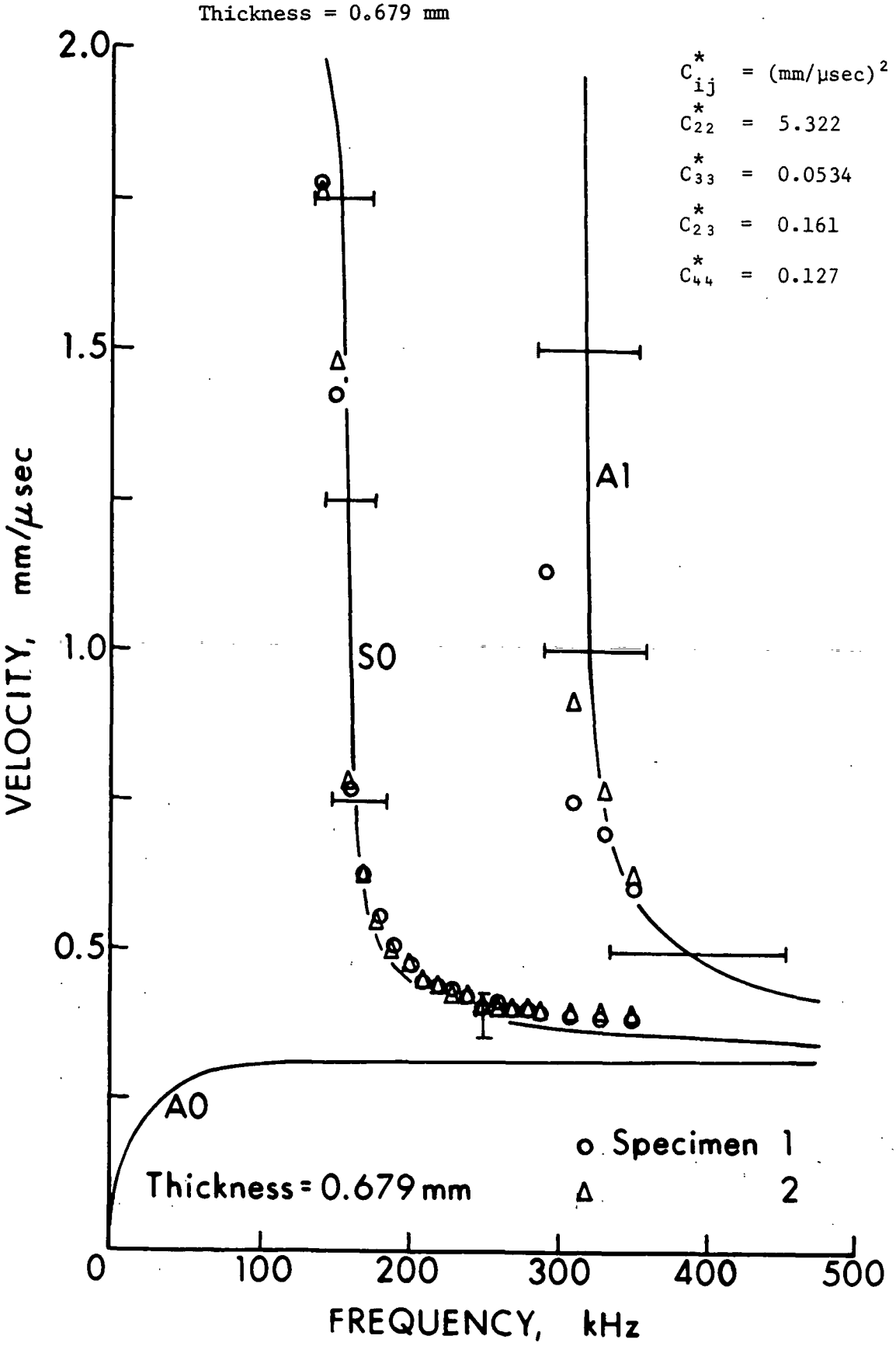

Figure 24. Theoretical and Experimental Dispersion Curves for Milk Carton Stock, Y-direction Propagation

Portions of the theoretical curves have also been presented. The experimental plate wave velocities are tabulated in Appendix IV.

From Table V it is seen that the shear velocities range between 0.351 and 0.431 mm/μsec. The lower values in this range correspond to Z-direction shear waves polarized in the Y-direction. As stated previously, the plate wave resonance technique is incapable of detecting plate waves travelling slower than about 0.38 mm/μsec. Consequently, A0 experimental data is absent from Fig. 20, 22, and 24 for Y-direction propagation.

When measuring the plate wave velocities, one could generally easily distinguish peaks on the received signal versus angle recordings. However, whenever two or more dispersion curves are in close proximity, corresponding peaks will tend to overlap. The extent of this overlap depends on how close the velocities of the modes are, but is also a function of the resolution characteristics of the measuring system. The result of this effect is either a shift in the locations of the peaks or a masking of peaks. This was not a serious problem in most cases.

The linerboard data were collected using the two smaller transducers. With this set-up, very little A1 data was obtained. For the milk carton stock, the larger transducer was used as the transmitter. This change increased the sensitivity considerably, permitting the measurement of A1 velocities at the high frequencies.

Additional plate wave data appear in Fig. 29 (see p. 125) for X-direction propagation in the milk carton stock. These S1 velocities, measured using a pulse propagation technique, constitute additional experimental evidence supporting the validity of the orthotropic wave theories.

DISCUSSION

In order to determine how well the experimental data fits the theoretically predicted dispersion curves, it is necessary to know how sensitive the dispersion curves are to errors in the parameters on which they depend. For X-direction propagation these parameters are T, C^*_{11}, C^*_{33}, C^*_{13}, and C^*_{55}. The actual measured parameters, however, are T, V_{Lx}, V_{Ly}, V_{Sx-z}, and V_{SOx}. Density is not a factor.

When one of these parameters is changed a little, the dispersion curves are shifted, while the basic shape of the curves is not altered significantly. Two quantities are defined in order to assess the sensitivity of the curves. A computer program has been written for the purpose of determining the sensitivity of these two quantities with respect to the four velocities on which they depend. Partial derivatives were calculated in each case.

The first quantity is the frequency at which the SO mode drops off. This is taken as the SO frequency which corresponds to a velocity of 1.0 mm/μsec. This frequency can be used to monitor horizontal shifts in the dispersion curves. The other quantity is the AO velocity which corresponds to a frequency of 500 kHz. This velocity can be used to monitor vertical shifts in the dispersion curves.

Since the quantities represent horizontal and vertical displacements, it is convenient to plot all of the results as vectors. This has been done in Fig. 25 for the X-direction of the milk carton stock.

Each of the vectors corresponds to one of the four velocities. The magnitude of the vector shows how sensitive the dispersion curves are to that particular velocity. The direction of the vectors is in the general direction of

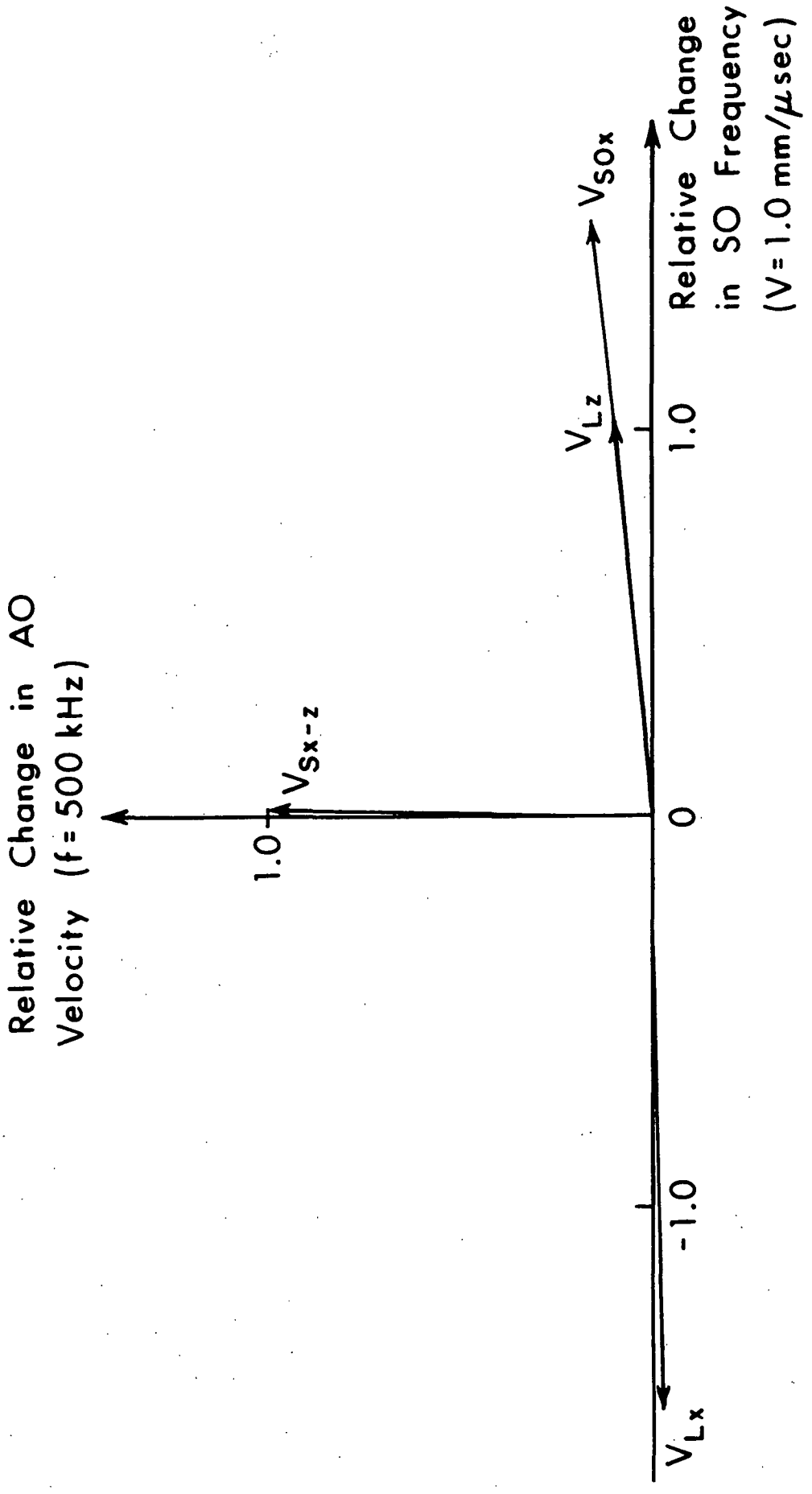

Figure 25. Polar Plot Showing how Dispersion Curves Shift with Changes in Measured Velocities

shift in the dispersion curves as the particular velocity is varied. As an example, a 1% increase in V_{Lz} would result in an equal 1% increase in the frequency at which the S0 velocity equals 1.0 mm/μsec. At the same time, the A0 velocity at 500 kHz would increase only 0.1%.

Vertical shifts are due predominantly to errors in V_{Sx-z}. This is expected in view of the previous discussion of surface waves. Horizontal shifts can result from errors in V_{Lx}, V_{Lz}, and V_{S0x}. Deviations in V_{Lx} and V_{S0x} affect horizontal shifts in an opposite sense. Consequently, it is the relative accuracy of these velocity measurements which is important. Horizontal shift is very sensitive to V_{Lz} and the thickness measurement. Dispersion curves are independent of the product of frequency and thickness. Therefore, an overestimation of thickness, T, will shift the curves to the left by a corresponding amount.

The estimated uncertainties associated with each of these parameters are given in Table VII. Limit bars appear in Fig. 23 and 24 in the case of the milk carton stock. These bars give the extremes which are accountable by the uncertainties given in Table VII. All of the data fall very close to the lower limit.

Table VII and Fig. 25 can be combined to estimate the maximum horizontal shift which is accountable by experimental error. The total amount comes to ±11%.

It is seen in Fig. 19 through 22 that in general the experimental S0 plate wave velocities for the two linerboard samples are considerably left of the predicted S0 curves. The deviation is approximately 25% for Sample No. 1, and 15% for Sample No. 2. It is concluded that these deviations cannot entirely be accounted for by experimental error.

TABLE VII

ESTIMATED UNCERTAINTIES IN THE PARAMETERS AFFECTING DISPERSION CURVES

Parameter	Estimated Uncertainty
T	± 3%
V_{Lx}, V_{Ly}	± 1%
V_{Lz}	± 5%
V_{SOx}, V_{SOy}	± 1%
V_{Sx-z}, V_{Sy-z}	± 5%

The deviations for the linerboard samples are assumed to result from two-sidedness, characteristic of double headbox fourdrinier linerboards. The top 20% of the linerboards consists of a more refined pulp. This results in a better bonded and more dense top layer. The bottoms of the linerboards were open and exhibited high fiber orientation in the machine direction. The milk carton stock is a much more homogeneous material, and the experimental results in this case were very good.

The scarcity of experimental data in Fig. 20 is indicative of problems encountered in resolving peaks for Y-direction propagation through linerboard Sample No. 1. This was the only instance of poor resolution, and it was not attributed to the experimental apparatus. It was concluded that large variations in the Y-direction elastic properties through the sheet were responsible for the poor resolution.

A second trend involves C^*_{33}. Horizontal shifts were less pronounced for higher values of C^*_{33}. C^*_{33} was lowest for linerboard Sample No. 1 and highest for the milk carton stock. To shift the predicted curves for the linerboard sample to the left it is necessary to decrease C^*_{33}. One possibility, then,

is that the Z-direction bulk velocities are too high. Since the accuracy of this velocity measurement has been estimated to be ±5%, the additional error in this velocity measurement would have to be about 15% for linerboard Sample No. 1 in order to account for the observed deviations.

CONCLUSIONS

The prediction of plate wave propagation using orthotropic bulk wave and orthotropic plate wave theories has been demonstrated for three heavy board samples. In all three cases, the form of the experimental data was found to agree with the orthotropic theory.

The experimental plate wave data for the two linerboard samples were found to deviate from theoretical predictions by more than was expected considering measurement uncertainties. It has been suggested that this anomalous behavior results from a two-sidedness which characterizes both linerboard samples. The milk carton stock was more homogeneous, and, in this case, close correlation of experimental data to the predicted dispersion curves was found.

These results clearly demonstrate the validity of using these theories. It is concluded that, in general, machine-made paper can be considered a three-dimensional orthotropic material. Orthotropic wave theories, developed assuming a continuous homogeneous material, apply to paper.

DETERMINATION OF C_{12} AND C_{66}

In order to predict plate wave dispersion curves for both X and Y-direction propagation through orthotropic plates, it was necessary to specify seven of the nine orthotropic stiffness coefficients. The determination of these seven constants was the subject of previous discussion. The two remaining stiffness coefficients are C_{12} and C_{66}.

C_{66} is most easily determined by propagating either shear bulk waves or shear plate waves in the X or Y-direction. C_{12}, on the other hand, can only be determined by propagating waves in the X-Y plane in a direction other than along the principle axes.

In the sections below, various ways of evaluating these remaining two orthotropic stiffness constants are discussed. Of particular interest are measurement techniques which simplify the determination of these elastic constants.

GOVERNING EQUATIONS

The equations which govern longitudinal and shear wave propagation in the X-Y plane, from Equations (53) and (54), are as follows:

$$\rho V_L^2(\theta) = \tfrac{1}{2}(c^2C_{11}+s^2C_{22}+C_{66}) + \tfrac{1}{2}[(c^2(C_{11}-C_{66}) + s^2(C_{66}-C_{22}))^2 + 4c^2s^2(C_{12}+C_{66})^2]^{\frac{1}{2}} \quad (112)$$

$$\rho V_S^2(\theta) = \tfrac{1}{2}(c^2C_{11}+s^2C_{22}+C_{66}) - \tfrac{1}{2}[(c^2(C_{11}-C_{66}) + s^2(C_{66}-C_{22}))^2 + 4c^2s^2(C_{12}+C_{66})\ ]^{\frac{1}{2}}, \quad (113)$$

where $c = \cos\theta$

$s = \sin\theta$

θ = angle between propagation direction and X-direction

V_L = longitudinal velocity

V_S = shear velocity

Equations (112) and (113) are valid theoretical relationships for bulk materials. In addition, it can be shown that these equations are also valid for thin materials in the zero frequency limit (57). In the latter case,

the planar orthotropic stiffness coefficients must be used. In either case, C_{66} (= C'_{66}) is given by the following expression:

$$C_{66} = \rho V_S^2(0°) = \rho V_S^2(90°) \tag{114}$$

Since C_{12} appears in both Equations (112) and (113), it can be determined by propagating either longitudinal or shear waves. A convenient angle for wave propagation is 45°. In this case, C_{12} is given by either of the following relationships:

$$C_{12} = [(2\rho V_L^2(45°) - \tfrac{1}{2}(C_{11}+C_{22}) - C_{66})^2 - ((C_{11}-C_{22})/2)^2]^{\frac{1}{2}} - C_{66} \tag{115}$$

$$C_{12} = [(2\rho V_S^2(45°) - \tfrac{1}{2}(C_{11}+C_{22}) - C_{66})^2 - ((C_{11}-C_{22})/2\ ^2]^{\frac{1}{2}} - C_{66} \tag{116}$$

A third possibility involves measuring both $V_L(45°)$ and $V_S(45°)$. In this case:

$$C_{12} = [(\rho V_L^2(45°) - \rho V_S^2(45°))^2 - ((C_{11}-C_{22})/2)^2]^{\frac{1}{2}} - C_{66} \tag{117}$$

Assuming that $V_L(45°)$ and $V_S(45°)$ can be measured with the same accuracy, it can be argued that Equation (116) is generally more accurate. This stems from the fact that $V_L(45°) > V_S(45°)$. Consequently, the maximum error in $V_S^2(45°)$ will be less than the maximum error in $V_L^2(45°)$. Therefore, Equation (116) has been selected for determining C_{12}.

MILK CARTON STOCK RESULTS

The resulting bulk shear velocities for the milk carton stock are given in Table VIII. These velocities represent shear wave propagation through three glued stacks. No correction was made for the effect of the glue. This effect should be very small as discussed earlier.

TABLE VIII

BULK SHEAR VELOCITIES FOR X-Y PLANE PROPAGATION THROUGH MILK CARTON STOCK

θ	$V_S(\theta)$ (mm/μsec)	$V_S^2(\theta)$ ($mm^2/\mu sec^2$)
0°	1.613	2.602
45°	1.596	2.549
90°	1.618	2.616

C_{66}^* is taken to be average of V_S^2 at 0 and 90°, i.e., 2.609 $mm^2/\mu sec^2$. As before, the stiffness coefficients are normalized with respect to density. Equation (116) is then used to determine C_{12}^*, yielding a value of 2.229 $mm^2/\mu sec^2$.

DISCUSSION

C_{12}' can be determined using Equation (116) by measuring $V_S(45°)$ through the plate material and by using the planar stiffness coefficients:

$$C_{11}' = \rho V_{S0x}^2 \tag{118}$$

$$C_{22}' = \rho V_{S0y}^2 \tag{119}$$

The bulk C_{12} is then given as follows:

$$C_{12} = C_{12}' + C_{13}C_{23}/C_{33} \tag{120}$$

The advantage of this method is that only two in-plane bulk velocities must be measured. These are V_{Lx} and V_{Ly}. This simplifies the procedure in that only two rather than three glued stacks are required. Also, errors associated with the gluing of stacks are reduced.

The closeness of the three shear velocities in Table VIII seems to be characteristic of many paper grades. Similar results were obtained by others

(20). Simplifying expressions result for C_{12} when various assumptions are made with respect to the in-plane shear velocity.

If it is assumed that $V_S(0°) = V_S(45°) = C_{66}$, the following relationship results from Equation (113):

$$C_{12} = (C_{66}^2 - C_{66}(C_{11}+C_{22}) + C_{11}C_{22})^{\frac{1}{2}} - C_{66} \tag{121}$$

For milk carton stock, Equation (121) predicts a value of 2.091 $mm^2/\mu sec^2$ for C_{12}^*, compared with 2.229 $mm^2/\mu sec^2$ as previously determined. An expression identical to Equation (121) results if one assumes that $V_S(0°) = V_S(\phi)$, where ϕ is the special angle for which the shear and longitudinal modes become pure modes. Furthermore, Equation (121) is also obtained when $V_S(45°) = V_S(\phi)$ is assumed. It follows, then, that when C_{12} is given by Equation (121), $V_S(0°) = V_S(45°) = V_S(\phi)$.

For the milk carton stock, these three velocities are as follows:

$$V_S(0°) = 1.613 \text{ mm/}\mu\text{sec}$$
$$V_S(45°) = 1.596 \text{ mm/}\mu\text{sec}$$
$$V_S(\phi) = 1.595 \text{ mm/}\mu\text{sec},$$

where $\phi = 52.7°$. It is evident that the assumption that $V_S(45°) = V_S(\phi)$ is a very good one, at least in this case. Setting $V_S^2(45°)$ equal to $V_S^2(\phi)$ in Equation (62) gives the following relationship:

$$C_{12}^* = (V_S^4(45°) - V_S^2(45°)(C_{11}^*C_{22}^*) + C_{11}^*C_{22}^*)^{\frac{1}{2}} - V_S^2(45°) \tag{122}$$

The value for C_{12}^* obtained from Equation (122) is 2.220 $mm^2/\mu sec^2$. This value is very close to the value of 2.229 $mm^2/\mu sec^2$ obtained using the exact relationship of Equation (116).

A third approximation is obtained when Campbell's relationship is assumed. Campbell's relationship implies that the shear modulus is independent of angle θ. It can be shown that this will be true if and only if $C_{66}(0°) = C_{66}(45°)$. Now, the shear modulus is related to angle as follows:

$$C_{66}(\theta) = (c^2-s^2)^2 C_{66} + c^2 s^2 (C_{11}+C_{22}-2C_{12}) \tag{123}$$

Campbell's relationship reduces, then, to:

$$C_{66}(0°) = C_{66} = \tfrac{1}{4}(C_{11}+C_{22}-2C_{12}) \tag{124}$$

C_{12} is then given as follows:

$$C_{12} = \tfrac{1}{2}(C_{11}+C_{22}-4C_{66}) \tag{125}$$

For the milk carton stock, Equation (125) predicts a value of 2.818 $mm^2/\mu sec^2$ for C_{12}^*.

Equation (122) undoubtedly gives a very good approximation to C_{12}^* for paper. ϕ from Equation (60) will be between about 50° and 57° for most machine-made paper. The shear velocity, as given by Equation (113), varies very gradually with angle. Consequently, $V_S(45°)$ and $V_S(\phi)$ should be very nearly equal for all machine-made papers.

The first assumption made, that $V_S(0°) = V_S(45°)$, is not as good, since $V_S(0°)$ is greater by 1.1%. However, if $V_S^2(45°)$ is used in Equation (121) instead of C_{66}, i.e., $V_S^2(0°)$, then the resulting expression is identical to Equation (122). The third approximation invoking Campbell's relationship leads to a very inaccurate prediction of C_{12}^*.

Equation (122) can also be used for thin materials. In this case, the shear velocity is measured on the plate material and C_{11} and C_{22} are replaced

with C'_{11} and C'_{22} of Equations (118) and (119). Now, the in-plane Poisson ratio, ν_{12}, is equal to C'_{12}/C'_{11}. Therefore, Equation (122) can be used to directly evaluate ν_{12}. The resulting expression is as follows:

$$\nu_{12} = A^2 - A(1+R) + R)^{\frac{1}{2}} - A, \tag{126}$$

where $A = V_S^2(45°)/V_{SOx}^2$

$R = V_{SOy}^2/V_{SOx}^2$

Equation (126) is identical to the one used by Bornhoeft (11) in her Poisson ratio determinations of various linerboards. For the milk carton stock, ν_{12} calculated from Equation (126) is 0.165, which is 0.9% less than the true value. For this calculation a planar value for $V_S(45°)$ was calculated using Equations (116) and (118)-(120).

It is concluded that C_{12}, C'_{12}, and ν_{12} can all be very nearly approximated by making three independent velocity measurements in the X-Y plane rather than four, if the shear velocity at 45° is used in the equations rather than the shear velocity at 0°. It is also concluded that Campbell's relationship is invalid.

The most accurate and direct way to approximate ν_{12} is on thin paper specimens, using Equation (126). Three velocity measurements are required, including longitudinal velocities along the X and Y-directions, and the shear velocity at 45°.

MEASUREMENT OF V_{Lx} AND V_{Ly} ON SINGLE THICKNESS SHEETS

INTRODUCTION

The in-plane bulk longitudinal velocities, V_{Lx} and V_{Ly}, are important in several ways. By themselves, they determine C_{11} and C_{22}, respectively. Together

with V_{Lz}, V_{SOx}, and V_{SOy}, these bulk velocities determine C_{13} and C_{23}. C_{13} and C_{23} dominate the determination of the out-of-plane Poisson ratios. For instance, ν_{31} is given, from Equation (21), as follows:

$$\nu_{31} = (C_{13}C_{22}-C_{12}C_{23})/(C_{22}C_{33}-C_{23}^2) \qquad (21)$$

The accuracy of the method previously discussed for determining C_{13} and C_{23} depends greatly on the relative accuracy of the in-plane bulk longitudinal and SO velocity measurements. This fact is apparent from Equations (110) and (111). Since the bulk and SO velocities differ by only a few percent (see Table V), it is necessary to measure these velocities very accurately. Improved techniques for doing this are discussed in this section.

A useful outcome of the work has been the observation that plateau regions exist for the symmetric modes. As discussed earlier, these are characteristic of materials like paper which have relatively little Z-direction stiffness. These nondispersive plateau regions are found to occur very close to the bulk longitudinal velocities. This is illustrated for the milk carton stock in Fig. 26 and 27. The bulk longitudinal velocities are indicated by the broken lines. Apparently, with the low Z-direction stiffness, the plate behaves very much like a bulk material. The tendency for the symmetric modes to propagate at nearly the bulk velocities over such a wide frequency range is evidence of this.

The effect of changing C_{33}^* on these plateau regions can be seen in Fig. 28. Curve 1 corresponds to X-direction propagation through the milk carton stock. Curve 2 represents a hypothetical material which has a much higher C_{33}^* value. In this case, C_{33}^* was taken to be 0.8544 $mm^2/\mu sec^2$, compared to 0.0534 $mm^2/\mu sec^2$ for the milk carton stock. C_{11}^* was kept the same so that the bulk longitudinal velocity would be the same. In general, as C_{33}^* increases, the slope of the S1 curve becomes steeper.

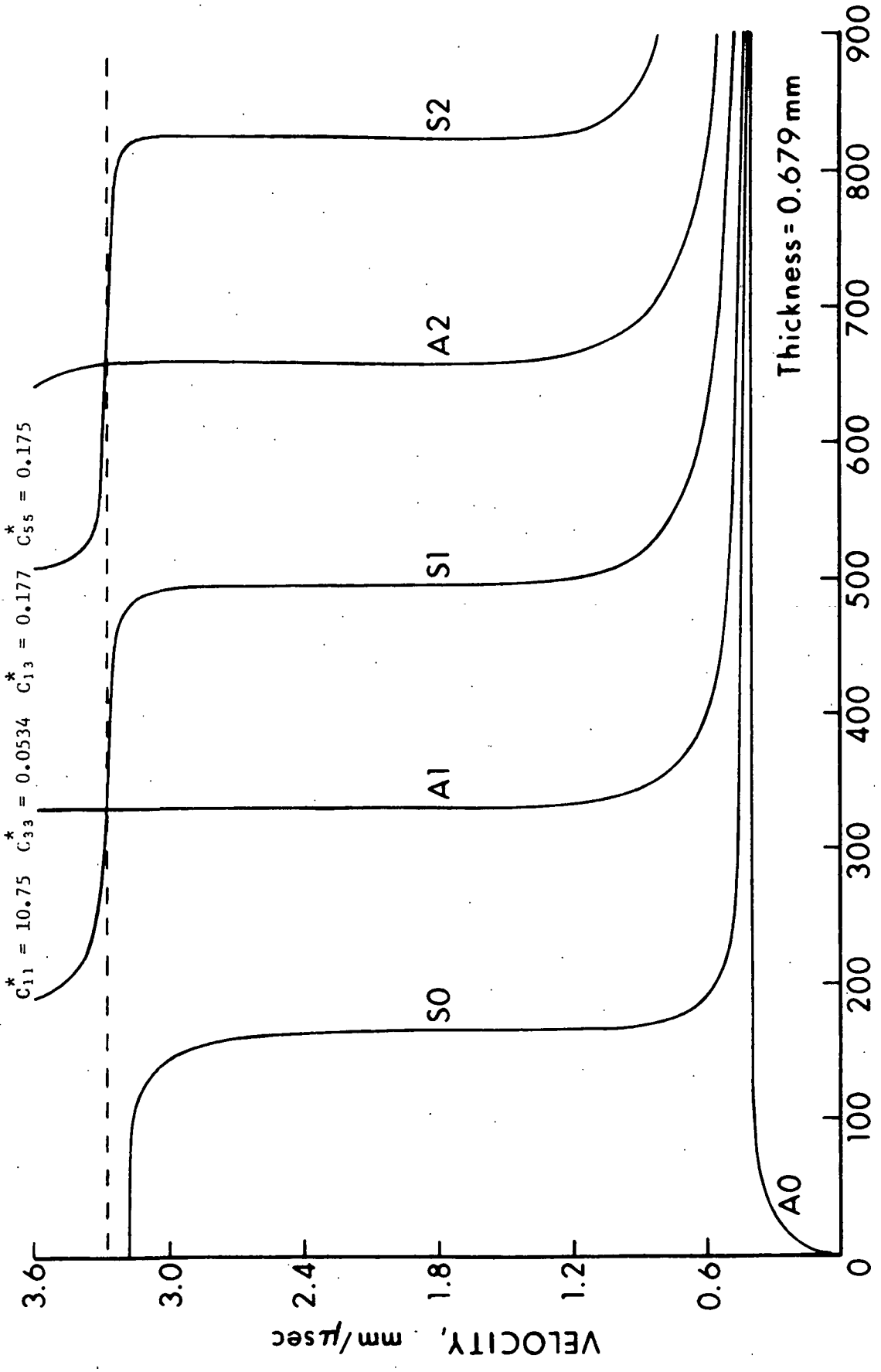

Figure 26. Theoretical Dispersion Curves for Milk Carton Stock, X-direction Propagation

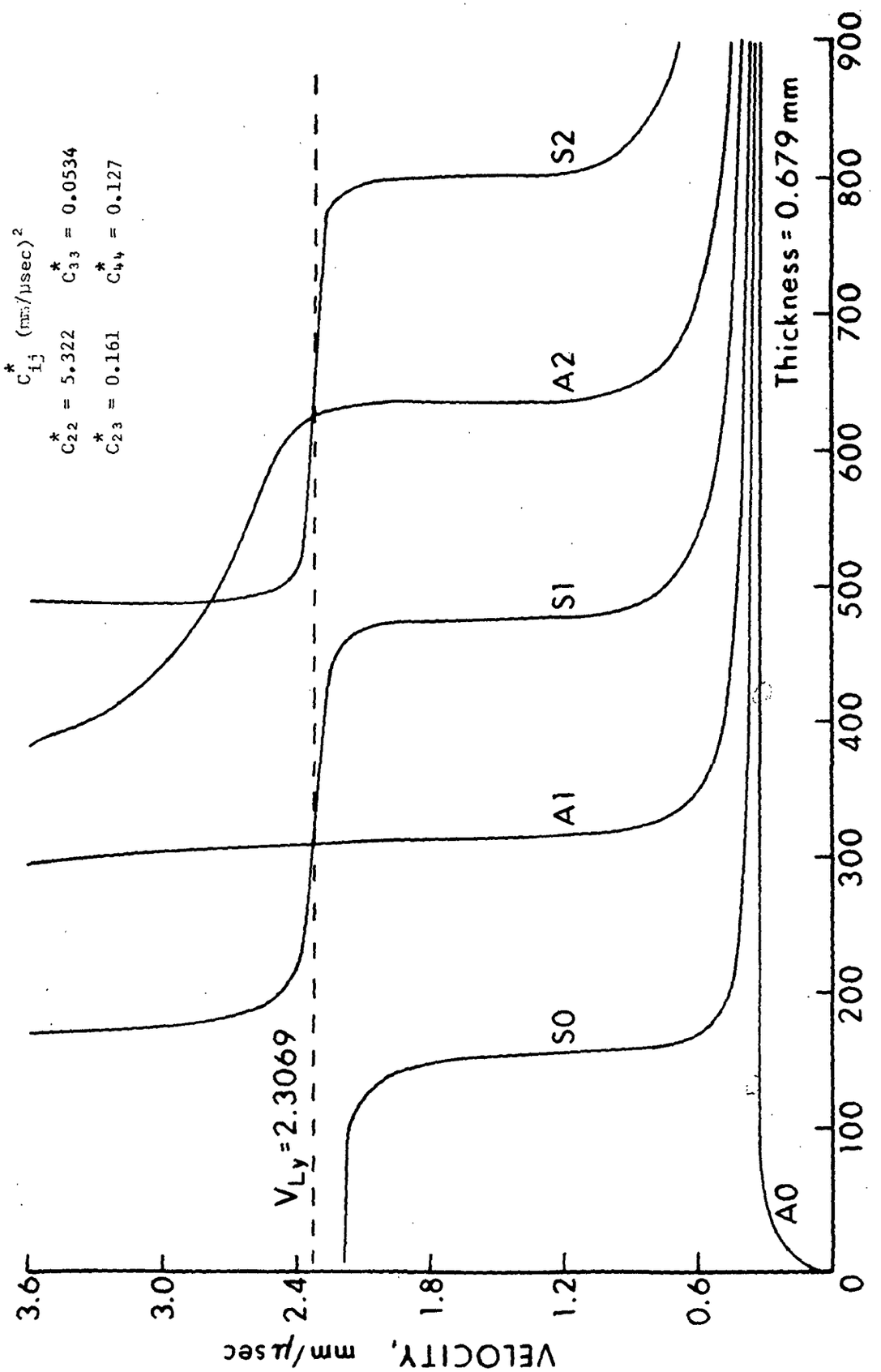

Figure 27. Theoretical Dispersion Curves for Milk Carton Stock, Y-direction Propgation

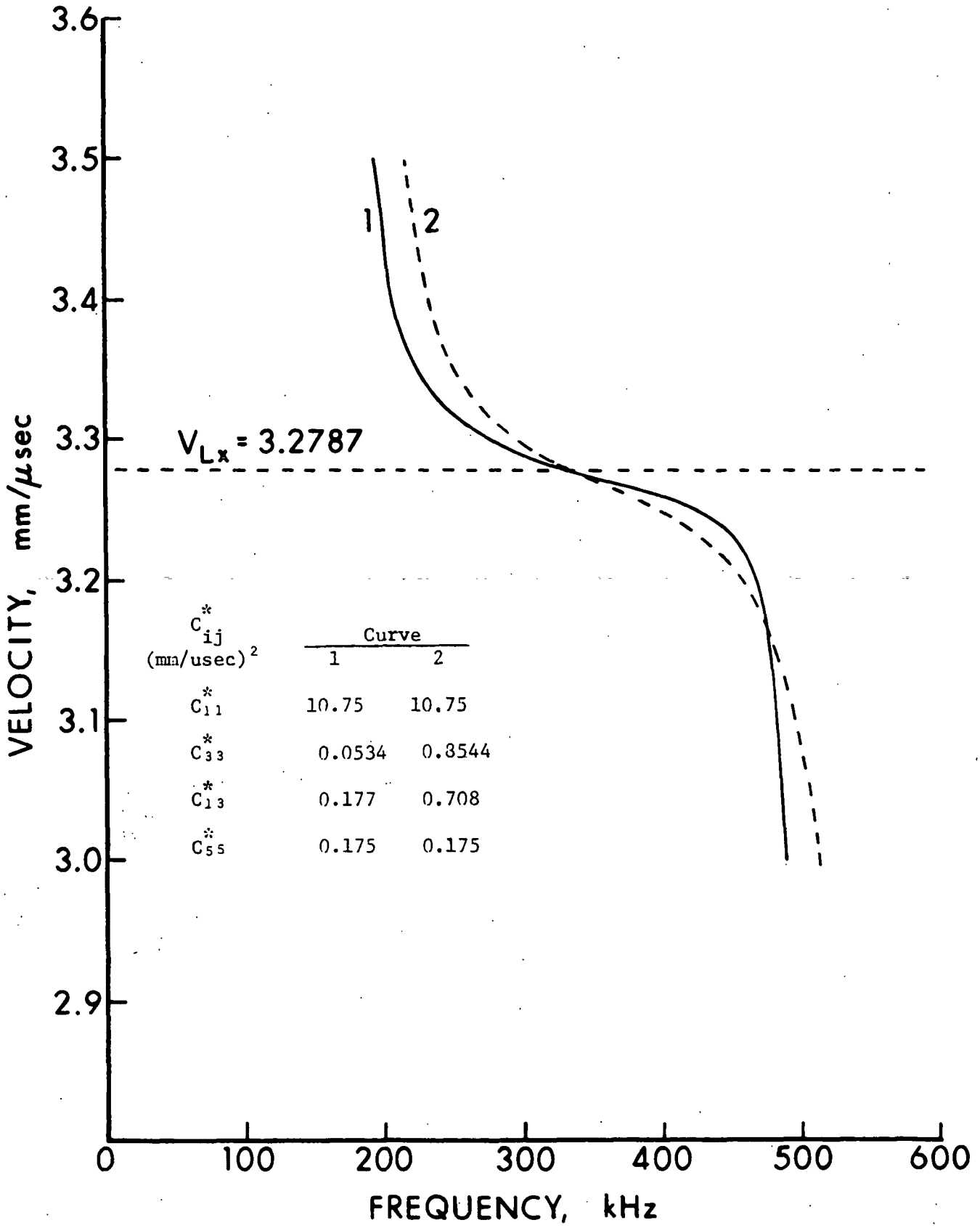

Figure 28. S1 Plateaus for Milk Carton Stock (Curve 1) and Hypothetical Sample Having a Much Higher C_{33} (Curve 2)

The frequency for which the S1 velocity is exactly equal to the bulk velocity is given by Equation (100):

$$f_1 = \frac{V_{Lz}}{T} \left[\frac{1}{\frac{1 + C_{13}(C_{13}+2C_{55})}{C_{11}C_{55}}} \right]^{\frac{1}{2}} \qquad (100)$$

The square root term is very nearly equal to unity (actually 0.976) in the case of the milk carton stock. This will be the case whenever C_{11} is much greater than C_{13} and C_{55}. For paper, this is probably a reasonable expectation. It is seen, then, that Equation (100) can be used to easily and accurately estimate the frequency for which the S1 plate wave velocity is equal to the bulk longitudinal velocity.

Bulk longitudinal velocities can be measured on single thickness specimens. To do so, one needs only to first measure the Z-direction bulk longitudinal velocity. Equation (100) can then be used to determine the frequency at which to propagate the S1 plate wave.

An alternative method is to construct the plateau regions of the S1 curve experimentally. As an approximation, the bulk longitudinal velocity would be taken as the point of inflection on the experimental curves. This would require the measurement of several S1 velocities over the frequency range spanning the nondispersive plateau region.

Not shown in Fig. 28 are the locations of inflection points on the curves. It was initially thought that inflection points were located at the bulk velocities. A separate computer program was written to generate these dispersion curves. This program was capable of calculating the slope of the curve as a function of frequency. Hence, these inflection points were easily located.

In Fig. 28, the bulk velocity is 3.2787 mm/μsec and f_1 is 332 kHz. The inflection point for the milk carton stock, Curve 1, occurs at a velocity of 3.2720 mm/μsec and a frequency of 357 kHz. In the second case, the inflection point is further from the bulk velocity, at 3.2645 mm/μsec. This trend was found to hold for other values of C_{33}^*. As C_{33}^* increased, the velocity at the inflection point was found further from the actual bulk longitudinal velocity. In general, these velocities should be very close for paper.

The existence of plateau regions should make it possible to measure plate wave velocities in these flat regions with pulse propagation techniques. Furthermore, the use of Equation (100) to compute the frequencies which correspond to the bulk longitudinal velocities should permit the determination of these bulk velocities, V_{Lx} and V_{Ly}. A second possibility is to use the frequency of the inflection point determined experimentally for this purpose. Though the two frequencies differ by roughly 10%, the error in the measured bulk velocity will be small due to the small plateau slope.

EXPERIMENTAL TECHNIQUE

The nondispersive S1 velocities were measured using the same technique used to measure S0 velocities employing contact transducers. In this case, 1 MHz immersion transducers were used instead of the 5 MHz transducers because the former functioned better at these higher frequencies.

Sample preparation was the same as before, though the specimens tended to be narrower due to higher attenuation. Vacuum grease was used to improve the coupling of transducers to specimens.

The thickness of the specimen is important in three ways. First, the thickness of the specimen greatly affects f_1, the frequency for which the S1

plate velocity equals the bulk longitudinal velocity. For thin sheets this frequency will be high, and attenuation may be too severe. Second, thicker sheets will contact the transducers over a larger area, thereby reducing signal losses. Third, thicker sheets are generally more rigid, capable of withstanding contact pressure applied to the transducers.

The specimen width is important also. The maximum specimen width is determined by the degree of attenuation at the operating frequency. Generally, a width of 6 inches was the limit. The lower limit is determined by the occurrence of interference due to reflections. Delay times were typically measured out to Peak 4 through 8 on the received pulse. This insured that measurements were made to the undistorted middle region of the pulse. It was necessary, then, that the first echo arrive later than about 8 periods in order to preclude interference effects. The minimum width for this was usually 2 to 3 inches.

As with the SO velocity measurements, various schemes can be used for measuring time delays. One method was to make several delay time measurements first along a 6-inch wide specimen. A 1/2-inch strip would be trimmed off the specimen, and delay time measurements would be repeated on the narrower specimen. This procedure would be repeated until the lower specimen width limit was reached. A linear regression of the average delay time versus specimen width data would yield an average velocity representing that part of the specimen which was trimmed off.

More commonly, after the initial delay time measurements, the 6-inch specimen would be cut in half and time delay measurements would be made on both 3-inch pieces. The velocity calculated this way would represent all of the original specimen. This method requires fewer delay time measurements for a given level of accuracy.

The results for X-direction propagation through the milk carton stock are presented in Fig. 29. Velocities were calculated at several frequencies. A portion of the predicted S1 curve is included for comparison. It is seen that the experimental curve follows the predicted curve closely. The deviation of about 2% in the velocities is not unexpected, since only one specimen was tested. The bulk longitudinal velocity, V_{Lx}, is determined by computing the crossover frequency, f_1, and reading the velocity at this frequency off the experimental curve. Normally, one would compute this frequency first, and then measure just the one velocity at this frequency.

These results clearly indicate that pulse propagation techniques can be used to measure plate velocities in regions where the velocity is not a strong function of frequency. This technique is particularly useful, though, when SO velocities are determined concurrently. When this is done using the same specimens, the resulting velocities, e.g., V_{SOx} and V_{Lx}, will have been measured with high relative accuracy. This high relative accuracy is required in order to determine C_{13} and C_{23} accurately.

RESULTS AND DISCUSSION

V_{SOx} and V_{Lx} were determined for the milk carton stock on four specimens cut from four 14-inch by 28-inch sheets. The same material was used in each velocity measurement. A frequency of about 340 kHz was used to determine V_{Lx}. Results are presented in Table IX.

The absolute accuracies of these measurements are not easily determined. The differences between velocities calculated using delay times to different peaks give some indication of experimental error. In the V_{SOx} measurement at 50 kHz, the delay times out to the first peaks were recorded. A velocity

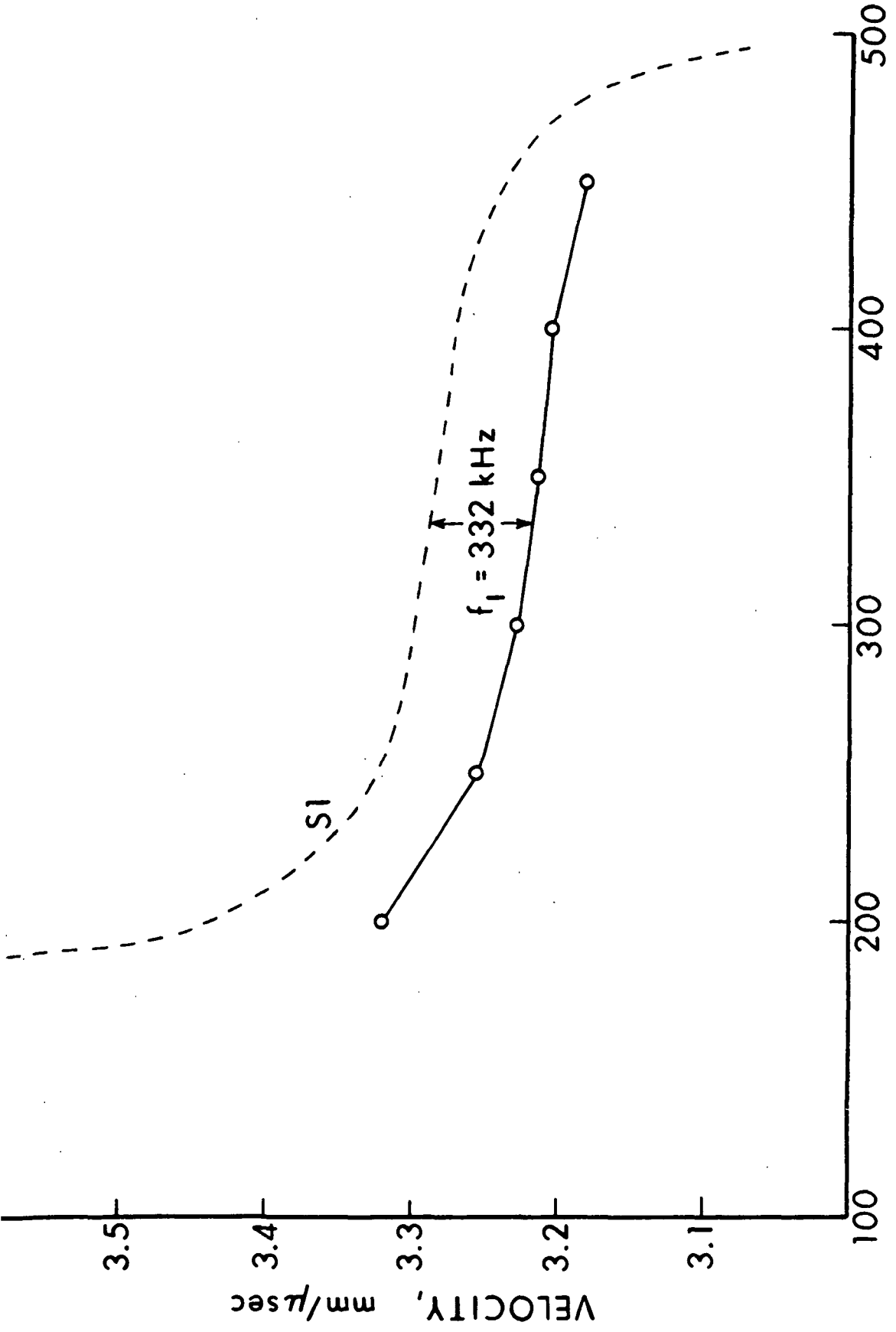

Figure 29. Theoretical and Experimental S1 Plate Wave Velocities for X-direction Propagation Through Milk Carton Stock

was calculated for each peak. The two velocities were found to differ by 0.30%. For V_{Lx} at 340 kHz, delay times to Peaks 4 and 5 were recorded. In this case, the two velocities differed by 0.32%.

TABLE IX

V_{SOx} AND V_{Lx} RESULTS FOR MILK CARTON STOCK

V_{SOx}	3.164 mm/μsec
V_{Lx}	3.205 mm/μsec
V_{SOx}/V_{Lx}	0.9874

Allowing for errors in predicting the frequency at which to measure V_{Lx}, one can estimate that each velocity is measured to ±0.25%. The ratio of the two velocities is therefore known to ±0.50%, and V_{SOx}/V_{Lx} is equal to 0.9874 ±0.0050.

Data for the Y-direction was also obtained. At the higher frequency of 340 kHz, attenuation was significantly greater than for X-direction propagation. In this case, the maximum usable specimen width was 4 inches.

V_{SOy} and V_{Ly} were determined for three specimens as presented in Table X. Specimens 1 and 2 were from the same 14-inch by 28-inch sheet, while the third specimen was from a different sheet. As with the X-direction velocities, experimental error was estimated to be ±0.25% for each velocity, and hence V_{SOy}/V_{Ly} is given as 0.9737 ± 0.0050.

The experimental work with milk carton stock has demonstrated that it is possible to make in-plane bulk longitudinal velocity measurements on single thickness specimens. It is possible, therefore, to determine all nine independent orthotropic elastic stiffness constants using only single thickness specimens for the velocity measurements. Some of the techniques, however, can be

used on fairly thick board materials only. The new method of calculating V_{Lx} and V_{Ly} on single sheets also permits very accurate determinations of V_{SOx}/V_{Lx} and V_{SOy}/V_{Ly}. This greatly improves the accuracy of determining C_{13} and C_{23}.

TABLE X

V_{SOy} AND V_{Ly} DATA FOR MILK CARTON STOCK

Specimen	V_{SOy}(mm/μsec)	V_{Ly}(mm/μsec)	V_{SOy}/V_{Ly}
1	2.152	2.209	0.9741
2	2.148	2.206	0.9740
3	2.182	2.243	0.9730
average	2.161	2.219	0.9737

ELASTIC CONSTANTS FOR MILK CARTON STOCK

The final results for the milk carton stock will now be presented. This was the only sample which was examined with the new techniques, for measuring in-plane bulk longitudinal and SO velocities.

The nine orthotropic stiffness coefficients are presented along with estimates of their measurement errors. These estimates are specific to the velocity measurement techniques used. A discussion of these stiffness constants follows.

MEASURED VELOCITIES

The nine independent velocity measurements for the milk carton stock are given in Table XI, along with estimates of measurement accuracy. All velocity measurements were made on single thickness specimens.

TABLE XI

NINE VELOCITY MEASUREMENTS FOR MILK CARTON STOCK

Velocity (mmμsec)	Accuracy
$V_{Lx} = 3.205$	± 0.5% absolute
$V_{Ly} = 2.219$	± 0.5% absolute
$V_{Lz} = 0.231$	± 5.0% absolute
$V_{SOx} = 3.164$	± 0.25% relative to V_{Lx}
$V_{SOy} = 2.161$	± 0.25% relative to V_{Ly}
$V_S(0°) = 1.615$	± 0.5% absolute
$V_S(45°) = 1.596$	± 0.25% relative to $V_S(0°)$
$V_{Sx-z} = 0.418$	± 5.0% absolute
$V_{Sy-z} = 0.351$	± 5.0% absolute

Absolute accuracy refers to how accurately the particular velocity measurement characterizes the whole sample. For instance, it is estimated that V_{Lx}, measured on a few small specimens, is within 0.25% of the true average velocity for those specimens. However, considering the variation between specimens, it is estimated that the measured value of V_{Lx} is only within 0.5% of the true sample average. While the same argument applies to V_{SOx}, both V_{SOx} and V_{Lx} were measured on the same specimens. Hence, the accuracy of either measurement, relative to the other, is higher in this case. The same holds for the measurement of V_{SOy} and V_{Ly}, and for $V_S(0°)$ and $V_S(45°)$.

ELASTIC CONSTANTS

The velocities cited in Table XI yield the orthotropic elastic constants given in Table XII. All elastic constants, except for the Poisson ratios, are normalized with respect to density, and have units of $mm^2/\mu sec^2$.

TABLE XII

ELASTIC CONSTANTS FOR THE MILK CARTON STOCK

$C_{11}^* =$		$E_{11}^* = 9.537$
$C_{22}^* =$		$E_{22}^* = 4.451$
$C_{33}^* = 0.0534$		$E_{33}^* = 0.0501$
$C_{12}^* =$	$\nu_{12} = 0.15$	$\nu_{21} = 0.32$
$C_{13}^* = 0.118$	$\nu_{13} = 0.008$	$\nu_{31} = 1.52$
$C_{23}^* = 0.116$	$\nu_{23} = 0.021$	$\nu_{32} = 1.84$
$C_{44}^* = 0.127$		$G_{44}^* = 0.127$
$C_{55}^* = 0.175$		$G_{55}^* = 0.175$
$C_{66}^* = 2.609$		$G_{66}^* = 2.609$

The errors associated with determining some of these elastic constants can be analyzed in a straightforward manner. These are the elastic constants which depend upon only one velocity measurement. These constants constitute the first six entries in Table XIII. The errors involved in determining the remaining elastic constants are not so easily obtained. A computer program has been written which determines $d(\ln C_{ij})/d(\ln V_i)$ coefficients for each of these elastic constants. By multiplying these coefficients by the accuracies of the measured velocities and summing absolute values, one can estimate the maximum errors associated with these elastic constants. The errors are also presented in Table XIII.

DISCUSSION

The strain level associated with the propagation of ultrasonic waves is very low. At the same time, the frequency of the oscillations is very high. Essentially no time is permitted for viscoelastic deformations to occur.

consequently, the elastic constants determined with ultrasonic techniques should characterize strictly the elastic response of the milk carton stock as to applied strains.

TABLE XIII

ESTIMATED MEASUREMENT ERRORS
FOR MILK CARTON STOCK ELASTIC CONSTANTS

Elastic Constant	Error
C_{11}^*	± 1%
C_{22}^*	± 1%
C_{33}^*	± 10%
C_{44}^*, G_{44}^*	± 10%
C_{55}^*, G_{55}^*	± 10%
C_{66}^*, G_{66}^*	± 1%
E_{11}^*	± 1.3%
E_{22}^*	± 1.4%
E_{33}^*	± 12%
C_{12}^*	± 7.7%
C_{13}^*	± 36%
C_{23}^*	± 19%
ν_{21}	± 10%
ν_{31}	± 61%
ν_{32}	± 28%

Mechanical measurements of Young's modulus for the milk carton stock in the X and Y-directions were found to be significantly lower than the values reported in Table XII. The measurements were made on 1-inch by 10-inch test strips employing an Instron tensile tester. The results of the load-elongation runs at three different strain rates are given below in Table XIV. It is seen

that the discrepancy between mechanical and sonic Young's moduli decreases as the strain rate of the mechanical test is increased. This trend strongly suggests that viscoelastic effects are operative during the mechanical test.

TABLE XIV

MECHANICAL MEASUREMENTS OF YOUNG'S MODULI ON MILK CARTON STOCK

	Strain Rate (per minute)		
	0.1%	0.5%	2.0%
$E_{11}^{*'}$ ($mm^2/\mu sec^2$)	7.053	7.351	7.789
$E_{22}^{*'}$ ($mm^2/\mu sec^2$)	3.060	3.159	3.923
$100\%(E_{11}^{*'}-E_{11}^{*})/E_{11}^{*}$	-26.0%	-22.9%	-18.3%
$100\%(E_{22}^{*'}-E_{22}^{*})/E_{22}^{*}$	-31.3%	-29.3%	-11.9%

(' indicates mechanically determined Young's Moduli)

The elastic constants for the milk carton stock are typical of all three board samples tested. These constants indicate that the elastic properties of these materials are highly unusual. Perhaps the most unique characteristic is the high degree of anisotropy between the in-plane and Z-direction properties. This is indicated by the high E_{11}^{*}/E_{33}^{*} ratio of 190. It is also seen that the two Z-direction shear moduli are both greater than the Z-direction tensile modulus.

The high out-of-plane Poisson ratios are also unusual. A high positive value of 1.52 means that a 1% tensile strain in the X-direction results in a 1.52% contraction in the Z-direction. The two out-of-plane Poisson ratios, ν_{31} and ν_{32}, are measured least accurately of all the elastic constants. With an accuracy of ±61%, ν_{31} is located in the range 0.59 to 2.45. ν_{32} is known to lie between 1.32 and 2.36. Clearly, then, at least ν_{32} must be greater than 1.

It is recalled that C_{13}^* and C_{23}^* were taken to be the positive roots of Equations (110) and (111). This assumption necessarily results in the calculation of positive out-of-plane Poisson ratios. Had the negative roots been chosen, ν_{31} and ν_{32} would have become negative. It is not obvious from the sonic measurements whether C_{13}^* and C_{23}^* are positive or negative.

Choosing the negative roots results in negative out-of-plane Poisson ratios, but does not affect any of the other elastic constants. The dispersion curves, however, are slightly affected by assuming negative values for C_{13}^* and C_{23}^*. The theoretical curves are found to shift horizontally to the right a few percent when negative values are substituted. This effect is relatively small, and consequently, the experimental data is not precise enough to indicate whether C_{13}^* and C_{23}^* are actually negative or positive.

It has been assumed in all of the previous discussion that C_{13}^* and C_{23}^* (and hence the out-of-plane Poisson ratios) were indeed positive. In the absence of other evidence, this assumption would be very reasonable. The mechanical measurements of thickness changes with tensile loading reported earlier (7,9, 12) were inconclusive. Both thickness increases and decreases were reported for various samples and under various conditions. Gottsching and Baumgarten (9) in the most recent work, found that paper thickness usually decreased initially during tensile loading, passed through a minimum, and then increased. The suggestion was that multiple processes are involved in the thickness changes. Apparently, for small strain levels, the thickness decrease predominates. This gives a basis, then, for assuming that the out-of-plane Poisson ratios measured sonically are indeed positive.

It would not be difficult to propose a mechanism which would account for these high out-of-plane Poisson ratios. To do so, however, would be highly

speculative. Obviously, the fibrous structure of paper is unusual, with the more or less parallel alignment of fibers in the plane of the sheet greatly determining the Z-direction elastic properties.

CONCLUSIONS

The present investigation has shown that waves propagate in paper according to wave theories developed for homogeneous materials. The fibrous structure does not interact with the waves to produce anomalous behavior below about 1 MHz.

Attenuation of waves in paper depends on frequency, and is a function of the direction of propagation. At a given frequency, attenuation is greatest in the Z-direction and least in the X-direction.

Pulse propagation techniques have been successfully adapted for measuring wave velocities in thick paper samples. With these techniques, delay times are measured to a certain peak near the middle of the received pulse for two or more transducer separations.

The experimental results clearly indicate that orthotropic wave theories are valid for machine-made paper. Consequently, paper has been established as a three-dimensional orthotropic material. The elastic constants are determined from various wave velocities. Orthotropic bulk wave and orthotropic plate wave theories furnish the necessary equations relating the measured velocities to the orthotropic elastic constants.

Nine velocity measurements are required to determine the nine independent orthotropic elastic constants. Three of the velocities are for waves propagated in the Z-direction. Two of these, V_{Sx-z} and V_{Xy-z} are for shear waves polarized in the X and Y-directions, respectively. The third, V_{Lz}, is for the longitudinal wave. These velocities can be measured to roughly ±5% on samples about 25 mils thick. The accuracy decreases with sample thickness. Generally, it is advantageous to operate above 200 kHz, where the transit time is longer than one period.

Four more velocities, V_{SOx}, V_{SOy}, $V_S(0°)$ and $V_S(45°)$, can be easily obtained for sheets of any thickness. These are for low frequency (around 10 kHz) longitudinal and shear waves propagated in the X-Y plane. The longitudinal waves are to be propagated along the X and Y-directions. The shear waves are to be propagated in either principal direction and in a direction 45° from the X-direction.

The remaining two velocities, V_{Lx} and V_{Ly}, are bulk longitudinal velocities in the X and Y-directions. These velocities can be accurately measured for thick samples on single thickness specimens by operating at a specific predetermined frequency. Otherwise, it is possible to construct glued or loose stacks which have been shown to approximate bulk materials.

For the milk carton stock, the orthotropic elastic constants determined from these nine measurements exhibited the following characteristics:

1. very high in-plane to Z-direction anisotropy;
2. very low Z-direction moduli; and
3. out-of-plane Poisson ratios greater than 1.

Young's moduli determined sonically have been found to be somewhat higher than mechanically determined moduli. From recent experimental results (32), it is concluded that the sonic technique measures strictly elastic responses, whereas the much slower mechanical tests involve viscoelastic responses as well.

LIST OF SYMBOLS

AO,A1,etc.	designation given to zeroth, first, etc., antisymmetric plate wave modes
A.F.	attenuation factor
C	stiffness matrix
C_{ij}	orthotropic stiffness coefficient
C^*_{ij}	normalized (with respect to density) orthotropic stiffness coefficient
C'_{ij}	planar orthotropic stiffness coefficients
c	$\cos\theta$
d	specimen width
e	strain matrix
e_{ij}	strain component in the j direction having the plane of action normal to the i direction
E	Young's modulus for an isotropic material
E_{11},E_{22},E_{33}	for an orthotropic material, Young's moduli in the X, Y, and Z-directions, respectively
E_θ	Young's modulus along the direction which makes an angle θ with the X-direction
f	frequency
G_{44},G_{55},G_{66}	for an orthotropic material, shear moduli characteristic of principle directions in the Y-Z, X-Z, and X-Y planes, respectively
$\vec{K}$	wave vector
$\vec{K}_{SV},\vec{K}_p$	wave vectors of SV and P type waves, respectively
k_x,k_z	component of wave vector in X and Z-directions, respectively
k_{z+},k_{z-}	Z-direction wave vector components belonging to SV and P type partial waves, respectively
l,m,n	direction cosines of wave vector, $\vec{K}$
P	designation given the bulk longitudinal wave
Q	quality factor

$\vec{r}$	position vector
s	sin θ
S	compliance matrix
SH	designation given the shear wave polarized normal to the plane under consideration
SV	designation given the shear wave polarized in the plane under consideration
S0,S1,etc.	designation given to zeroth, first, etc., symmetric plate wave modes
t	time
T	plate thickness
t_d	total delay time
T_t	extraneous delay time
$\vec{U}(x,y,z)$	displacement vector field, the difference between a particle's location after deformation and its original location with respect to a fixed coordinate system
$\vec{U}_0$	maximum displacement vector
u_x, u_y, u_z	components of displacement vector
u_{0x}, u_{0y}	components of maximum displacement vector
V	phase velocity
V_{air}	velocity of sound in air
V_L	velocity of a longitudinal wave propagated in the X-Y plane
V_{Lx}, V_{Ly}, V_{Lz}	bulk longitudinal velocities for propagation along the X, Y, and Z-direction, respectively
V_p	velocity of a plate wave
V_S	velocity of a shear wave propagated in the X-Y plane
V_{Sx-z}	bulk shear velocity in the Z-direction, polarization in the X-direction
V_{Sy-z}	bulk shear velocity in the Z-direction, polarization in the Y-direction

V_{SOx}, V_{SOy}	low frequency SO plate wave velocity for X and Y-direction propagation, respectively
V_1, V_2, V_3	phase velocities of orthogonal set of waves propagated in the X-Y plane of an orthotropic bulk material
x,y,z	coordinates along the X, Y, and Z-directions, respectively
α	angle of incidence in plate wave resonance technique, measured to plate normal
θ	angle specifying orientation with respect to X-direction
λ	wavelength
ν	Poisson ratio for an isotropic material
$\nu_{xy}, \nu_{yx}, \nu_{xz}$	Poisson ratios (stress applied in the direction given by the second subscript)
ν_{ij}	Poisson ratios (stress applied in the direction given by the second subscript)
ρ	bulk density
σ	stress matrix
σ_{ij}	stress component in j direction having the plane of action normal to the i direction
ϕ	specific angle ψ for which the wave vector $(\vec{K})$ and particle displacement vector $(\vec{U})$ are either parallel or normal to each other
ψ	for bulk wave propagation in the X-Y plane of an orthotropic material, the angle between the particle displacement vector and the X-direction
ψ_1, ψ_2	ψ for bulk waves having phase velocities V_1 and V_2, respectively
ω	angular frequency

ACKNOWLEDGMENTS

I would like to extend my sincere gratitude and appreciation to my advisory committee of Gary Baum, Chuck Habeger, and Bob Stratton, for their guidance and assistance throughout the course of this work, and also to Jimmy Hung who served on my advisory committee during the initial phases of the work.

Special thanks are due Drs. Baum and Habeger for many helpful and invaluable discussions on many aspects of this work.

I also wish to express my gratitude to the membership of The Institute of Paper Chemistry for their support of not only this work, but for the support of my family as well.

I also acknowledge the contribution of my wife, Deborah, to the outcome of this work. While Deborah never came to know one wave from another, she is not unfamiliar with propagation.

LITERATURE CITED

1. Brezinski, J. P., Tappi 39(2):116(1956).

2. Riemen, W. P. and Kurath, S. F., Tappi 47(10):629(1964).

3. Horio, M. and Onogi, S., J. Appl. Physics 22(7):971(1951).

4. Kubat, J. and Lindbergson, B., Svensk Papperstid. 68(21):743(1965).

5. Seve, R. and Perrin, H., Assoc. Tech. Ind. Papetiere 1:1(1954).

6. Kubat, J., Nyborg, L. and Steenberg, B., Svensk Papperstid. 66(19):754 (1963).

7. Ranger, A. E. and Hopkins, L. F. In Bolam's The formation and structure of paper. Vol. 1. p. 277-310. London, Technical Section of the British Paper and Board Makers' Association, 1962.

8. Jones, A. F., Tappi 51(5):203(1968).

9. Gottsching, L. and Baumgarten, H. L. In Bolam's The fundamental properties of paper related to its uses. Vol. 1. p. 227-52. London, Technical Division of the British Paper and Board Industry Federation, 1974.

10. Brezinski, J. P. Progress Report No. 7, Project 2733, Appleton, Wis., The Institute of Paper Chemistry, 1973.

11. Bornhoeft, L. R. The determination of elastic constants in paper by sound velocity measurements. A-291 Research Topic. Appleton, Wis., The Institute of Paper Chemistry, 1978.

12. Ohrn, O. E., Svensk Papperstid. 5:141(1965).

13. Van Liew, G. P., Tappi 57(11):121(1974).

14. Truell, R., Elbaum, C. and Chick, B. B. Ultrasonic methods in solid state physics. New York, Academic Press, 1969.

15. Mason, W. P. Physical acoustics and the properties of solids. Princeton, N.J., Van Nostrand, 1958.

16. Krautkramer, J. and Krautkramer, H. Ultrasonic testing of materials. 2nd ed. Berlin, Germany, Springer-Verlag, 1977.

17. Mason, W. P. Physical acoustics. Vol. I. New York, Academic Press, 1964.

18. ASTM Standard F 89-68, Part 21, p. 345-51, 1974.

19. Craver, J. K. and Taylor, D. L., Tappi 48(3):142(1965).

20. Taylor, D. L. and Craver, J. K. In Bolam's Consolidation of the paper web. Vol. 2. p. 852-72. London, Technical Section of the British Paper and Board Makers' Association, 1966.

21. Craver, J. K. and Taylor, D. L., Pulp Paper Mag. Can. 67:T331-6(1966).

22. Chatterjee, P. K., Svensk Papperstid. 74(17):503(1971).

23. Back, E. L. and Didriksson, E. I. E., Svensk Papperstid. 72(21):697(1969).

24. Jackson, M. and Gavelin, G., Svensk Papperstid. 70(3):63(1967).

25. Chatterjee, P. K., Tappi 52(4):699(1969).

26. Yastrebov, O. I. and Kundzich, G. A. Continuous control of the physico-mechanical properties and defects of the paper web. Chap. VI. Moscow, Lesnaya Promyshlennost, 1975.

27. Papadakis, E. P., Tappi 56(2):74(1973).

28. Luukkala, M., Heikkila, P. and Surakka, J., Ultrasonics 9(3):201(1971).

29. Kolsky, H. Stress waves in solids. Oxford, Clarendon Press, 1953.

30. Graff, K. F. Wave motion in elastic solids. Ohio State University Press, 1975.

31. Viktorov, I. A. Rayleigh and Lamb waves. New York, Plenum Press, 1967.

32. Austin, J. N. An investigation of elastic moduli measured sonically and mechanically. A-291 Research Topic. Appleton, Wis., The Institute of Paper Chemistry, 1978.

33. Nissan, A., Tappi 60(10):98(1977).

34. Weatherwax, R. C. and Caulfield, D. F., Tappi 59(8):85(1976).

35. Button, A. F. Interfiber bonding as measured by a sonic velocity technique. Master's Dissertation. University Park, Penn., Pennsylvania State University, 1972.

36. Ballou, J. W. and Smith, J. C., J. Appl. Physics 20(6):493(1949).

37. Moseley, W. W., J. Appl. Polymer Sci. 3(9):266(1960).

38. Zorowski, C. F. and Murayama, T., Textile Res. J. 37:852(1967).

39. Eden, H. F. and Felsenthal, P., J. Acoust. Soc. Am. 53(2):464(1973).

40. Peck, J. C. and Gurtman, G. A., J. Appl. Mechanics 36(3):479(1969).

41. Zimmer, J. E. and Cost, J. R., J. Acoust. Soc. Am. 47(3):793(1970).

42. Markham, M. F., Composites 1:145(1970).

43. Dean, G. D. and Turner, P., Composites 4:174(1973).

44. Reynolds, W. N. and Wilkinson, S. J., Ultrasonics 12(3):109(1974).

45. Felix, M. P., J. Composite Materials 8(7):275(1974).

46. Chan, O. K., Chen, F. C., Choy, C. L., and Ward, I. M., J. Phys. D: Appl. Phys. 11:617(1978).

47. Campbell, J. G., Austral. J. Appl. Sci. 12(3):356(1961).

48. API Report No. 60. Measurement of thickness. Appleton, Wis., The Institute of Paper Chemistry, 1975.

49. Love, A. E. H. The mathematical theory of elasticity. 4th ed. New York, Dover, 1944.

50. Borngis, F. E., Phys. Rev. 98(4):1000(1955).

51. Musgrave, M. J. P., Proc. Royal Soc. A226(1166):339(1954).

52. Habeger, C. C., Mann, R. W., and Baum, G. A., Ultrasonics, 1979.

53. Solie, L. P. and Auld, B. A., J. Acoust. Soc. Am. 54:50(1973).

54. Mason, W. P. Piezoelectric crystals and their application to ultrasonics. New York, Van Nostrand, 1950.

55. Weast, R. C., ed. CRC Handbook of Chemistry and Physics. 54th ed. p. E-47. Cleveland, Ohio, CRC Press, 1973.

56. Curtis, G., Ultrasonics 12(4):148(1974).

57. Baum, G. A. and Bornhoeft, L. R., unpublished work, Appleton, Wis., The Institute of Paper Chemistry.

APPENDIX I

FORTRAN IV LISTING: SOLUTIONS TO ORTHOTROPIC DISPERSION EQUATION

The computer program listed in this appendix finds solutions to the orthotropic dispersion equation, Equation (83). The primary inputs to the program are as follows:

1. Stiffness coefficients: C_{11}, C_{33}, C_{13}, and C_{55} for X-direction propagation; C_{22}, C_{33}, C_{23}, and C_{44} for Y-direction propagation.
2. Maximum phase velocity for which solutions are to be sought (CPI).
3. Number of velocities for which solutions are to be sought (NC).
4. Maximum frequency for which solutions are to be sought (FMAX).
5. Plate thickness (T).
6. Integer parameter indicating how results are to be plotted (IGRAPH).
7. Lengths of coordinate axes (XHM and YHM).

In addition, there are several secondary inputs, i.e., those specified in the program. These are:

8. Minimum frequency for which solutions are to be sought (FI).
9. Frequency increment used in iterative search (DELF).
10. Maximum number of solutions to be located (NMR).
11. Plate density (RHO).

The main program consists of a large DO loop within another DO loop. The outer DO loop sets the wave symmetry. Solutions for antisymmetric modes are sought first. The inner DO loop sets the phase velocity. Within the inner DO loop, frequency is stepped by increments of DELF from FI to FMAX. For each velocity, the right side of Equation (83), being independent of frequency, is

evaluated. Then, for each frequency, the left side of Equation (83) is evaluated and a comparison is made. When the two sides are approximately equal, solution is indicated. When the right side of Equation (83) is either very large or very small, which occurs in certain velocity ranges, solutions are sometimes not located.

The first time through the inner main DO loop, solutions are sought for the maximum phase velocity, CPI. With succeeding passes, the velocity is decreased in NC-1 steps of CPI/NC. No program itself is described via comments within the FORTRAN statements.

```
C
C
C     DETERMINATION OF ORTHOTROPIC PLATE WAVE DISPERSION CURVES
C
C
C     RESULTS CAN BE PLOTTED IN THE FOLLOWING FORMATS
C     IGRAPH       X-AXIS          Y-AXIS
C     ------       ------          ------
C        0            F               V
C        1          F*T/V             V
C        2          F*T/V             F
C        3            F             F/(V*V)
C
C
/JOB GO,TIME=60
      DIMENSION ID(300),VEL(300),FREQ(150,15),X(1000),Y(1000),A(20)
      DIMENSION LX(13),LY(13)
      REAL KP,KM,KPS,KMS
      READ (5,4) CPI,NC,FMAX,T,XHM,YHM
      FI = 0.001
      DELF = 0.001
      XSF = FMAX/XHM
      YSF = CPI/YHM
      NUMF = FMAX/DELF
      MNR = 5
      DELCP = CPI/NC
      RHO = 1.00
C.....THE NEXT LINE IN THE DATA FILE IS LITERAL INFORMATION.
      READ (6,5) QRT
    1 FORMAT (4F10.3/I1)
    2 FORMAT (1HO,///,'STIFFNESS COEFICIENTS ARE',/,T5,4F10.2)
    3 FORMAT (1H ,'C = ',F5.2,5X,'B*B-4*D IS ZERO OR LESS')
    4 FORMAT (F10.4,I2,8X,6F10.4)
    5 FORMAT (8X,F2.0)
  400 READ (5,1) C11,C22,C12,C66,IGRAPH
      IF (IGRAPH-3) 7,6,7
    6 IG = 3
      IGRAPH = 0
    7 IF (C11) 123,500,123
  123 WRITE (6,2) C11,C22,C12,C66
      CALL RON1(RHO,C11,C22,C12,C66,A1,A2,A3,A4,A5,A6)
C.....OUTER DO LOOP, L=1 FOR ANTISYMMETRIC MODES
C.....               L=2 FOR SYMMETRIC MODES
      DO 200 L=1,2
      DO 9 I=1,100
      ID(I) = 0
      DO 9 J=1,10
    9 FREQ(I,J) = 0.
C.....EACH TIME THROUGH THIS NEXT DO LOOP, A NEW VALUE OF
C.....VELOCITY IS USED.
      DO 100 I=1,NC
      IK = 0
      IF (IGRAPH-1) 32,32,31
   31 ANGLE = -(ATAN(CPI)/NC)*(I-1) + ATAN(CPI)
      C = SIN(ANGLE)/COS(ANGLE)
      GO TO 33
   32 C = CPI- (I-1)*DELCP
C.....PHASE VELOCITY, C=VEL(I)
   33 VEL(I) = C
```

```
      IF (C-0.001) 150,150,10
C.....SUBROUTINE RON2 THEN EVALUATES SQUARES OF THE Z-DIRECTION
C.....WAVE VECTORS.  INDEX INDICATES IMAGINARY QUANTITIES.
   10 CALL RON2(C,A1,A2,A3,A4,A5,KPS,KMS,INDEX)
      IF (INDEX) 30,30,20
   20 WRITE (6,3) C
      GO TO 100
   30 IF (KMS) 40,100,50
   40 IK = 1
      KMS  = -KMS
      IF (KPS) 45,100,50
   45 IK = -1
      KPS = -KPS
C.....THE Z-DIRECTION WAVE VECTORS ARE THEN CALCULATED.  THE
C.....SQUARE ROOTS OF THE ABSOLUTE VALUES ARE TAKEN.
   50 KP = SQRT(KPS)
      KM = SQRT(KMS)
C.....SUBROUTINE RON3 DETERMINES THE RIGHT HAND SIDE OF THE
C.....DISPERSION EQUATION (AS CONST) AND ALSO DETERMINES THE
C.....COEFFICIENTS IN THE ARGUMENTS OF THE TANGENT FUNCTIONS.
C.....ALPHA AND BETA MUST BE MULTIPLIED BY THE FREQUENCY, F.
      CALL RON3(KP,KM,T,C,RHO,C11,C12,A6,C66,ALPHA,BETA,CONST,IK)
C.....THE RIGHT SIDE OF THE DISPERSION EQUATION IS INVERTED,
C.....OR NOT, DEPENDING ON THE SYMMETRY.
      IF (L-2) 52,51,51
   51 CONST =  1./CONST
      GO TO 55
   52 IF (IK-1) 55,53,55
   53 CONST = - CONST
C.....IF CONST IS TOO LARGE OR SMALL, SEARCH INCREMENT ON F IS
C.....DECREASED.
   55 IF (ABS(CONST)-40.0) 56,56,57
C  56 IF (ABS(CONST)-0.025) 57,59,59
   56 GO TO 59
   57 DEL = DELF/5.0
      NUM = NUMF*5
      GO TO 61
   59 DEL = DELF
      NUM = NUMF
   61 IQ = 0
      IF (IGRAPH-1) 22,22,21
   21 NUM = NUM*C
C.....WITH THIS DO LOOP, FREQENCY IS SCANNED.
   22 DO 90 J=1,NUM
      F = FI + (J-1)*DEL
      IF (F-FMAX) 15,15,100
   15 IF (IGRAPH-1) 12,11,12
   11 F = F*C/T
C.....TANGENT FUNCTIONS ARE EVALUATED.
   12 SA =  SIN(ALPHA*F)/COS(ALPHA*F)
      IF (IK) 64,60,65
   60 SB =  SIN(BETA*F)/COS(BETA*F)
      GO TO 69
   64 IF (ALPHA*F-5.0) 164,165,165
  164 SA = (EXP(ALPHA*F)-EXP(-ALPHA*F))/(EXP(ALPHA*F)+EXP(-ALPHA*F))
      GO TO 65
  165 SA = 1.0
   65 IF (BETA*F-5.0) 66,67,67
   66 SB = (EXP(BETA*F)-EXP(-BETA*F))/(EXP(BETA*F)+EXP(-BETA*F))
      GO TO 69
```

```
   67 SB = 1.0
   69 IF (SB) 70,90,70
C.....THEIR RATIO IS THEN CALCULATED.
   70 RATIO = SA/SB
  170 IF (J-1) 72,71,72
   71 F2 = F
      Q2 = RATIO
      GO TO 90
C.....STARTING WITH THE SECOND FREQUENCY, SUBROUTINE RON4
C.....DETERMINES IF RATIO=CONST.
   72 F1 = F2
      Q1 = Q2
      F2 = F
      Q2 = RATIO
      CALL RON4(Q1,CONST,Q2,IND)
      IF (IND) 90,90,75
   75 FV = F1 + (CONST-Q1)*DEL/(Q2-Q1)
      IF (IGRAPH-1) 17,16,16
   16 FV = T*FV/C
   17 IQ = 1 + IQ
      ID(I) = IQ
      FAC = FV/(VEL(I)*VEL(I))
      IF (IG-3) 19,18,19
   18 VEL(I) = FAC
C.....SOLUTIONS ARE STORED IN FREQ(I,IQ).  IQ IS A COUNTER
C.....USED IN RON5.
   19 FREQ(I,IQ) = FV
C     WRITE (6,5) SA,SB,FP,VEL(I),FV,FAC
      IF (IQ-MNR) 90,100,100
   90 CONTINUE
C.....PROCEDURE IS REPEATED FOR NEXT VELOCITY.
  100 N = I
  150 CONTINUE
C.....WHEN SOLUTIONS FOR ALL VELOCITIES HAVE BEEN SOUGHT,
C.....SUBROUTINE RON5 IS CALLED TO PUT THE DATA IN FINAL FORM
C.....FOR PLOTTING.
      CALL RON5(VEL,FREQ,ID,N,X,Y,A,IGRAPH,T)
C.....SUBROUTINE RON6 IS CALLED TO PLOT DATA.
      CALL RON6(N,X,Y,L,XHM,YHM,XSF,YSF)
  200 CONTINUE
      GO TO 400
  500 STOP
      END
C
      SUBROUTINE RON1 (RHO,C11,C22,C12,C66,A1,A2,A3,A4,A5,A6)
      A1 = (C11*C22 - C12*(C12+2.*C66))/(C22*C66)
      A2 = -RHO*(C22+C66)/(C22*C66)
      A3 = C11/C22
      A4 = -RHO*(1.+C11/C66)/C22
      A5 = RHO*RHO/(C22*C66)
      A6 = -C11 + C12*(C12+C66)/C22
      WRITE (6,1) A1,A2,A3,A4,A5,A6
    1 FORMAT (1HO,///,'THE A CONSTANTS ARE',/,T5,6F10.3)
      RETURN
      END
C
      SUBROUTINE RON2(C,A1,A2,A3,A4,A5,KPS,KMS,INDEX)
      REAL KPS,KMS
      B = A1 + A2*C*C
      D = A3 + A4*C*C + A5*C*C*C*C
```

```
      D = B*B - 4*D
      IF (D) 10,10,20
   10 INDEX = 1
      GO TO 100
   20 KPS = (-B + SQRT(D))/2.
      KMS = (-B - SQRT(D))/2.
      INDEX = 0
  100 RETURN
      END
C
      SUBROUTINE RON3(KP,KM,T,C,RHO,C11,C12,A6,C66,ALPHA,BETA,CONST,IK)
      REAL KP,KM
      ALPHA = (KP*T*3.141592)/C
      BETA = (KM*T*3.141592)/C
      IF (IK) 10,20,10
   10 CSS = -C66
      COT = -C12
      CON = C12
      CSX = C66
      IF (IK) 15,20,30
   15 CON = -C12
      CSX = -C66
      GO TO 30
   20 CSS = C66
      COT = C12
      CON = C12
      CSX = C66
   30 CONST = KM*(RHO*C*C - C11 + CON*KP*KP)
      CONST = CONST*(RHO*C*C + A6 - CSS*KM*KM)/KP
      CONST = CONST/(RHO*C*C - C11 + COT*KM*KM)
      CONST =  CONST/(RHO*C*C + A6 - CSX*KP*KP)
      WRITE (6,1) C,KP,KM,ALPHA,BETA, CONST
    1 FORMAT (1H ,3F10.4,5X,3F10.4)
      RETURN
      END
C
      SUBROUTINE RON4(Q1,CONST,Q2,IND)
      IF (Q1*Q2) 5,10,10
    5 IF (ABS(Q1-Q2)-2.0) 10,10,100
   10 IF (Q1-CONST) 20,20,50
   20 IF (CONST-Q2) 200,200,100
   50 IF (CONST-Q2) 100,200,200
  100 IND = 0
      GO TO 300
  200 IND = 1
  300 RETURN
      END
C
      SUBROUTINE RON5(VEL,FREQ,ID,N,X,Y,A,IGRAPH,T)
      DIMENSION A(20),FREQ(150,15),ID(300),X(1000),Y(1000),VEL(300)
      K = 0
      M = -1
      DO 100 I=1,N
      MM = ID(I)
      IF (ID(I)-1) 100,40,10
   10 M = -M
      IF (M) 20,20,50
   20 DO 25 J=1,MM
   25 A(J) = FREQ(I,J)
      DO 30 J=1,MM
```

```
      INDEX = MM + 1 - J
   30 FREQ(I,J) = A(INDEX)
      GO TO 50
   40 K = K + 1
      X(K) = FREQ(I,MM)
      IF (IGRAPH-1) 42,42,41
   41 Y(K) = X(K)*VEL(I)/T
      GO TO 100
   42 Y(K) = VEL(I)
      GO TO 100
   50 DO 70 J=1,MM
      K = K + 1
      X(K) = FREQ(I,J)
      IF (IGRAPH-1) 60,60,55
   55 Y(K) = X(K)*VEL(I)/T
      GO TO 70
   60 Y(K) = VEL(I)
   70 CONTINUE
  100 CONTINUE
      N = K
  200 CONTINUE
      RETURN
      END
C
      SUBROUTINE RON6(N,X,Y,L,XHM,YHM,XSF,YSF)
      DIMENSION X(1000),Y(1000),LX(13),LY(13),IBCD(12)
      IF (L-1) 10,10,20
   10 CALL ITLZ
      CALL DPT(1,4)
      CALL PLOT(0.0,-11.0,-2)
      CALL PLOT(1.5,1.25,-3)
   15 READ (5,1) (LX(I),I=1,13),(LY(I),I=1,13)
    1 FORMAT (12A4,I2/12A4,I2)
   25 CALL AXIS(0.0,0.0,LX,-LX(13),XHM,0.0,0.0,XSF)
      CALL AXIS(0.0,0.0,LY,LY(13),YHM,90.0,0.0,YSF)
   20 NN = N + 1
      NNN = NN + 1
      X(NN) = 0.0
      X(NNN) = XSF
      Y(NN) = 0.0
      Y(NNN) = YSF
      INP = 2
      IF (L-2) 29,28,28
   28 INP = 6
   29 CALL LINE(X,Y,N,1,-1,INP)
      IF (L-1) 40,40,30
    2 FORMAT (2F5.2,I2,12A4)
   30 READ (5,2) XPAGE,YPAGE,NCHAR,(IBCD(I),I=1,12)
      IF (NCHAR) 35,45,35
   35 CALL SYMBOL (XPAGE,YPAGE,0.14,IBCD,0.0,NCHAR)
      GO TO 30
   45 CALL FINAL
   40 RETURN
      END
C.....SAMPLE DATA FILE
/DATA
1.6         16          0.4         0.625       6.0         8.0
MAX VEL.    NO. PTS.    MAX FREQ    THICK.      X-AXIS      Y-AXIS
12.137      0.0644      0.100       0.300
0
```

```
FREQUENCY (MEGAHERTZ)                                    21
PHASE VELOCITY (MM/USEC)                                 24
1.5  8.8  31RHO = 1.0, THICKNESS = 0.625 MM
1.5  8.6  30C11 = 12.137, C33 = 0.0644
1.5  8.4  30C13 =  0.100, C55 = 0.300
0
12.137     0.0644     0.100      0.100
0
FREQUENCY (MEGAHERTZ)                                    21
PHASE VELOCITY (MM/USEC)                                 24
1.5  8.8  31RHO = 1.0, THICKNESS = 0.625 MM
1.5  8.6  30C11 = 12.137, C33 = 0.0644
1.5  8.4  30C13 =  0.100, C55 = 0.100


/END CARD READ, JOB TERMINATED
```

APPENDIX II

FORTRAN IV LISTING: PLOTTING OF PLATE WAVE DEFORMATIONS

This computer program plots actual plate wave deformations. Part of the program solves the dispersion equation for a particular velocity and mode in order to locate the frequency. At the same time the wave vectors are computed.

The program will plot any number of waves at a time, though only 7 to a page. Each wave is described on a separate input data card. For each it is necessary to give a minimum frequency for which to start the search.

Most of the symbols are explained in the comments preceding the program. Additional comments within the program serve to describe the flow of computations.

```
C
C
C          PLOTTING OF ORTHOTROPIC PLATE WAVES
C
C
C**********PARAMETERS SPECIFIED IN THE MAIN PROGRAM**********
C      N = NO. OF POINTS PLOTTED ON VERTICAL DEFORMATION LINES
C      PLI = INCHES UP ON 11 INCH PAPER TO FIRST WAVE PLOT
C      NV = NO. OF VERTICAL DEFORMATIONS LINES PLOTTED PER WAVELENGTH
C      XMA = LENGTH OF WAVE AS PLOTTED IN INCHES
C      YMAX = PLATE THICKNESS AS PLOTTED, IN INCHES
C      PRNT = PRINT PARAMETER.  WITH PRNT = 2, MUCH OF THE
C                 PRINT OUT IS DELETED.
C      FD = FREQUENCY INCREMENT (IN MHZ) USED IN SEARCHING FOR SOLUTIONS
C                 TO DISPERSION EQUATION
C      T = ACTUAL PLATE THICKNESS IN MM
C      NF = MAXIMUM NO. OF FREQUENCIES TO BE TRIED IN SEARCH
C      RHO = PLATE BULK DENSITY (GMS/CM3)
C      INK = MAXIMUM NO. OF PLOTS PER PAGE
C      M = NO. OF HORIZONTAL LINES PLOTTED
C
C
C**********PARAMETERS SPECIFIED IN DATA FILE**********
C      C11,C33,C13,C55 = ELASTIC STIFFNESS COEFFICIENTS
C      LN1,LN2,LN3 = LITERAL INFORMATION AS STRINGS, FOR PRINTING THE
C                 VELOCITY, FREQUENCY, AND DISPLACEMENT RATIO (PROVISION
C                 FOR 28 CHARACTERS EACH)
C      NC = NO. OF WAVES TO BE PLOTTED
C      S = VELOCITY OF WAVE
C      FI = FIRST FREQUENCY IN SEARCH
C      NVL = ADDITIONAL VERTICAL LINES PLOTTED PER WAVELENGTH
C      SCA = SCALE FACTOR (SAME FOR X AND Z DISPLACEMENTS) IN INCHES
C      SYM = SYMMETRY PARAMETER (1-SYMMETRIC, 2-ANTISYMMETRIC)
C      XMAX = ADDITIONAL LENGTH OF WAVE (INCHES)
C
C
C**********DATA FILE FORMAT**********
C      4F10.3                        C11,C33,C13,C55
C      7A4/7A4,7A4                   LN1,LN2,LN3
C      I2                            NC
C      2F5.2,I5,4F5.2                S,FI,NVL,SCA,SYM,XMAX
C      ETC.
C      ETC.
C
C
/JOB GO,TIME=15
      DIMENSION ARG(2),KS(2),K(2,2),G(2,2),H(2,2),A(2),B(2),C(2),D(2)
      DIMENSION TX(2),TY(2),CX(2),CY(2),V(2),V1(2),V2(2),W(2),LN3(30)
      DIMENSION U(2),T1(2),T2(2),T3(2),T4(2),XP(2),XM(2),YP(2),YM(2)
      DIMENSION U1(100,2),U2(100,2),XC(501),YC(501),LN1(30),LN2(30)
      REAL KS,K,KPS,KMS
C
      N = 25
      PL1 = 9.0
      NV = 8
      XMA= 45.0
      YMAX = 1.00
      SCA = 0.050
      PRNT = 2.0
```

```
      SYM = 1.0
      FD = 0.0001
      T = 0.679
      NF = 10000
      RHO = 1.0
      INK = 7
      M = 5
C
      READ (5,1) C11,C33,C13,C55
      READ (5,18) (LN1(I),I=1,7),(LN2(I),I=1,7),(LN3(I),I=1,7)
      WRITE (6,2) C11,C33,C13,C55,RHO,T
    1 FORMAT (4F10.3)
    2 FORMAT (1HO,///,'STIFFNESS COEFICIENTS ARE',/,T5,4F10.3,/,
     + 'RHO = ',F4.2,'  THICKNESS = ',F4.2)
    3 FORMAT (1H ,'C = ',F5.2,5X,'B*B-4*D IS ZERO OR LESS')
    4 FORMAT (1H ,//,'KZ+B/F = ',F10.4,/'KZ-B/F = ',F10.4/' CONST = ',
     + F11.5)
    5 FORMAT (1HO,/,50('-'))
    7 FORMAT (1HO,/,T24,'C = ',F5.3,'  MM/USEC',/T24,'F = ',F5.3,
     + ' MHZ',//,T2,'KS+ = ',F10.4,/,T2,'KS- = ',F10.4,///,T12,'REAL',
     + T22,'IMAG',/,T12,'----',T22,'----',//,T3,'K+ = ',2F10.4,/,T3,
     + 'K- = ',2F10.4,//,T4,'X = ',F10.4,/,T4,'Y = ',F10.4,//)
    8 FORMAT (1H ,T4,'A = ',2F10.4,/,T4,'B = ',2F10.4,/,
     + T4,'C = ',2F10.4,/,T4,'D = ',2F10.4/)
C   9 FORMAT (1H ,2F10.4,10X,2F10.4)
   14 FORMAT (I2)
   15 FORMAT (2F5.2,I5,4F5.2)
   16 FORMAT (1HO/,T24,'C = ',F5.3,'  MM/USEC'/T24,'F = ',F5.3,
     + '  MHZ'/)
   18 FORMAT (7A4/7A4,7A4)
C
C.....SUBROUTINE RON1 CALCULATES SEVERAL PARAMETERS FROM
C.....DENSITY AND STIFFNESS COEFFICIENTS.
      CALL RON1(RHO,C11,C33,C13,C55,A7,A8,A3,A4,A5,A6)
      READ (5,14) NC
      IF (NC-1) 40,40,30
C.....MAIN DO LOOP ON LBJ WHEN MORE THAN 1 WAVE IS TO BE DRAWN.
   30 DO 900 LBJ=1,NC
   40 READ (5,15) S,FI,NVL,SCA,SYM,XMAX
      NVL = NVL + NV
      XMAX = XMAX + XMA
C.....SUBROUTINE RON2 CALCULATES SQUARES OF Z-DIRECTION WAVE
C.....VECTORS.
      CALL RON2(S,A7,A8,A3,A4,A5,KPS,KMS,INDEX)
      IF (INDEX) 60,60,50
   50 WRITE (6,3) S,KPS,KMS
      GO TO 900
C
C.....SUBROUTINE RON3 CALCULATES RIGHT SIDE OF DISPERSION EQUATION.
   60 CALL RON3(KPS,KMS,S,RHO,C11,C13,C55,A6,CONST)
C.....ARGUMENTS TO TANGENT FUNCTIONS ARE DEFINED.
      ARG(1) = (SQRT(ABS(KPS))*T*3.141592)/S
      ARG(2) = (SQRT(ABS(KMS))*T*3.141592)/S
      WRITE (6,5)
      IF (PRNT - 2.0) 61,62,61
   61 WRITE (6,4) ARG(1),ARG(2),CONST
   62 KS(1) = KPS
      KS(2) = KMS
      IF (SYM-1.0) 80,70,80
   70 CONST = 1./CONST
```

```
C
C.....FREQUENCY SEARCH BEGINS WITH DO LOOP ON I.
   80 DO 300 I=1,NF
      F = FI + (I-1)*FD
C.....SUBROUTINE RON4 CALCULATES LEFT SIDE OF DISPERSION
C.....EQUATION.
      CALL RON4(ARG,KS,F,RATIO)
      IF (I-1) 100,90,100
   90 F2 = F
      Q2 = RATIO
      GO TO 300
  100 F1 = F2
      Q1 = Q2
      F2 = F
      Q2 = RATIO
C.....SUBROUTINE RON5 DETERMINES WHEN A SOLUTION HAS BEEN FOUND.
      CALL RON5(Q1,CONST,Q2,IND)
      IF (IND) 300,300,110
  110 F = F1 + (CONST-Q1)*FD/(Q2-Q1)
      GO TO 305
  300 CONTINUE
C
  305 CONTINUE
C
C
C
C.....HAVING FOUND THE SOLUTION TO THE DISPERSION EQUATION, F,
C.....THE PARTICLE DISPLACEMENT VECTORS CAN NOW BE SOUGHT.
      X = ARG(1)*F
      Y = ARG(2)*F
C.....THE GOVERNING DISPLACEMENT EQUATIONS ARE COMPLEX.  SUBROU-
C.....TINE RON6 DEFINES SEVERAL COMPLEX QUANTITIES.
C.....K = Z-DIRECTION WAVE VECTORS
C.....TX,TY = TANGENTS OF ARGUMENTS X AND Y
C.....CX,CY = COSINES OF ARGUMENTS X AND Y
      CALL RON6(KS,K,F,TX,TY,CX,CY,X,Y)
C.....IN THIS DO LOOP THE G AND H PARAMETERS ARE DETERMINED.
C.....THE SECOND SUBSCRIPT INDICATES REAL AND IMAGINARY COMPONENTS.
      DO 400 I=1,2
      G(I,1) = C33*(RHO*S*S - C11 - C55*KS(I))/(C55+C13) + C13
      G(I,2) = 0.0
      AA= (RHO*S*S - C11 -C55*KS(I))/(C55+C13)
      IF (KS(I)) 320,320,310
  310 H(I,1) = K(I,1) +AA/K(I,1)
      H(I,2) = 0.0
      GO TO 400
  320 H(I,2) = K(I,2) -AA/K(I,2)
      H(I,1) = 0.0
  400 CONTINUE
C
C     WRITE (6,12)  G(1,1),G(1,2),G(2,1),G(2,2)
C     WRITE (6,13)  H(1,1),H(1,2),H(2,1),H(2,2)
C  12 FORMAT (1H ,T5,'G+ = ',2F10.4,/,T5,'G- = ',2F10.4)
C  13 FORMAT (1H ,T5,'H+ = ',2F10.4,/,T5,'H- = ',2F10.4)
      IF (PRNT - 2.0) 401,402,401
  401 WRITE (6,7) S,F,KS(1),KS(2),K(1,1),K(1,2),K(2,1),K(2,2),X,Y
      GO TO 403
C
  402 WRITE (6,16) S,F
  403 A(1) = 1.0
```

```
      A(2) = 0.0
      B(2) = 0.0
      IF (SYM-1.0) 442,441,442
  441 B(1) = 1.0
      GO TO 443
  442 B(1) = -1.0
C.....SUBROUTINE RON9 DIVIDES THE FIRST VECTOR BY THE SECOND,
C.....RETURNING THE THIRD.
  443 CALL RON9(-G(1,1),-G(1,2),G(2,1),G(2,2),V(1),V(2))
      CALL RON9(CX(1),CX(2),CY(1),CY(2),V1(1),V1(2))
      CALL RON9(TX(1),TX(2),TY(1),TY(2),V2(1),V2(2))
C.....SUBROUTINE RON7 MULTIPLIES THE FIRST AND SECOND VECTORS,
C.....RETURNING THE THIRD.
      CALL RON7(V(1),V(2),V1(1),V1(2),A1,A2)
      IF (SYM-1.0) 445,444,445
  444 C(1) = A1
      C(2) = A2
      D(1) = A1
      D(2) = A2
      GO TO 446
C
  445 CALL RON7(A1,A2,V2(1),V2(2),C(1),C(2))
      D(1) = -C(1)
      D(2) = -C(2)
C
  446 IF (PRNT - 2.0) 447,448,447
C.....THE A,B,C, AND D QUANTITIES GIVE THE MAGNITUDES OF THE
C.....PARTIAL WAVES.
  447 WRITE (6,8) A(1),A(2),B(1),B(2),C(1),C(2),D(1),D(2)
C
  448 CONTINUE
C.....THESE NEXT STATEMENTS SET SOME OF THE PLOTTING PARAMETERS.
      XWL = S*YMAX/(F*T)
      WN = XMAX/XWL
      NLX=NVL*WN + 2
      SCALE = SCA*YMAX*S/(3.0*F)
      NS = INT(S)
      NSP = INT(1000*S) - 1000*NS
      NF2 = INT(1000*F)
C.....SUBROUTINE NUMB INCORPORATES INTEGER NUMBERS INTO STRINGS TO
C.....BE PRINTED BY THE PLOTTER.  IN THIS CASE, VELOCITY AND
C.....FREQUENCY ARE PLACED IN STRINGS LN1 AND LN2, RESPECTIVELY.
      CALL NUMB(NS,LN1,13,13)
      CALL NUMB(NSP,LN1,15,17)
      CALL NUMB(NF2,LN2,14,17)
C
C.....SUBROUTINE RON11 COMPUTES THE MAXIMUM X (U1) AND Z (U2)
C.....PARTICLE DISPLACEMENTS.  THESE ARE NORMALIZED.
      CALL RON11(A,B,C,D,H,X,Y,KS,K,N,U1,U2,R)
C.....R GIVES THE RATIO OF WAVELENGTH TO MAXIMUM Z-DIRECTION
C.....DEFORMATION.
      R = S/(R*F*T)
      NR = INT(R)
      CALL NUMB(NR,LN3,14,17)
C
C     IF (N-50) 505,601,601
C 505 DO 600 I=1,N
C 600 WRITE (6,9) U1(I,1),U1(I,2),U2(I,1),U2(I,2)
C
C.....PLOTTING OF THE LITERAL INFORMATION IS PERFORMED.
```

```
  601 IF (N) 900,900,602
  602 INK = INK + 1
      IF (INK-7) 605,605,603
  603 IF (NC-1) 606,604,606
  604 PL1 = 5.5 - YMAX/2.0
  606 CALL ITLZ
      CALL DPT(1,4)
      CALL PLOT(0.0,-11.0,-2)
      CALL PLOT(4.0,PL1,-3)
      CALL SYMBOL(-3.5,0.00,0.14,LN1,0.0,25)
      CALL SYMBOL(-3.5,0.25,0.14,LN2,0.0,25)
C     CALL SYMBOL(-3.5,0.5,0.14,LN3,0.0,25)
      INK = INK - 7
      GO TO 610
  605 PL2 = (2.0*PL1-11.0)/(NC-1)
      CALL PLOT(0.0,-PL2,-3)
      CALL SYMBOL(-3.5,0.00,0.14,LN1,0.0,25)
      CALL SYMBOL(-3.5,0.25,0.14,LN2,0.0,25)
C     CALL SYMBOL(-3.5,0.5,0.14,LN3,0.0,25)
  610 XC(N+1) = 0.0
      XC(N+2) = 1.0
      YC(N+1) = 0.0
      YC(N+2) = 1.0
C
      NX = 301
C
      IN = 1
C.....HORIZONTAL DEFORMATION LINES ARE PLOTTED FIRST.
      DO 700 I=1,NLX
      IN = -IN
      XI = XWL*(I-1)/NVL + XWL/4.0
      XA = 2.0*3.141592*XI/XWL
      DO 650 J=1,N
      JJ = J
      IF (IN) 621,620,620
  620 JJ = N - J + 1
  621 YI = YMAX*(JJ-1)/(N-1)
C.....XC AND YC ARE THE ACTUAL X,Y COORDINATES (IN INCHES) OF
C.....THE INITIALLY UNDEFORMED HORIZONTAL GRID LINE.
      XC(J) = XI +(COS(XA)*U1(JJ,1)-SIN(XA)*U1(JJ,2))*SCALE  -XWL/4.0
  650 YC(J) = YI +(COS(XA)*U2(JJ,1)-SIN(XA)*U2(JJ,2))*SCALE
C.....SUBROUTINE LINE DOES THE PLOTTING.
      CALL LINE(XC,YC,N,1,0,1)
  700 CONTINUE
C
      XC(NX+1)= 0.0
      XC(NX+2)= 1.0
      YC(NX+1)= 0.0
      YC(NX+2)= 1.0
C
      IN =-1
C.....VERTICAL DEFORMATION LINES ARE THEN PLOTTED.
      DO 800 L=1,M
      IN = -IN
      J = 1 + (L-1)*(N-1)/(M-1)
      YI = YMAX*(J-1)/(N-1)
      DO 750 I=1,NX
      XI = XWL*(I-1)*(NLX-1)/((NX-1)*NVL) + XWL/4.0
      II = I
      IF (IN) 721,720,720
```

```
  720 II = NX - I + 1
  721 XA = 2.0*3.141592*XI/XWL
      XC(II)= XI +(COS(XA)*U1(J,1) - SIN(XA)*U1(J,2))*SCALE -XWL/4.0
  750 YC(II)= YI +(COS(XA)*U2(J,1) - SIN(XA)*U2(J,2))*SCALE
      CALL LINE(XC,YC,NX,1,0,1)
  800 CONTINUE
      IF (INK-7) 900,850,900
  850 CALL FINAL
C
C.....PROCEDURE IS REPEATED FOR NEXT WAVE.
  900 CONTINUE
      IF (N) 950,1000,950
  950 CALL FINAL
 1000 STOP
      END
      SUBROUTINE RON1(RHO,C11,C33,C13,C55,A1,A2,A3,A4,A5,A6)
      A1 = (C11*C33 - C13*(C13+2.*C55))/(C33*C55)
      A2 = -RHO*(C33+C55)/(C33*C55)
      A3 = C11/C33
      A4 = -RHO*(1.+C11/C55)/C33
      A5 = RHO*RHO/(C33*C55)
      A6 = -C11 + C13*(C13+C55)/C33
      WRITE (6,1) A1,A2,A3,A4,A5,A6
    1 FORMAT (1HO,///,'THE A CONSTANTS ARE',/,T5,6F10.4)
      RETURN
      END
C
      SUBROUTINE RON2(S,A1,A2,A3,A4,A5,KPS,KMS,INDEX)
      REAL KPS,KMS
      B = A1 + A2*S*S
      D = A3 + A4*S*S + A5*S*S*S*S
      D = B*B - 4.0*D
      IF (D) 10,10,20
   10 INDEX = 1
      GO TO 100
   20 INDEX = 0
      KPS = (-B + SQRT(D))/2.0
      KMS = (-B - SQRT(D))/2.0
  100 RETURN
      END
C
      SUBROUTINE RON3(KPS,KMS,S,RHO,C11,C13,C55,A6,CONST)
      REAL KPS,KMS
      CONST = SQRT(ABS(KMS))*(RHO*S*S-C11+C13*KPS)
      CONST = CONST*(RHO*S*S+A6-C55*KMS)/SQRT(ABS(KPS))
      CONST = CONST/(RHO*S*S-C11+C13*KMS)
      CONST = CONST/(RHO*S*S+A6-C55*KPS)
      RETURN
      END
C
      SUBROUTINE RON4(ARG,KS,F,RATIO)
      DIMENSION ARG(2),KS(2),V(2)
      REAL KS
      DO 100 I=1,2
      A = ARG(I)*F
      IF (KS(I)) 20,10,10
   10 V(I) = SIN(A)/COS(A)
      GO TO 100
   20 V(I) = (EXP(A)-EXP(-A))/(EXP(A)+EXP(-A))
  100 CONTINUE
```

```
      RATIO = V(1)/V(2)
      RETURN
      END
C
C
C
      SUBROUTINE RON5(Q1,CONST,Q2,IND)
      IF (Q1*Q2) 5,10,10
    5 IF (ABS(Q1-Q2)-2.0) 10,10,100
   10 IF (Q1-CONST) 20,20,50
   20 IF (CONST-Q2) 200,200,100
   50 IF (CONST-Q2) 100,200,200
  100 IND = 0
      GO TO 300
  200 IND = 1
  300 RETURN
      END
C
      SUBROUTINE RON6(KS,K,F,TX,TY,CX,CY,X,Y)
      DIMENSION KS(2),K(2,2),TX(2),TY(2),CX(2),CY(2)
      REAL KS,K
      IF (KS(1)) 20,10,10
   10 K(1,1) = SQRT(KS(1))
      K(1,2) = 0.0
      TX(1) = SIN(X)/COS(X)
      TX(2) = 0.0
      CX(1) = COS(X)
      CX(2) = 0.0
      GO TO 25
   20 K(1,1) = 0.0
      K(1,2) = SQRT(-KS(1))
      TX(1) = 0.0
      TX(2) = (EXP(X)-EXP(-X))/(EXP(X)+EXP(-X))
      CX(1) = (EXP(X)+EXP(-X))/2.0
      CX(2) = 0.0
   25 IF (KS(2)) 40,30,30
   30 K(2,1) = SQRT(KS(2))
      K(2,2) = 0.0
      TY(1) = SIN(Y)/COS(Y)
      TY(2) = 0.0
      CY(1) = COS(Y)
      CY(2) = 0.0
      GO TO 50
   40 K(2,1) = 0.0
      K(2,2) = SQRT(-KS(2))
      TY(1) = 0.0
      TY(2) = (EXP(Y)-EXP(-Y))/(EXP(Y)+EXP(-Y))
      CY(1) = (EXP(Y)+EXP(-Y))/2.0
      CY(2) = 0.0
   50 RETURN
      END
C
      SUBROUTINE RON7(A,B,C,D,E,F)
      E = A*C - B*D
      F = A*D + B*C
      RETURN
      END
      SUBROUTINE RON9(A,B,C,D,E,F)
      R1 = C*C + D*D
      E = (A*C + B*D)/R1
```

```
      F = (B*C - A*D)/R1
      RETURN
      END
C
      SUBROUTINE RON11(A,B,C,D,H,X,Y,KS,K,N,U1,U2,R)
      DIMENSION A(2),B(2),C(2),D(2),E(4,2),F(4,2),G(4,2),H(2,2)
      DIMENSION FG(4,2),KS(2),K(2,2),U1(100,2),U2(100,2)
      REAL KS,K
      E(1,1) = H(1,1) - K(1,1)
      E(1,2) = H(1,2) - K(1,2)
      E(3,1) = H(2,1) - K(2,1)
      E(3,2) = H(2,2) - K(2,2)
      E(2,1) = - E(1,1)
      E(2,2) = - E(1,2)
      E(4,1) = - E(3,1)
      E(4,2) = - E(3,2)
      F(1,1) = A(1)
      F(1,2) = A(2)
      F(2,1) = B(1)
      F(2,2) = B(2)
      F(3,1) = C(1)
      F(3,2) = C(2)
      F(4,1) = D(1)
      F(4,2) = D(2)
C
      X1 = X
      Y1 = Y
      DUD = 0.
      DUB = 0.
C
      DO 500 I=1,N
      X = X1*(2*I-N-1)/(N-1)
      Y = Y1*(2*I-N-1)/(N-1)
C
      IF (KS(1)) 20,10,10
   10 G(1,1) = COS(X)
      G(1,2) = SIN(X)
      G(2,1) = COS(-X)
      G(2,2) = SIN(-X)
      GO TO 30
   20 G(1,1) = EXP(-X)
      G(1,2) = 0.0
      G(2,1) = EXP(X)
      G(2,2) = 0.0
   30 IF (KS(2)) 50,40,40
   40 G(3,1) = COS(Y)
      G(3,2) = SIN(Y)
      G(4,1) = COS(-Y)
      G(4,2) = SIN(-Y)
      GO TO 60
   50 G(3,1) = EXP(-Y)
      G(3,2) = 0.0
      G(4,1) = EXP(Y)
      G(4,2) = 0.0
C
   60 U1(I,1) = 0.0
      U1(I,2) = 0.0
      U2(I,1) = 0.0
      U2(I,2) = 0.0
C
```

```
      DO 100 J=1,4
      CALL RON7(F(J,1),F(J,2),G(J,1),G(J,2),FG(J,1),FG(J,2))
      U1(I,1) = U1(I,1) + FG(J,1)
      U1(I,2) = U1(I,2) + FG(J,2)
      CALL RON7(E(J,1),E(J,2),FG(J,1),FG(J,2),P,Q)
      U2(I,1) = U2(I,1) + P
  100 U2(I,2) = U2(I,2) + Q
C
      IF (DUD - ABS(U1(I,1))) 110,120,120
  110 DUD = ABS(U1(I,1))
  120 IF (DUD - ABS(U1(I,2))) 130,140,140
  130 DUD = ABS(U1(I,2))
  140 IF (DUB - ABS(U2(I,1))) 150,160,160
  150 DUB = ABS(U2(I,1))
  160 IF (DUB - ABS(U2(I,2))) 170,500,500
  170 DUB = ABS(U2(I,2))
C
  500 CONTINUE
C
      R = DUD/DUB
      IF (DUD-DUB) 510,520,520
  510 DUD = DUB
  520 DO 600 I=1,N
      DO 550 J=1,2
      U1(I,J) = U1(I,J)/DUD
  550 U2(I,J) = U2(I,J)/DUD
      WRITE (6,5) U1(I,1),U1(I,2),U2(I,1),U2(I,2)
    5 FORMAT (1H ,2F10.4,10X,2F10.4)
  600 CONTINUE
C
      RETURN
      END

/END CARD READ, JOB TERMINATED
```

APPENDIX III

SEM PHOTOMICROGRAPHS OF BOARD SAMPLES

On the following pages, SEM photomicrographs are presented for the three board samples tested extensively in this investigation.

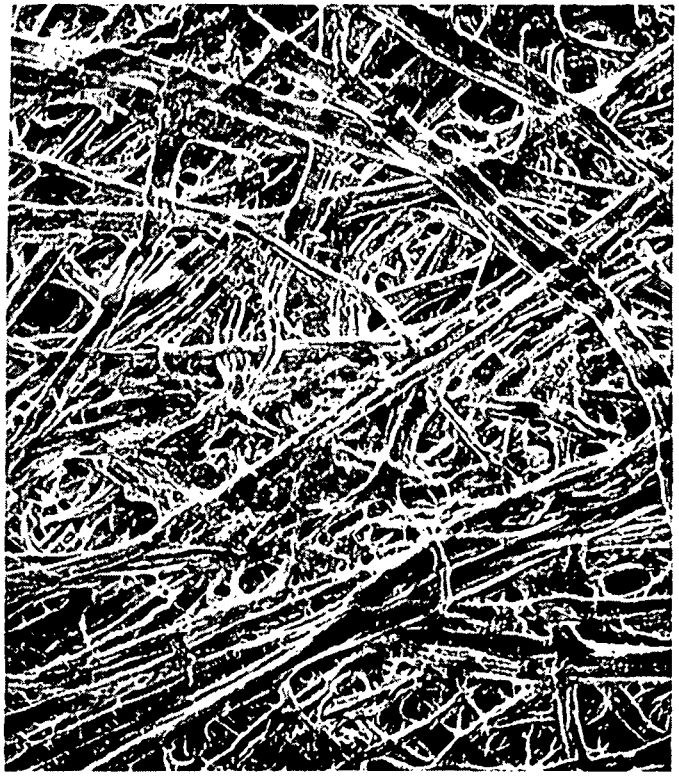

(a) Top View, 100X

(b) Bottom View, 100X

90 lbLinerboard Sample No. 1

(c) Bottom View, 300X

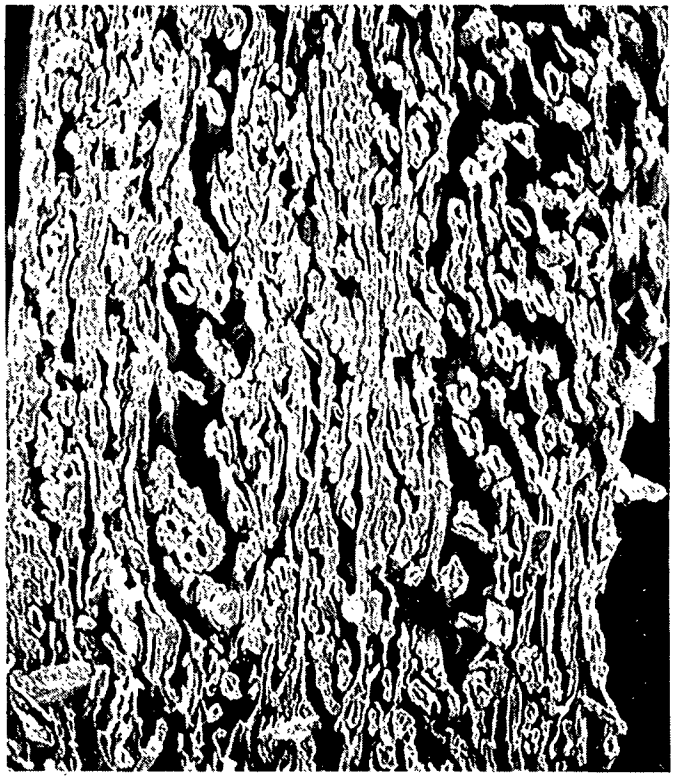

(d) Edge View, 120X

90 lb Linerboard Sample No. 1

(a) Top View, 100X

(b) Bottom View, 100X

90 lb Linerboard Sample No. 2

(c) Bottom View, 300X

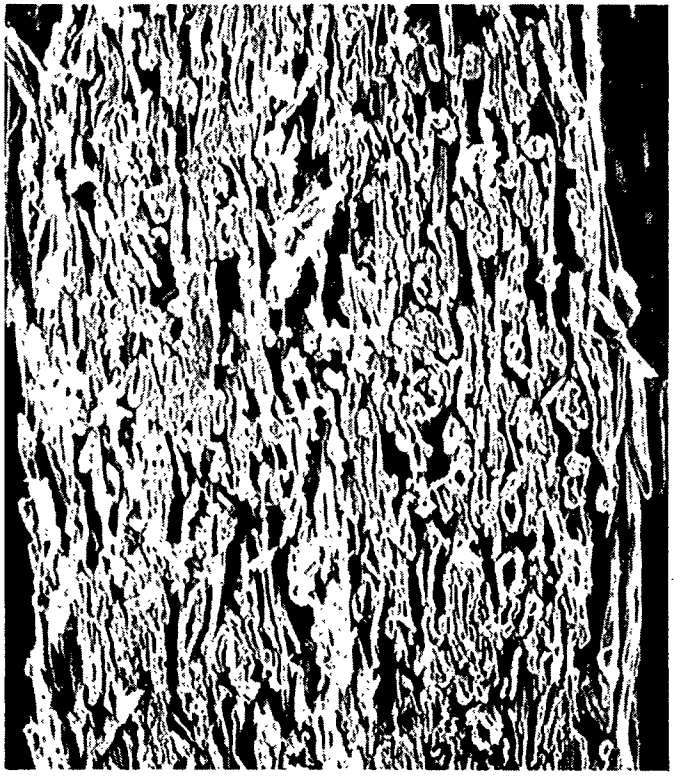

(d) Edge View, 120X

90 lb Linerboard Sample No. 2

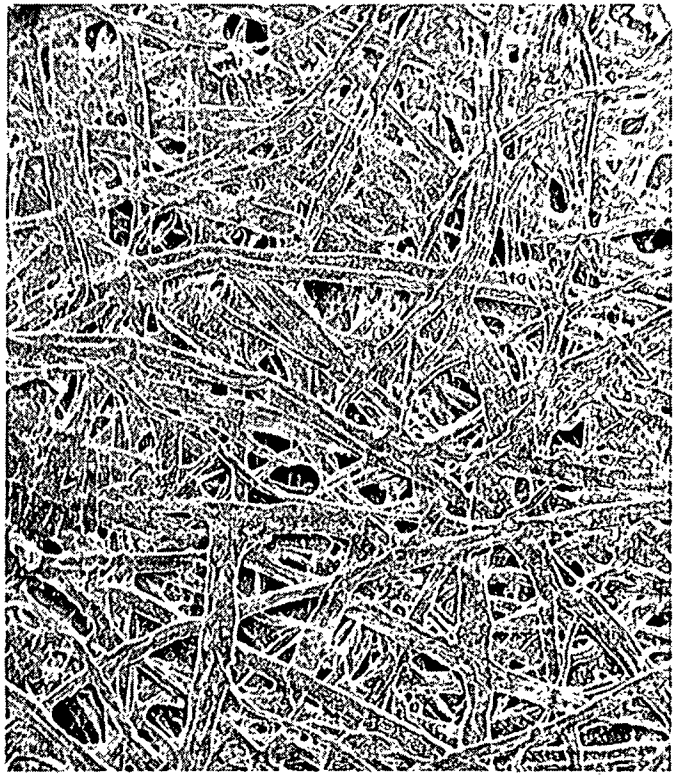

(a) Top View, 100X

(b) Bottom View, 100X

Milk Carton Stock

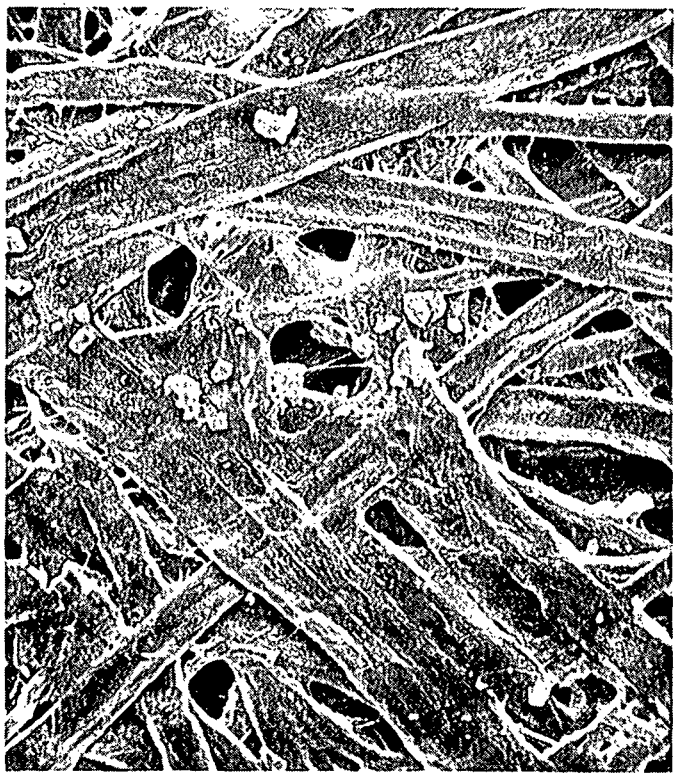

(c) Bottom View, 300X

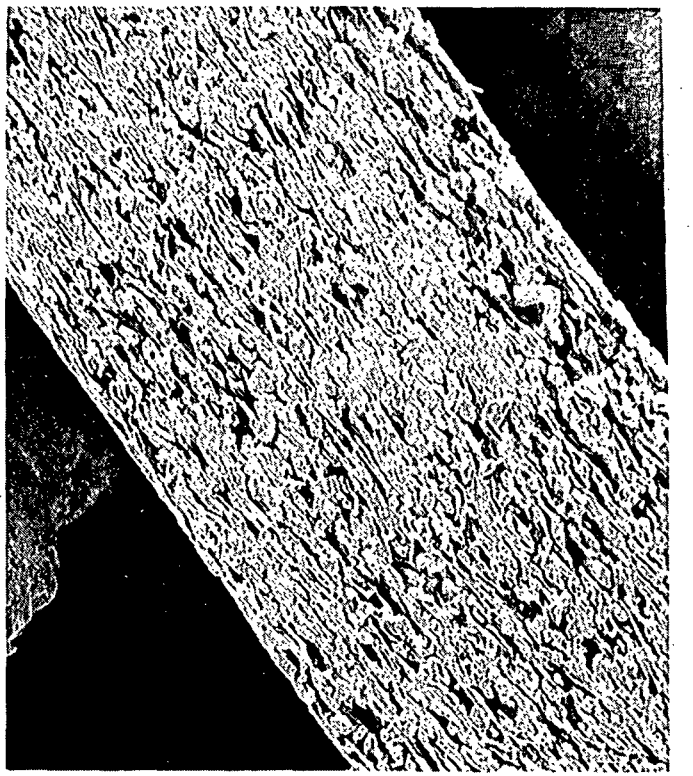

(d) Edge View, 100X

Milk Carton Stock

APPENDIX IV

PLATE WAVE VELOCITY DATA

Listed in the tables (Tables XV-XVII) in this appendix are the plate wave velocities measured at various frequencies for the three board samples. These data have been plotted in Fig. 19 through 24.

TABLE XV

PLATE WAVE VELOCITIES FOR 90 LB. LINERBOARD SAMPLE 1

	Frequency (kHz)	Velocity (m/sec)		
		Specimen 1	Specimen 2	Specimen 3
X-direction	100	1935	-	-
	110	925	677	595
	120	554	579	598
	130	479	477	384, 521
	140	439	417	381, 453
	150	426	455	379, 453
	160	402	432	392, 413
	170	390	416	386
	180	387	409	384
	190	379	400	-
	200	376	396	-
	210	-	867	-
	220	643	663	-
	230	581	-	-
	240	369, 498	-	-
	250	372, 479	399	-
	260	374, 472	405	-
	270	373, 472	410	-
	280	374, 453	407	-
	290	374, 439	410	-
	300	374, 434	415	-
	310	383, 429	-	-
	320	396, 439	-	-
Y-direction	100	1836	-	1340
	110	782	666	677
	115	509	575	-
	120	515	-	435
	125	-	-	420
	130	414	496	400
	140	-	477	-
	150	380	-	-

TABLE XVI

PLATE WAVE VELOCITIES FOR 90 LB. LINERBOARD SAMPLE 2

	Frequency (kHz)	Velocity (m/sec)		
		Specimen 1	Specimen 2	Specimen 3
X-direction	110	-	-	1941
	120	2493	-	1877
	125	-	-	1234
	130	1626	-	924
	140	832	1876	703
	150	620	876	616
	160	656	697	559
	170	-	634	515
	180	546	563	487
	190	539	527	-
	200	509	366, 504	483
	210	503	369, 485	-
	220	384, 477	372, 481	365, 460
	230	453	373, 463	-
	240	385, 453	376, 453	379, 452
	250	393, 438	379, 449	-
	260	391, 464	381, 442	382, 442
	270	-	382, 441	-
	280	404, 453	384, 439	384, 436
	290	-	387, 434	-
	300	451	387, 439	386, 440
	310	-	437	-
	320	-	442	440
Y-direction	120	-	1755	1384
	130	-	1307	691
	140	892	644	640
	150	489	508	554
	160	513	456	512
	170	446	432	490
	180	431	407	455
	190	412	395	428
	200	394	384	409
	210	387	-	-
	220	382	-	393
	230	377	-	-
	240	-	-	385
	260	-	-	381
	270	-	1092	-
	280	-	800	-
	290	-	640	-
	300	-	644	-

TABLE XVII

PLATE WAVE DATA FOR MILK CARTON STOCK

	Frequency (kHz)	Velocity (m/sec) Specimen 1	Specimen 2
X-direction	150	1100	1441
	160	724	807
	170	623	676
	180	562	605
	190	530	366, 567
	200	369, 514	372, 540
	210	374, 498	375, 526
	220	375, 478	378, 509
	230	379, 471	379, 493
	250	387, 460	383, 477
	270	393, 449	389, 468
	290	452, 1610	392, 465
	310	444, 873	396, 456
	330	465, 751	464, 948
	350	440, 589	402, 461, 810
	360	-	397, 457, 779
	370	-	457, 667
	380	-	462, 669
	390	-	459, 627
	400	-	448, 582
	410	-	456, 587
	420	-	597
Y-direction	140	1774	1765
	150	1426	1483
	160	769	782
	170	625	626
	180	555	542
	190	510	498
	200	474	473
	210	459	450
	220	446	438
	230	438	432
	240	425	424
	250	419	415
	260	412	408
	270	404	404
	280	-	402
	290	397, 1133	400
	310	389, 747	394, 914
	330	383, 697	396, 763
	350	389, 600	393, 629